Shear Localization in Viscoplastic Solids

by

Kwon Hee Kim

B.S., Mechanical Engineering, Seoul National University(1979)
M.S., Mechanics and Design, Seoul National University(1981)

SUBMITTED IN PARTIAL FULFILLMENT
OF THE REQUIREMENT FOR THE
DEGREE OF
DOCTOR OF PHILOSOPHY
IN MECHANICAL ENGINEERING

at the

MASSACHUSETTS INSTITUTE OF TECHNOLOGY
August 1987

©Massachusetts Institute of Technology 1987

Signature of Author _____
Department of Mechanical Engineering
August, 1987

Certified by _____
Professor Lallit Anand
Thesis Supervisor

Accepted by _____
Professor Ain Ants Sonin, Chairman
Departmental Committee on Graduate Studies

MASSACHUSETTS INSTITUTE
OF TECHNOLOGY

NOV 04 1987

SHEAR LOCALIZATION IN VISCOPLASTIC SOLIDS

by

KWON HEE KIM

Submitted to the Department of Mechanical Engineering in
partial fulfillment of the requirements for the Degree of
Doctor of Philosophy in Mechanical Engineering

ABSTRACT

An outstanding problem in mechanics is the modeling of the phenomenon of initiation and development of localized shear bands in materials whose inelastic deformation behavior is inherently rate-dependent. Clifton (1980) and Bai (1982) have presented a one-dimensional linear perturbation stability analysis for the initiation of shear bands in viscoplastic solids deforming in simple shear. Although this one-dimensional analysis provides much insight into the phenomenon of shear localization, the results are not directly applicable to the practically more interesting problems in two and three dimensions. Accordingly, here, a three-dimensional generalization of this linear perturbation stability analysis is presented for a J_2 flow theory of plasticity which exhibits isotropic strain hardening or softening, strain rate hardening, and thermal softening. The results are then specialized to the simpler case of plane motions and the limiting cases of quasi-static isothermal deformations and dynamic adiabatic deformations are thoroughly analyzed.

An inherent limitation of this linear perturbation analyses is that it provides only (a) the *necessary* conditions for the *initiation* of shear bands, and (b) the *orientations* and the *incipient rate of growth* of the *emergent* shear bands. It does not provide any information regarding the more interesting stages of localization when the strain, strain rate, and temperature in the shear bands becomes much larger than elsewhere. To predict the beginning stages of *significant* flow localization a new criterion has been developed for *adiabatic* flow localization. A history dependent dimensionless parameter λ which represents the integral in time of the ratio of the rate of flow softening to the rate of strain-rate hardening is identified as a possible flow localization parameter, and the attainment of a critically large value λ_c of λ is suggested as a simple criterion for monitoring the beginning of severe adiabatic flow localization. Fully two dimensional large deformation finite element simulations of plane strain compression, tension and U-notch bending tests on a class of thermo-elasto-viscoplastic materials under adiabatic conditions have been performed and the initiation and growth of naturally appearing band-like regions of localization is followed from slow early growth to severe localization. By simultaneously monitoring level contours of λ it is demonstrated that the time when there appears a zone of noticeable size in which $\lambda > \lambda_c$ within the specimen *correlates* very well with the beginning of significant shear localization.

Thesis Supervisor: Lallit Anand
Title: Associate Professor of Mechanical Engineering

VITA

Education

- Master of Science in Engineering, Seoul National University in Seoul, Korea, February, 1981.
- Bachelor of Science in Mechanical Engineering, Seoul National University, February, 1979.

Professional

- Research Staff, Korea Institute of Machinery and Metals, Seoul, Korea, 1981 to 1983.

Personal

- Born, August 12, 1956 in Seoul, Korea.
- Married in August 1983.

ACKNOWLEDGEMENTS

I offer my greatest appreciation to Professor Lallit Anand who provided support and guidance during my stay here at MIT since I have joined his research group in January 1984.

Next, I must acknowledge the help of Allen Lush for computational problems related to the study and the guidance and inspiration from Tarek Shawki. My great officemates Stuart Brown, Charles White, Mehrdad Haghi, Shoichi Hashimoto, Curt Bronkhorst and Tresa Pollock have made my life at MIT valuable and memorable in terms of friendship and guidance. I appreciate the support and advice from Bill Henry for my experimentations during the last three and half years.

The linear perturbation analysis has been performed jointely with Anand and Shawki and the content of chapter 2 is essentially the one which is in press for publication in the Journal of the Mechanics and Physics of Solids. The integral localization criterion in chapter 3 and the numerical simulation of a plane strain tension test AMS 6418 steel in chapter 4 has been submitted for publication in the proceedings of the International Conference on Computational Methods for Predicting Material Processing Defects which is to be held in September 8 - 11, 1987, Cachan, France.

Funding for the research has been provided partially by the overseas education program of Korea Science and Engineering Foundation and partially by National Science Foundation under the contract no. MEA - 8315117.

Contents

1. Introduction....1
2. Linear Perturbation Stability Analysis for Shear Localization....9
2.1 Field Equations....10
2.2 Linear Perturbation Stability Analysis for 3-Dimensions....13
2.3 Initiation of Localized Shear Bands in Plane Motions....20
2.3.1 Quasi-Static, Isothermal Deformations....23
2.3.1a Pressure Insensitive Materials....24
2.3.1b Pressure Sensitive Materials....25
2.3.2 Dynamic, Adiabatic Deformations....28
2.3.2a Pressure Insensitive Materials....29
2.3.2b Pressure Sensitive Materials....32
2.4 Discussion....33
3. Integral Flow Localization Criterion....36
3.1 Background....36
3.2 Localization Criterion....39
4. Numerical Examples....44
4.1 Plane Strain Compression....48
4.2 Plane Strain Tension....51
4.3 Plane Strain Bending of a U-notched Specimen....54
5. Discussion and Conclusions....57
References....65
Appendix....71
List of Figures....88
Figures....91

Chapter 1
Introduction

Localization of plastic flow into shear bands is a widely observed phenomenon. Once such bands are formed, they persist and the strains inside the bands can become very large. In situations where the attendant principal stresses are positive and large, the formation of shear bands is an important precursor to imminent ductile fracture. However, in compressive stress fields, some materials can sustain considerable subsequent inelastic deformation by continued shearing within the bands and by the formation of additional shear bands. Of course, even in compressive stress fields ductile fracture nuclei may be formed by local micro-tensile fracturing which may (if dominantly tensile type of fracture can be suppressed by say the application of large hydrostatic pressure) lead to sliding-off types of fracture along the shear bands.

Shear band formation is usually associated with a flow softening behavior of the material with increasing deformation. Various softening mechanisms are possible. For quasi-static deformation conditions a major reason for flow softening is internal damage, for example that due to void nucleation and growth. Under high-rate plastic deformation conditions, any softening due to internal damage is enhanced due to thermal effects and the shear bands that form are called "adiabatic shear bands". In either case, the process of shear banding is an autocatalytic one : an increase in the strain in a soft zone causes a further softening of the material which causes a local increase in the strain and so on.

Since the pioneering observation of adiabatic shear bands formed in a steel plate during punching by Zener and Hollomon [1944], various experimental observations has been

made in different deformation processes such as machining (e.g., Recht [1964], Semiatin, Lahoti and Oh [1982]), dynamic torsion of hollow tubes (e.g., Culver [1973], Costin, Crisman, Hawley, and Duffy [1979]), ballistic impact (e.g., Backman and Finnegan [1973], Rogers and Shastry [1981], Leech [1985]), explosive loading of thick walled tubes (e.g., Thornton and Heiser [1971], Staker [1981]), isothermal and non-isothermal hot forging (e.g. Semiatin, Lahoti and Oh [1982]), sheet metal stretching (e.g., Bird and Carlson [1986]) and plane strain tension and compression (e.g., Anand and Spitzig [1980, 1982]). Along with the experimental observations, considerable theoretical attention has been paid to this phenomenon with most studies confining their attention to the initiation of such a flow localization. For materials which can be modeled as *rate-independent* and considered to be deforming *quasi-statically* and isothermally, a mathematical method is available for analyzing the onset of shear band formation (cf. e.g., Rudnicki and Rice [1975], Rice [1977]). In this method, the onset of localization is viewed as a material instability, and critical conditions are sought at which the rate-independent elastic-plastic constitutive relations first allow a bifurcation from a homogenous deformation into a shear band mode. It is found that a necessary condition for the existence of shear bands is that the velocity equations of continuing equilibrium suffer a loss of ellipticity, and this occurs when the rate of strain hardening reaches a critical value. Further, the boundaries of the emergent shear bands correspond to the associated characteristic lines.

For *rate-dependent* plastic flow, shear localization of plastic deformation is believed to be controlled by the interaction between softening and hardening features of the material behavior which include thermal softening, strain hardening and strain rate hardening. In an effort to predict the formation of shear bands in dynamic deformation

processes, Recht [1964] suggested that "Catastrophic shear occurs when the local rate of change of temperature has a negative effect on strength which is equal or greater than the positive effect of strain hardening". This is equivalent to saying that the critical strain at which plastic instability takes place is that at which the slope of the true stress - strain curve vanishes. For quasi-static, isothermal deformation processes, this criterion requires that the rate of strain hardening should vanish or be negative for the occurence of shear band formation. Because of its simplicity, this criterion has been applied to shear localization problems in a wide variety of deformation processes by different investigators (e.g., Culver [1973], Staker [1981], Rogers and Shastry [1981], Semiatin, Staker and Jonas [1984]).

An alternative approach to the study of the criteria for the onset of shear localization has been recently considered by Clifton [1980] and Bai [1982]. These authors also treat shear localization as material instability, however, the method of mathematical analysis differs from that of the bifurcation analysis for rate-independent materials and the simple stress maximum criterion outlined above. In their approach, Clifton and Bai seek critical conditions at which the rate-dependent constitutive relations, which exhibit strain hardening or softening, strain-rate hardening and thermal softening first allow the growth of infinitesimal periodic non-uniformities in an otherwise homogeneous *simple shearing* motion. The effects of inertia and heat conduction are included in the analysis.

It is interesting to note here that the linear perturbation stability analyses for adiabatic simple shear deformation gives a necessary condition for shear localization which is the same as the one for shear band formation given by maximum flow stress criterion. Both types of analyses require that the strain hardening should be overcome by

thermal softening such that the slope of the adiabatic flow stress-strain curve vanishes (e.g., compare equation (3) in Culver [1973] with equation (4.3) in Bai [1982]).

The history of linear perturbation stability analyses for viscoplastic solids can be traced back to the paper by Rabotnov and Shesterikov [1958] on creep buckling of axially compressed columns and plates. They define stability against buckling of columns and plates made from viscoplastic materials as follows: "If at a certain moment a deviation from straightness or plane form is given to the compressed column or plate under creep, the deflection will increase of decrease during a subsequent short interval of time. According to whether the deflection increases or decreases, the initial state is considered unstable of stable". As emphasized by Hoff [1958], an analysis based on such a notion of stability ".... simply indicates stability or instability in the classical sense immediately following the disturbance. It cannot predict the motion over an extended period of time."

In addition to the work of Clifton and Bai on one-dimensional shear localization, and the papers of Rabotnov and Shesterikov and Hoff on creep buckling of axially compressed columns, of pertinence to the present discussion is the recent paper by Fressengeas and Molinari [1985] on the necking mode of localization during uniaxial tensile testing of viscoplastic solids. These authors present a one-dimensional linear perturbation analysis for this problem, and elucidate a the role played by inertia and thermal effects on this localization phenomenon. Their analysis proceeds along lines similar to those of Clifton and Bai and they too arrive at a characteristic stability equation from which they determine the conditions for the *onset* of necking type of instability. Fressengeas and Molinari also carry out a numerical study of their full nonlinear boundary value problem with an *initial* non-uniformity in the cross-sectional area

of the bar, and a particular power-law type of viscoplastic constitutive equation. They obtain numerical predictions for the evolution of the initial defect size, and calculate the evolution of strains in cross-sections with and without the defect as a function of the nominal strain. Also, for *small* geometric non-uniformity they linearize their problem and obtain similar predictions, and then compare the predictions from their linearized boundary value problem against those from their non-linear analysis. They find that although the linearized theory qualitatively predicts the necking instability, it predicts significant localization at nominal strains which are much smaller than those predicted by the full non-linear analysis. Similar conclusions have been previously reached by Hutchinson and Obrecht [1977] who have also studied problem of necking instabilities in viscoplastic solids, but have not accounted for inertia and thermal effects in their analysis.

For most engineering materials which have positive strain-rate hardening, the speeds of the growth of perturbations are strongly controlled by the rate sensitivity. Unless the value of strain-rate hardening is extremely small such that a material is almost rate independent, the perturbations will growth with finite speeds and thus the stage of significant flow localization with unbounded strains and strain rates inside the localization zone will be postponed far after the onset of the growth of perturbations predicted by linear perturbation stability analyses. This feature of the shear localization in viscoplastic solids can be observed in the fully nonlinear numerical simulations of simple shear deformation processes with the introduction of small geometric or temperature perturbations (e.g., Merzer [1982], Wright and Batra [1985], Shawki [1986]). Thus it should be emphasized that although linear perturbations stability analyses predict the instability qualitatively, they cannot predict the amount of "attainable strains" before

the strains inside the localization zone become unbounded. This type of analysis can only predict the *necessary* conditions for the *onset* of flow localization. The same is true for the maximum flow stress criterion which agrees with the perturbation stability analyses upon the necessary condition for shear localization in adiabatic simple shear deformation process.

In spite of these limitations of the linear perturbation analysis as compared to the full non-linear analysis, the linear perturbation stability analysis does predict the necessary conditions for the onset of formation of shear bands for a wide class of constitutive equations whereas the non-linear analysis requires the assumption of a special form for the viscoplastic constitutive equation and the use of numerical techniques.

The plan of this thesis is as follows. In chapter 2, a 3-dimensional linear perturbation stability analysis for shear localization in viscoplastic solids will be presented. This analysis is a generalization of the 1-dimensional analysis prevously performed by Clifton and Bai. The constitutive equations considered here model isotropic, incompressible, viscoplastic materials which exhibit strain hardening or softening, strain-rate hardening, thermal softening and pressure sensitivity. Elastic effects are neglected. After briefly discussing the field equations, the linear perturbation stability analysis which helps determine the necessary conditions for the formation of shear bands will be presented. Then attention will be paid to plane motions and the criteria for the onset of shear localization and the directions of the emergent shear bands for the physically important special cases of quasi-static isothermal deformations and dynamic adiabatic deformations will be discussed. An important prediction of the perturbation analysis is that shear bands can initiate in two directions even in simple shear. This is contrary to the common perturbation analysis assumption (e.g., Clifton [1980], Bai [1982]) that in

simple shear, a shear band can initiate only in the direction parallel to the direction of shear. This theoretical prediction is shown to be in agreement with some simple shear experiments on the polymer polycarbonate. This and some other observations will be made in this chapter.

In Chapter 3, a new approach to the problem of flow localization in viscoplastic solids will be taken. To overcome the difficulty of the underestimation of critical strains predicted by linear perturbation stability analyses, a new flow localization criterion for *adiabatic shear banding* in viscoplastic solids will be developed. In contrast to the linear perturbation stability analysis which predicts the onset of shear localization as when the strain hardening is overcome by thermal softening, the new criterion predicts that the beginning of significant flow localization is possible when the time history of the ratio of the rate of flow softening to the rate of strain rate hardening attains a critically large value.

In chapter 4, the results from the numerical simulations of a few adiabatic deformation processes: plane strain compression, plane strain tension, and plane strain bending of a u-notched specimen, are presented. Fully non-linear solutions to these problems are compared against the predictions of the linear perturbation analysis and the new localization criterion developed in chapter 3. Classical underestimation of critical strains to significant shear localization is obtained by the linear perturbation analysis. On the other hand, it is observed that the new criterion gives reasonable predictions for the beginning of shear localization in plane strain deformations.

Finally in chapter 5, some conclusions regarding the performance of the linear perturbation stability analysis and the new localization criterion are presented, and some aspects of the shear localization phenomenon which needs to be investigated further

are discussed.

Chapter 2

Linear Perturbation Stability Analysis for Shear Localization

Since the introduction of linear perturbation stability analysis for the prediction of thermo-mechanical shear instability in simple shear deformation of viscoplastic solids by Clifton [1982] and Bai [1982], linear perturbation stability analysis has received considerable attention as an analytical tool for the prediction of the critical conditions for the onset of shear localization. Various analyses (see e.g., Clifton, Duffy, Hartley and Shawki [1984], Shawki [1986], Molinari and Clifton [1986]) show that even in simple shear, the shear localization is the result of a complex interplay between various factors such as the strain hardening and softening features of a material, heat transfer, inertial effects, initial field inhomogeneity and boundary conditions.

Although the results from 1-dimensional linear perturbation analysis of simple shear provides much insight into the nature of shear localization phenomenon in viscoplastic solids, these results are not directly applicable to the practically important 2-dimensional or 3-dimensional deformation processes. In the following, a 3-dimensional generalization of the 1-dimensional linear perturbation stability analysis of Clifton and Bai will be presented.

2.1 Field Equations

In the following analysis, $\mathbf{x}$ denotes the position of a particle of a body in the current configuration at time t. Also, $\mathbf{v}(\mathbf{x},t)$ denotes the spatial description of velocity. $\mathbf{L}(\mathbf{x},t) \equiv$ grad $\mathbf{v}$ the velocity gradient, $\mathbf{D}(\mathbf{x},t) \equiv$ sym $\mathbf{L}$ the stretching, $\mathbf{T}(\mathbf{x},t)$ the Cauchy stress, and $\theta(\mathbf{x},t)$ the absolute temperature.

It will be assumed that the effects of elasticity are negligible, and that the flow rule is given by[1]

$$\mathbf{L} = \dot{\bar{\gamma}}\mathbf{N} \tag{1}$$

Here, with

$$\mathbf{T}' \equiv \mathbf{T} + \bar{p}\mathbf{1} \tag{2}$$

denoting the stress deviator,

$$\bar{p} \equiv -(1/3)tr\mathbf{T} \tag{3}$$

the mean normal pressure, and

$$\bar{\tau} \equiv \sqrt{(1/2)\mathbf{T}' \cdot \mathbf{T}'} \tag{4}$$

the equivalent shear stress,

$$\mathbf{N} \equiv [\mathbf{T}'/2\bar{\tau}] \tag{5}$$

is the "direction" of plastic flow, and

$$\dot{\bar{\gamma}} = f(\bar{\tau}, \bar{p}, \theta, \bar{\gamma}) > 0 \tag{6}$$

[1]No yield condition and switching rules are assumed

with

$$f(0, \bar{p}, \theta, \bar{\gamma}) = 0$$

is the equivalent plastic shear strain rate. In equation (6)

$$\bar{\gamma}(t) = \int_0^t \dot{\bar{\gamma}} dt \tag{7}$$

is the equivalent plastic shear strain.

It is assumed that the strain-rate function f in equation (6) is invertible such that

$$\bar{\tau} = g(\dot{\bar{\gamma}}, \bar{\gamma}, \theta, \bar{p}). \tag{8}$$

For later use, the rates of strain-rate hardening, strain hardening, thermal softening, and pressure hardening are defined by

$$\left.\begin{aligned} R &\equiv \partial g / \partial \dot{\bar{\gamma}}, \\ S &\equiv \partial g / \partial \bar{\gamma}, \\ T &\equiv -\partial g / \partial \theta, \end{aligned}\right\} \tag{9}$$

and

$$P \equiv \partial g / \partial \bar{p},$$

respectively.

The constitutive equations (1) - (7) may be alternatively witten as

$$\left.\begin{aligned} \mathbf{T} &= -\bar{p}\mathbf{1} + 2\mu\mathbf{D}, \\ &\text{where the scalar function} \\ \mu &\equiv \bar{\tau}/\dot{\bar{\gamma}} = \hat{\mu}(\bar{\tau}, \bar{p}, \theta, \bar{\gamma}) \end{aligned}\right\} \tag{10}$$

by analogy to the constitutive equation for a Newtonian fluid, is called the *viscosity* of the viscoplastic solid. However, unlike a Newtonian fluid, this viscosity is not a constant but given by the constitutive equation (10b).

The equation of motion in the absence of body force is

$$\rho \dot{\mathbf{v}} = \mathrm{div}\mathbf{T} \tag{11}$$

and the energy balance equation is

$$\rho c \dot{\theta} \doteq \kappa \triangle \theta + \omega \mathbf{T} \cdot \mathbf{D} \tag{12}$$

Here, ρ is the mass density, c is the specific heat, κ is the thermal conductivity (here assumed to be independent of position), $\triangle\theta$ is the Laplacian of θ and ω, a scalar in the range $0.85 \leq \omega \leq 1$, is the fraction of plastic work that is converted to heat.

2.2 Linear Perturbation Stability Analysis for 3-Dimensions

Let B_t and B_τ denote configurations of a body at times t and $\tau > t$, respectively. The relative motion of the body is characterized by a function

$$\mathbf{p}_t(\mathbf{x}, \tau) \tag{13}$$

which gives the place occupied at time τ by a material particle which at time t occupied the place $\mathbf{x}$. The vector valued functions

$$\begin{aligned} \mathbf{u}_t(\mathbf{x}, \tau) &\equiv \mathbf{p}_t(\mathbf{x}, \tau) - \mathbf{x} \\ \dot{\mathbf{u}}_t(\mathbf{x}, \tau) &\equiv \frac{\partial}{\partial \tau}\mathbf{u}_t(\mathbf{x}, \tau), \\ \ddot{\mathbf{u}}_t(\mathbf{x}, \tau) &\equiv \frac{\partial^2}{\partial \tau^2}\mathbf{u}_t(\mathbf{x}, \tau), \end{aligned} \tag{14}$$

describe the relative displacement, the relative velocity, and the relative acceleration, respectively.

Equation (11) for the balance of linear momentum (in the absence of body forces) at time τ may be expressed as

$$\rho \ddot{\mathbf{u}}_t(\mathbf{x}, \tau) = \mathrm{div}\bar{\mathbf{S}}_t(\mathbf{x}, \tau) \tag{15}$$

where $\bar{\mathbf{S}}_t$ is the relative first Piola Kirchhoff stress tensor which describes the actual forces in the configuration B_τ per unit area of the configuration B_t. It is defined by the relation

$$\bar{\mathbf{S}}_t(\mathbf{x}, \tau) \equiv (\det \mathbf{F}_t(\mathbf{x}, \tau))\mathbf{T}(\mathbf{p}_t(\mathbf{x}, \tau), \tau)\mathbf{F}_t^{-T}(\mathbf{x}, \tau), \tag{16}$$

where $\mathbf{F}_t = \partial \mathbf{p}_t / \partial \mathbf{x}$ is the relative deformation gradient, $(\det \mathbf{F}_t)$ its determinant, $\mathbf{F}_t^{-T}$ the transpose of its inverse. Also, equation (12) for the balance of energy at time τ may be expressed as

$$\rho c\dot{\theta}(\mathbf{x},\tau) \doteq \kappa \triangle \theta(\mathbf{x},\tau) + \omega \bar{\mathbf{S}}_t(\mathbf{x},\tau) \cdot \dot{\mathbf{F}}_t(\mathbf{x},\tau) \tag{17}$$

For the perturbation stability analysis, the body is considered to be homogeneous and homogeneously deformed in its current configuration B_t. If the body is subjected to boundary conditions which could give rise to continued homogeneous deformation, then the field equations together with the appropriate boundary conditions determine the homogeneous solution $[\dot{\mathbf{u}}_t^\circ, \theta^\circ, \bar{\mathbf{S}}_t^\circ]$. Next, we wish to determine that if this homogeneous solution is perturbed so that the configuration B_τ of the body, with $\triangle t = (\tau - t) \to 0$, differs only by infinitesimal displacements of a shear band mode relative to B_t, then can this perturbation grow while the field variables still satisfy the field equations?

Let the normal to the shear band perturbation have an orientation $\mathbf{n}$ in B_t. The homogeneous solution $[\dot{\mathbf{u}}_t^\circ, \theta^\circ, \bar{\mathbf{S}}_t^\circ]$ is assumed to be perturbed by a small fluctuation which varies with $(\mathbf{x} - \mathbf{0}) \cdot \mathbf{n}$, that is, with position across the band. Accordingly, we assume that the relative velocity field can be written as

$$\left.\begin{aligned} &\dot{\mathbf{u}}_t(\mathbf{x},\tau) = \dot{\mathbf{u}}_t^\circ(\mathbf{x},\tau) + \epsilon\tilde{\mathbf{v}}, \quad \epsilon \ll 1, \\ &\text{corresponding to which} \\ &\dot{\mathbf{F}}_t(\mathbf{x},\tau) = \dot{\mathbf{F}}_t^\circ(\tau) + \epsilon \operatorname{grad}\tilde{\mathbf{v}} \end{aligned}\right\} \tag{18}$$

For the perturbation velocity field (18) to be of a form which may lead to shear band formation, it is required that

$$\left.\begin{aligned} &\operatorname{grad}\tilde{\mathbf{v}} = \mathbf{a} \otimes \mathbf{n} \\ &\text{where} \\ &\mathbf{a} = \mathbf{a}((\mathbf{x} - \mathbf{0}) \cdot \mathbf{n}, \triangle t), \\ &\text{is an amplitude vector, and} \end{aligned}\right\} \tag{19}$$

$$\mathbf{a} \cdot \mathbf{n} = 0$$

Further, we assume that the perturbations in the temperature and the stress are:

$$\left.\begin{aligned} &\theta(\mathbf{x}, \tau) = \theta^{\circ}(\tau) + \epsilon\tilde{\theta}, \\ &\text{with} \\ &\tilde{\theta} = \tilde{\theta}((\mathbf{x} - \mathbf{0}) \cdot \mathbf{n}, \triangle t), \end{aligned}\right\} \tag{20}$$

and

$$\left.\begin{aligned} &\bar{\mathbf{S}}_t(\mathbf{x}, \tau) = \bar{\mathbf{S}}_t^{\circ}(\tau) + \epsilon\tilde{\mathbf{T}}, \\ &\text{with} \\ &\tilde{\mathbf{T}} = \tilde{\mathbf{T}}((\mathbf{x} - \mathbf{0}) \cdot \mathbf{n}, \triangle t) \end{aligned}\right\} \tag{21}$$

Substituting from (18)-(21) into (15) and (17) and retaining only the terms of first order in ϵ, we obtain the following differential equations for the perturbed quantities:

$$\rho\dot{\tilde{\mathbf{v}}} = \mathrm{div}\tilde{\mathbf{T}}, \tag{22}$$

and

$$\rho c\dot{\tilde{\theta}} \doteq \kappa \triangle \tilde{\theta} + \omega[\tilde{\mathbf{T}} \cdot \dot{\mathbf{F}}_t^{\circ} + (\mathrm{grad}\tilde{\mathbf{v}}) \cdot \bar{\mathbf{S}}_t^{\circ}] \tag{23}$$

Since $\triangle t = (\tau - t) \to 0$, $\dot{\mathbf{F}}_t^{\circ} \approx \mathbf{L}^{\circ}$ and $\bar{\mathbf{S}}_t^{\circ} \approx \mathbf{T}^{\circ}$. Using this, the symmetry of $\mathbf{T}^{\circ}$, and the near symmetry of $\tilde{\mathbf{T}}$, we obtain

$$[\tilde{\mathbf{T}} \cdot \dot{\mathbf{F}}_t^{\circ} + (\mathrm{grad}\tilde{\mathbf{v}}) \cdot \bar{\mathbf{S}}_t^{\circ}] \doteq [\tilde{\mathbf{T}} \cdot \mathbf{D}^{\circ} + \tilde{\mathbf{D}} \cdot \mathbf{T}^{\circ}].$$

Also, since $\mathbf{T}\cdot\mathbf{D} = \bar{\tau}\dot{\bar{\gamma}}$, the term $[\tilde{\mathbf{T}}\cdot\mathbf{D}^{\circ} + \tilde{\mathbf{D}}\cdot\mathbf{T}^{\circ}]$ can be replaced by $[\tilde{\bar{\tau}}\dot{\bar{\gamma}}^{\circ} + \dot{\tilde{\bar{\gamma}}}\bar{\tau}^{\circ}]$, where $\tilde{\bar{\tau}}$ and $\dot{\tilde{\bar{\gamma}}}$ are the perturbations in the equivalent shear stress and the equivalent shear strain rate, respectively. With this, the energy balance equation (23) may be written as

$$\rho c\dot{\tilde{\theta}} \doteq \kappa \bigtriangledown^2 \tilde{\theta} + \omega[\tilde{\bar{\tau}}\dot{\bar{\gamma}}^{\circ} + \dot{\tilde{\bar{\gamma}}}\bar{\tau}^{\circ}] \tag{24}$$

In order to analyze the stability of the homogeneous solution, the following form of solutions for (22) and (24) is considered.

$$\left.\begin{aligned} &\tilde{\mathbf{v}} = \varphi\mathbf{v}_{\bullet}, \\ &\varphi = \exp\{i\xi(\mathbf{x}-0)\cdot\mathbf{n} + \eta\,\triangle t\} \\ &\mathbf{v}_{\bullet} \equiv \text{constant}, \quad \mathbf{v}_{\bullet}\cdot\mathbf{n} = 0. \end{aligned}\right\} \tag{25}$$

For this assumed form of the perturbation in the velocity

$$\left.\begin{aligned} &\text{grad}\tilde{\mathbf{v}} = \mathbf{a}\otimes\mathbf{n}, \\ &\text{with} \\ &\mathbf{a} = i\xi\tilde{\mathbf{v}}, \quad \mathbf{a}\cdot\mathbf{n} = 0, \end{aligned}\right\} \tag{25}$$

and this satisfies the requirement (19). In parallel, for the perturbations in the temperature and the stress, the following forms are considered.

$$\left.\begin{aligned} &\tilde{\theta} = \varphi\theta_{\bullet}, \quad \theta_{\bullet} \equiv \text{constant} \\ &\text{and} \\ &\tilde{\mathbf{T}} = \varphi\mathbf{T}_{\bullet}, \quad \mathbf{T}_{\bullet} \equiv \text{constant}. \end{aligned}\right\}$$

Here ξ is the reciprocal of the wavelength of the periodic perturbation in the direction normal to the shear band and is called the wave number. If a solution in the form of equations (25) exists with η real and positive, then the perturbation *may* grow with time and a shear band type instability is possible. However, if η is real and negative, then the perturbed solution is likely to decay with increasing time and the homogeneous solution is considered stable.

Since $\dot{\gamma}^2 = 2\mathbf{D}\cdot\mathbf{D}$, the perturbation $\tilde{\dot{\gamma}}$ can be written as

$$\left.\begin{aligned} &\tilde{\dot{\gamma}} = \varphi\dot{\gamma}_*, \\ &\text{where} \\ &\dot{\gamma}_* = (i\xi)\mathbf{g}\cdot\mathbf{v}_*, \\ &\text{with} \\ &\mathbf{g} = (2/\dot{\gamma}^\circ)\mathbf{D}^\circ\mathbf{n}. \end{aligned}\right\} \tag{26}$$

Also, since $(1/\eta)$ has dimensions of time, the perturbation $\tilde{\gamma}$ in the equivalent shear strain can be estimated by

$$\tilde{\gamma} \doteq \tilde{\dot{\gamma}}/\eta = \varphi(\dot{\gamma}_*/\eta). \tag{27}$$

Further, from the constitutive equations, the perturbation $\tilde{\tau}$ in the equivalent shear stress is

$$\tilde{\tau} = \varphi\tau_* \tag{28}$$

with

$$\tau_* = (R^\circ + S^\circ/\eta)\dot{\gamma}_* - T^\circ\theta_* + P^\circ p_*$$

where $R^\circ, S^\circ, T^\circ$ and P° are the values of the rates of strain-rate hardening, strain hardening, thermal softening and pressure hardening, respectively, evaluated at the homogeneous solution at time t. It is important to note that these are time varying quantities. Also, in writing (28), it has been assumed that the perturbation in the mean normal pressure $\bar{p}$ can be written as

$$\tilde{\bar{p}} = \varphi p_*. \tag{29}$$

Next, from the constitutive equations and equations (25)-(29), it follows that

$$\left.\begin{aligned} \mathbf{T}_* = &\left[\{R^\circ + S^\circ/\eta\}\dot{\bar{\gamma}}_*\bar{\mathbf{D}}^\circ + (\bar{\tau}^\circ/\dot{\bar{\gamma}}^\circ)\{(i\xi)(\mathbf{v}_* \otimes \mathbf{n} + \mathbf{n} \otimes \mathbf{v}_*) - \dot{\bar{\gamma}}_*\bar{\mathbf{D}}^\circ\}\right] \\ &-\{T^\circ\bar{\mathbf{D}}^\circ\}\theta_* + \{P^\circ\bar{\mathbf{D}}^\circ - \mathbf{1}\}p_*, \\ &\\ &\text{where} \\ &\\ \bar{\mathbf{D}}^\circ = &(2\mathbf{D}^\circ/\dot{\bar{\gamma}}^\circ) \end{aligned}\right\} \tag{30}$$

Finally, upon substituting (25) in (22) and (24), and upon further substitution from (26), (28) and (30) for $\dot{\bar{\gamma}}_*, \bar{\tau}_*$ and $\mathbf{T}_*$, we obtain

$$\begin{aligned} &\left[\xi^2\left\{(R^\circ + S^\circ/\eta)\mathbf{g}\otimes\mathbf{g} + (\bar{\tau}^\circ/\dot{\bar{\gamma}}^\circ)(\mathbf{1} - \mathbf{g}\otimes\mathbf{g})\right\} + \rho\eta\mathbf{1}\right]\mathbf{v}_* \\ &+ [(i\xi)(T^\circ\mathbf{g})]\,\theta_* + [(i\xi)(\mathbf{n} - P^\circ\mathbf{g})]\,p_* = 0 \end{aligned} \tag{31}$$

and

$$\begin{aligned} &\left[(i\xi)\left\{(R^\circ + S^\circ/\eta)\dot{\bar{\gamma}}^\circ + \bar{\tau}^\circ\right\}\mathbf{g}\right]\cdot\mathbf{v}_* \\ &+ \left[-(\frac{\rho c}{\omega}\eta + \frac{\kappa}{\omega}\xi^2 + T^\circ\dot{\bar{\gamma}}^\circ)\right]\theta_* + \left[P^\circ\dot{\bar{\gamma}}^\circ\right]p_* = 0 \end{aligned} \tag{32}$$

Equations (31) and (32), together with the kinematic constraint on the direction of velocity perturbation vector

$$\mathbf{v}_* \cdot \mathbf{n} = 0 \tag{33}$$

constitute the basic equations of the current perturbation analysis.

Let

$$\mathbf{D}^\circ = \sum_{i=1}^{3} \alpha_i \hat{\mathbf{e}}_i \otimes \hat{\mathbf{e}}_i, \tag{34}$$

denote a spectral representation of the homogeneous stretching. Here $\{\hat{\mathbf{e}}_i\}$ are the eigenvectors and $\{\alpha_i\}$ are the eigenvalues of $\mathbf{D}^\circ$. For the current constitutive model $\{\hat{\mathbf{e}}_i\}$ are also the principal directions of the stress $\mathbf{T}^\circ$. Next, let $\{v_{*i}\}$ denote the components of $\mathbf{v}_*$ relative to the basis $\{\hat{\mathbf{e}}_i\}$. Then the component form of system of equations (31) - (33), with respect to the basis $\{\hat{\mathbf{e}}_i\}$ may be written in the following form

$$\mathbf{A}\mathbf{y} = \mathbf{0} \tag{35}$$

where the solution vector is

$$\mathbf{y} = [v_{*1}, v_{*2}, v_{*3}, \theta_*, p_*]^T, \tag{36}$$

and the entries of the coefficient matrix $\mathbf{A}$ are given in Appendix A. For non-trivial $\mathbf{y}$, equation (35) implies that

$$\det \mathbf{A} = 0. \tag{37}$$

Equation (37) will yield a characteristic polynomial for η. If for a given state and a given wave number ξ this characteristic polynomial has real positive roots for η, then the perturbation may grow and a shear band instability is possible. The direction of the emergent shear band will be characterized by that η for which η has maximum real positive root.

In the next section, attention will be focused on plane motions and two important special cases of the resulting characteristic stability equation will be discussed.

2.3 Initiation of Localized Shear Bands in Plane Motions

For plane motions, $v_3 = 0$, and the homogeneous stretching tensor $\mathbf{D}^\circ$ can be put in the spectral form

$$\mathbf{D}^\circ = \alpha \hat{\mathbf{e}}_1 \otimes \hat{\mathbf{e}}_1 + (-\alpha)\hat{\mathbf{e}}_2 \otimes \hat{\mathbf{e}}_2, \quad \alpha > 0. \tag{38}$$

Since $\dot{\bar{\gamma}}^\circ = \sqrt{2\mathbf{D}^\circ \cdot \mathbf{D}^\circ}$, from (38), we obtain

$$\dot{\bar{\gamma}}^\circ = 2\alpha. \tag{39}$$

It will be assumed that the trace of the shear band lies in the plane of the motion, that is,

$$n_3 = 0 \tag{40}$$

Then, for plane motion, equation (35) reduces to

$$\mathbf{B}\mathbf{z} = \mathbf{0}, \tag{41}$$

where the solution vector is

$$\mathbf{z} = [v_{*1}, v_{*2}, \theta_*, p_*]^T, \tag{42}$$

and the entries of the coefficient matrix $\mathbf{B}$ are given in Appendix B.

For non-trivial $\mathbf{z}$, equation (41) implies that

$$\det \mathbf{B} = 0. \tag{43}$$

Upon evaluating this determinant, the following cubic equation for η is obtained :

$$
\left.
\begin{aligned}
& C_0\eta^3 + C_1\eta^2 + C_2\eta + C_3 = 0 \\
& \text{where} \\
& C_0 = (\rho^2 c)(1 + \chi_2 P^\circ) \\
& C_1 = \rho[\omega T^\circ \dot{\bar{\gamma}}^\circ + \{(1 + \chi_2 P^\circ)\kappa + \chi_1 c R^\circ + c(\bar{\tau}^\circ/\dot{\bar{\gamma}}^\circ)(1 - \chi_1 + \chi_2 P^\circ)\}\xi^2] \\
& C_2 = [\chi_1 \kappa R^\circ + \kappa(\bar{\tau}^\circ/\dot{\bar{\gamma}}^\circ)(1 - \chi_1 + \chi_2 P^\circ)]\xi^4 + [\chi_1 \rho c S^\circ - \omega \bar{\tau}^\circ T^\circ(2\chi_1 - 1)]\xi^2, \\
& C_3 = \chi_1 \kappa S^\circ \xi^4, \\
& \text{with} \\
& \chi_1 = \sin^2 2\chi \equiv 4n_1^2 n_2^2 \\
& \text{and} \\
& \chi_2 = \cos 2\chi \equiv n_2^2 - n_1^2
\end{aligned}
\right\} \quad (44)
$$

Here, χ stands for the inclination of the trace of the shear band relative to the maximum principal stretching (stress) axis $\hat{\mathbf{e}}_1$.

Equation (44) is the central equation for the problem[2]. If for a given state, a wave number ξ and an orientation χ, this cubic equation for η has real positive roots, then the periodic perturbation may grow and a shear band instability is possible.

It is important to note that whether or not such an instability *develops* when η is positive cannot be determined from this linear perturbation analysis because the

[2]It is noted here that if pressure sensitivity is neglected, i.e. $P = 0$, and if we assume a priori that shear bands form at angles $\chi = \pm\pi/4$ with respect to maximum principal stress direction, then equation (44) reduces to equation (3.10) in Bai's 1982 paper.

value of η is time-dependent since it is a root of the polynomial equation (44) whose coefficients C_0 through C_3 (which characterize the state of the material when the perturbation is introduced) are time-dependent. However, since these coefficients may be considered to be approximately constant during a short interval of time, the positive root η of this equation does give information about the incipient rate of growth of the localized mode. The linear perturbation theory can give information about the time for growth of the localized mode only under conditions in which it may be assumed that the perturbation grows on a time scale that is short relative to the variation of the coefficients in the characteristic stability equation; however, as mentioned previously, such an approach always underestimates the time for instability to develop (cf. e.g., Clifton et al. (1984), Fressengeas and Molinari (1985)).

In the following sub-sections, attention will be confined to the class of materials for which

$$R > 0, \quad -\infty < S < \infty, \quad T > 0, \quad 0 \leq P < 1; \tag{45}$$

that is , attention will be restricted to the materials which exhibit positive strain-rate hardening, strain hardening or strain softening, thermal softening, and which are either pressure insensitive or exhibit some pressure hardening.

2.3.1 Quasi-Static, Isothermal Deformations

This limit is obtained by neglecting the inertial term on the left hand side of the equation of motion (11), neglecting the energy balance equation (12), and assuming that the partial derivative T defined in (9) (corresponding to thermal softening) is zero-valued. With respect to the stability equation (44), this corresponds to neglecting all coefficients containing the mass density ρ, and letting the thermal conductivity κ become infinite. In this case, the characteristic equation reduces to

$$[\chi_1 R^\circ + (\bar{\tau}^\circ/\dot{\bar{\gamma}}^\circ)(1 - \chi_1 + \chi_2 P^\circ)]\eta + \chi_1 S^\circ = 0$$

from which, the only possible root for η is

$$\left.\begin{aligned} \eta &= \frac{-S^\circ}{\{R^\circ + \mu^\circ f_1(\chi, P^\circ)\}} \\ \text{where} \quad & \\ \mu^\circ &\equiv (\bar{\tau}^\circ/\dot{\bar{\gamma}}^\circ) > 0 \\ \text{and} \quad & \\ f_1(\chi, P^\circ) &= \{1 + P^\circ \sec(2\chi)\}\cot^2(2\chi) \end{aligned}\right\} \qquad (46)$$

It is noted here that this expression for η is independent of the wave number ξ of the perturbation.

2.3.1a Pressure-Insensitive Materials($P = 0$)

Here, equation (46) reduces to

$$\eta = \frac{-S^\circ}{\{R^\circ + \mu^\circ \cot^2(2\chi)\}}. \tag{47}$$

Since the denominator in (47) is always positive valued for $\chi \in \pm(0, \pi/2)$, a growing mode can exist only if

$$S^\circ < 0,$$

that is, if the material exhibits strain-softening. For a short period of time after S° becomes negative, η is positive and it may then be thought to represent the incipient rate of growth of the localized mode.

The angles χ which give the largest incipient rate of growth are

$$\chi_{cr} = \pm\pi/4, \tag{48}$$

and this maximum rate

$$\eta_{max} = -S^\circ/R^\circ \tag{49}$$

That is, the fastest growth rate is inversely proportional to the strain-rate sensitivity and directly proportional to the extent to which the localization is past the onset of instability. It is apparent from this expression that a weak strain rate sensitivity (i.e., small R°) promotes faster growth rates.

2.3.1b Pressure-Sensitive Materials($0 < P < 1$)

From (46), two conditions under which perturbations can grow are identified.

Case 1

If

$$R^\circ > -\mu^\circ f_1(\chi, P^\circ) \tag{50}$$

for a given $(R^\circ, P^\circ, \mu^\circ)$ and all possible orientations $\chi \in \pm(0, \pi/2)$, then for a growing mode to exist, it is necessary that

$$S^\circ < 0; \tag{51}$$

that is, for a shear band instability to be possible the material must exhibit strain softening.

In this case the most probable orientations of the shear bands are given by those χ for which $\{R^\circ + \mu^\circ f_1(\chi, P^\circ)\}$ has the least positive value. This occurs for

$$\left.\begin{aligned} \chi_{cr} &= \pm[(\pi/4) + (\beta/2)] \\ \text{with} \\ \beta &= \sin^{-1}\left[(1/P^\circ)(1 - \sqrt{1 - P^{\circ 2}})\right] \end{aligned}\right\} \tag{52}$$

For $0 < P^\circ \ll 1$, that is for only slightly pressure sensitive materials, (52) reduces to

$$\chi_{cr} = \pm[(\pi/4) + (P^\circ/4)] \tag{53}$$

and the corresponding maximum value of η is

$$\eta_{max} = [-S^\circ]/\left[R^\circ - \frac{\mu^\circ (P^\circ/2)^2}{[1 - (P^\circ/2)^2]}\right] \tag{54}$$

from which it is clear that for strain softening materials a slight pressure sensitivity accelerates the growth rate.

Case 2

If

$$R^\circ < -\mu^\circ f_1(\chi, P^\circ) \tag{55}$$

for a given $(R^\circ, P^\circ, \mu^\circ)$ and some orientation $\chi \in \pm(0, \pi/2)$, then instability is possible with $S^\circ > 0$. Let

$$f_2(\chi, P^\circ) \equiv \sin^2(2\chi) f_1(\chi, P^\circ) = \cos(2\chi)[\cos(2\chi) + P^\circ]. \tag{56}$$

The behavior of the function f_2 with respect to χ at a fixed P° is sketched in Fig. 1. Since attention has been confined to materials which exhibit a positive strain rate sensitivity, i.e., $R^\circ > 0$, it is seen that the instability condition can be satisfied for a sufficiently large P° and some $\chi \in \pm((\pi/4), (\pi/4 + P^\circ/2))$. From Fig. 1, for a given P°, the maximum negative value of f_2 is

$$f_2^* = -(P^\circ/2)^2 \tag{57}$$

and it occurs at

$$\chi^* = \pm[(\pi/4) + (P^\circ/4)]$$

In this case

$$\eta = [S^\circ] / \left[-\left\{ R^\circ + \frac{\mu^\circ}{\sin^2(2\chi)} f_2(\chi, P^\circ) \right\} \right], \tag{58}$$

and the most probable orientations of the shear bands are given by those χ for which

$$R^\circ + \frac{\mu^\circ}{\sin^2(2\chi)} f_2(\chi, P^\circ)$$

has the least negative value.

In the limit $R^\circ \to 0$, that is for nearly rate-independent materials, extremely fast finite rates of incipient growth are attained in the directions

$$\left.\begin{aligned} &\chi_{cr}^{(1)} = \pm[(\pi/4) + \delta] \\ &\text{or} \\ &\chi_{cr}^{(2)} = \pm[(\pi/4) + (P^\circ/2) - \delta] \\ &\text{with} \\ &\delta \ll 1.0 \end{aligned}\right\} \tag{59}$$

For R° finite, there are a pair of critical orientations which depend on the precise values of $(R^\circ, P^\circ, \mu^\circ)$. In any event, these critical orientations are bound from below by $(\pi/4)$, and from above by $[(\pi/4) + (P^\circ/2)]$.

2.3.2 Dynamic, Adiabatic Deformations

This limiting case is obtained by setting the thermal conductivity κ to zero in the characteristic equation (44). In this limit, the characteristic equation for η reduces to the following quadratic equation:

$$C_0\eta^2 + C_1\eta + C_2 = 0, \tag{60}$$

where

$$C_0 = \rho^2 c(1 + \chi_2 P^\circ)$$

$$C_1 = \rho\omega T^\circ \dot{\bar{\gamma}}^\circ + \rho c\xi^2[R^\circ\chi_1 + \mu^\circ(1 - \chi_1 + \chi_2 P^\circ)] \tag{61}$$

$$C_2 = H\xi^2$$

and

$$H(\chi) \equiv \rho c S^\circ \chi_1 - \omega\bar{\tau}^\circ T^\circ(2\chi_1 - 1) \tag{62}$$

The roots of the quadratic equation (60) are:

$$\eta_\pm = \frac{C_1}{2C_0}\left[-1 \pm \sqrt{1 - \frac{4C_0C_2}{C_1^2}}\right] \tag{63}$$

In what follows, we limit our attention to strain-hardening materials, $S^\circ > 0$, and treat pressure-insensitive materials separately from pressure-sensitive materials.

2.3.2a Pressure Insensitive Materials($P = 0$)

In this case, $C_0 > 0$ and $C_1 > 0$. Thus, for η to have a positive root, it is required that C_2, and hence the function $H(\chi)$, must be negative. The behavior of the function $H(\chi)$ is sketched in Fig. 2a, from which it is clear that the necessary condition for $H(\chi)$ to be negative is that $\rho c S^\circ < \omega \bar{\tau}^\circ T^\circ$, and this condition for instability may be written as

$$H_a^\circ \equiv (S^\circ - \Theta^\circ) < 0 \tag{64}$$

where

$$\Theta^\circ \equiv (\omega \bar{\tau}^\circ / \rho c) T^\circ \tag{65}$$

is an *effective rate of thermal softening.* The quantity H_a° is interpreted as a measure of the slope of the shear stress-strain curve at a constant shear strain rate under adiabatic conditions. Its value depends on the interaction between strain hardening and thermal softening.

It is important to note that the critical condition (64) is independent of the wave number ξ of the initial inhomogeneity and the strain rate sensitivity R of the material.

Although the critical condition (64) for instability is independent of ξ and R, the incipient rate of growth of the inhomogeneity depends on these quantities[3]. An indication of the form of this dependence can be obtained by observing that for small negative values of C_2, that is for conditions slightly beyond the onset of instability, the eigenvalue $\eta_+ \doteq -C_2/C_1$ is given by

$$\eta \doteq \frac{-H(\chi)}{\{\rho \omega T^\circ \dot{\bar{\gamma}}^\circ / \xi^2\} + \rho c [R^\circ \chi_1 + \mu^\circ (1 - \chi_1)]} \tag{66}$$

[3]Recall that the incipient rate of growth of the inhomogeneities in the case of quasi-static, isothermal deformations did not depend on the wave number.

Since η_+ increases with increasing wave number, the perturbation with the largest wave number is predicted to grow at the highest rate. Thus, as $\xi \to \infty$,

$$\eta_+ \to \frac{-H(\chi)}{\rho c[R^\circ \chi_1 + \mu^\circ(1-\chi_1)]} \tag{67}$$

The orientation dependent function in the denominator of (67) is sketched in Fig. 2b. Examining Figs. 2a and 2b, it is concluded that η_+ has its maximum value for an orientation χ^* in the ranges (χ_a, χ_b) and $(-\chi_a, -\chi_b)$ where

$$\left.\begin{aligned} \chi_a &= \frac{1}{2}\sin^{-1}\left(\frac{B}{2B-A}\right)^{1/2} \\ \chi_b &= \frac{\pi}{2} - \chi_a \end{aligned}\right\} \tag{68}$$

with

$$A = \rho c S^\circ$$

and

$$B = \omega \bar{\tau}^\circ T^\circ$$

.

Further, if $\mu^\circ > R^\circ$, then η_+ has an absolute maximum

$$\eta_+|_{max} = \frac{-H_a^\circ}{R^\circ}, \tag{69}$$

for

$$\chi_{cr} = \pm\frac{\pi}{4}$$

.

The considerations of this section clearly show the interplay between the stabilizing effect of strain hardening and the destabilizing effect of thermal softening. High

strength metallic materials generally exhibit relatively low strain hardening so the resistance to adiabatic shear localization in these materials is low. Note from (65) that the effective rate of thermal softening Θ increases with increasing flow stress $\bar{\tau}$ and decreasing density ρ. Also, the flow stress $\bar{\tau}$ increases, the specific heat decreases, and the thermal softening T is enhanced as the temperature decreases. Thus high strength materials which exhibit a low rate of strain and strain-rate hardening are very susceptible to adiabatic shear localization at low temperatures.

2.3.2b Pressure Sensitive Materials($0 < P < 1$)

From (60) - (63), two conditions under which perturbations can grow are identified:

Case 1

If $C_1 > 0$, i.e., if (with f_2 defined in equation (56))

$$\frac{\omega T^\circ \dot{\bar{\gamma}}^\circ}{c\xi^2} + R^\circ \xi > -\mu^\circ f_2(\chi, P^\circ), \tag{70}$$

for a given state and all possible orientations $\chi \in \pm(0, \pi/2)$, then, for a growing mode to exist, it is again necessary to satisfy the instability condition (64). The direction of the fastest growing modes are still in the ranges (χ_a, χ_b) and $(-\chi_a, -\chi_b)$ and are determined by requiring that $\eta_+(P^\circ \neq 0)$ attain the maximum positive value.

Case 2

If $C_1 < 0$, i.e., if

$$\frac{\omega T^\circ \dot{\bar{\gamma}}^\circ}{c\xi^2} + R^\circ \xi < -\mu^\circ f_2(\chi, P^\circ) \tag{71}$$

for a given P° and some $\chi \in \pm(0, \pi/2)$, then a growing mode exists even if $H_a^\circ > 0$.

Clearly, as $R^\circ \to 0$ smaller amounts of pressure sensitivity are necessary to satisfy (71). The orientation of the fastest growing mode is the one that gives the maximum η_+ for given values of $(R^\circ, S^\circ, T^\circ, P^\circ, \mu^\circ, \dot{\bar{\gamma}}^\circ, \xi)$. This orientation is not necessarily $\pm\pi/4$.

2.4 Discussion

In previous analyses of the onset of shear localization in viscoplastic materials, the problem of localization in simple shear has been the prototypical problem that has been considered(e.g., Clifton (1980), Bai (1982)). A common starting point for these analyses is the assumption that the deformation can localize only in one narrow band which is parallel to the direction of shear. However, simple shearing is a special plane motion and the current analysis for the onset of shear instability predicts that even in simple shear, shear bands can initiate in two directions. This will be briefly discussed in what follows and some experimental evidence in support of the current theoretical predictions will be presented.

In simple shearing motion the velocity $\mathbf{v}$ is given by

$$\mathbf{v} = 2\alpha(\mathbf{e}_1 \otimes \mathbf{e}_2)(\mathbf{x} - \mathbf{0}),$$

where α is a positive constant and $\mathbf{e}_1$ and $\mathbf{e}_2$ are orthogonal unit vectors. The stretching tensor corresponding to this velocity is

$$\mathbf{D} = \alpha(\hat{\mathbf{e}}_1 \otimes \hat{\mathbf{e}}_2 + \hat{\mathbf{e}}_2 \otimes \hat{\mathbf{e}}_1),$$

where

$$\hat{\mathbf{e}}_1 = (1/\sqrt{2})(\mathbf{e}_1 + \mathbf{e}_2)$$

and

$$\hat{\mathbf{e}}_2 = (1/\sqrt{2})(\mathbf{e}_1 - \mathbf{e}_2)$$

are the principal directions of stretching. According our analysis for quasi-static, isothermal deformations, shear bands are expected to form at angles

$$\chi = \pm[(\pi/4) + (\beta/2)],$$

with

$$\beta = \sin^{-1}\left[(1/P^{\circ})(1 - \sqrt{1 - P^{\circ}})\right]$$

For $P^{\circ} \ll 1$, $\beta \doteq P^{\circ}/2$ and as P° approaches zero, so does the angle β. Thus, for pressure insensitive materials, the traces of the shear bands are expected to coincide with the shear direction $\mathbf{e}_1$, and the direction $\mathbf{e}_2$ which is perpendicular to the shearing planes. For pressure sensitive materials, they are predicted to form at angles larger than $\pm(\pi/4)$ from the $\hat{\mathbf{e}}_1$ - direction, see Fig. 3. In Fig. 4, a micrograph of shear bands observed in a simple shear test conducted on the polymer polycarbonate at a shear strain rate of $10^{-3}/sec$ is shown. The shear bands were found to initiate just before the peak in the shear stress-strain curve. Note that, as predicted by the analysis, there are *two* sets of shear bands. Further, since plastic deformation in polycarbonate is pressure sensitive, the shear bands form at orientations which are qualitatively similar to those sketched in Fig. 3. Thus, the analysis clearly indicates, and the experiments show that shear bands can initiate in two directions even in simple shear. This is contrary to the common perturbation analysis assumption that in simple shear a shear band is initiated only in the direction of shear.

In summary, for materials whose rate-dependent plastic deformation behavior can be modeled by the simple phenomenological constitutive model of section 2, a linear perturbation stability analysis for the onset of formation of shear bands has been presented. The predictions of this analysis have been explored for the important limiting cases of (1) plane quasi-static, isothermal deformations and (2) plane dynamic, adiabatic deformations. The predictions of (a) the critical conditions for the formation of shear bands, (b) the direction of emergent shear bands, and (c) the incipient rate of

growth of these bands for these cases are qualitatively correct and intuitively satisfying. For the more general problems of localization of dynamic deformations in which heat conduction effects cannot be neglected, the predictions of the stability equations (44) and (37) remains to be explored.

Chapter 3

Integral Criterion for Adiabatic Flow Localization

3.1 Background

For the present discussion we note that an analysis of the stability of two-dimensional plane homogeneous deformations has been presented in chapter 2. In the previous analysis we assumed isotropy, neglected elasticity and used a flow rule for the (plastic) stretching in which the direction of viscoplastic flow is in the direction of the deviator $\mathbf{T}'$ of the Cauchy stress $\mathbf{T}$, while the magnitude of plastic flow is proportional to an equivalent plastic strain rate $\dot{\bar{\gamma}}^p$ which is constitutively defined by a function $\dot{\bar{\gamma}}^p = f(\bar{\tau}, \bar{\gamma}^p, \theta)$ with the neglect of pressure sensitivity. Here $\bar{\tau} \equiv \sqrt{(1/2)\mathbf{T}' \cdot \mathbf{T}'}$ is the equivalent shear stress; $\bar{\gamma}^p$, the time integral of $\dot{\bar{\gamma}}^p$, is the equivalent plastic shear strain; and θ is the absolute temperature. It has been assumed that the strain rate function f is invertible such that one can write

$$\bar{\tau} = g(\bar{\gamma}^p, \dot{\bar{\gamma}}^p, \theta). \tag{72}$$

Corresponding to (72), the partial derivatives

$$S \equiv \partial g / \partial \bar{\gamma}^p, \tag{73}$$

$$R \equiv \partial g / \partial \dot{\bar{\gamma}}^p, \tag{74}$$

$$T \equiv -\partial g / \partial \theta, \tag{75}$$

denote the rates of strain hardening, strain-rate hardening and thermal softening, respectively. Further, for adiabatic deformations we take the energy balance equation to be

$$\dot{\theta} \approx (\omega / \rho c)\, \bar{\tau} \dot{\bar{\gamma}}^p, \tag{76}$$

where ρ, c, and $\omega(\approx 0.9)$ are the mass density, specific heat, and the fraction of plastic work converted to heat. Confining attention to materials for which $S > 0$, $R > 0$ and $T > 0$, we have found that for dynamic (i.e., inclusion of inertial effects), adiabatic (i.e., neglect of heat conduction) deformations:

1. The *necessary condition* for the *initiation* of shear bands is

$$\left[S - \left(\frac{\omega \bar{\tau}}{\rho c}\right) T\right] < 0. \tag{77}$$

2. The maximum incipient rate of growth is for shear band perturbations at angles

$$\chi = \pm \pi/4 \tag{78}$$

relative to the maximum principal stress direction. Accordingly, the emergent shear bands are expected to form at orientations given by (78).

3. The *incipient rate of growth* of the *emergent* shear bands is given by (-P), where

$$P \equiv \left[\frac{S - (\omega \bar{\tau}/\rho c) T}{R}\right]. \tag{79}$$

These results clearly bring out the interactions of various material characteristics on adiabatic shear localization. They show the important interplay between the stabilizing effect of strain hardening and the destabilizing effect of thermal softening. High strength metallic materials generally exhibit relatively low strain hardening so that the resistance to adiabatic shear localization in these materials is low. Note that the effects of thermal softening increase with increasing flow stress $\bar{\tau}$ and decreasing density ρ. Also, the flow stress $\bar{\tau}$ increases, the specific heat c decreases, and the thermal softening T is enhanced as the temperature decreases. Thus, high strength materials which exhibit a low rate of strain hardening are very susceptible to adiabatic shear

localization at low temperatures. Note also that the incipient rate of growth of the shear band is inversely proportional to the rate of strain-rate hardening R. Thus a weak strain rate sensitivity, that is a small value of R, promotes faster growth rates.

An inherent limitation of this (and all other) linear perturbation analyses is that it provides only (a) the *necessary* conditions for the *initiation* of shear bands, and (b) the *orientations* and the *incipient rate of growth* of the *emergent* shear bands. It does not provide any information regarding the more interesting stages of localization when the strain, strain rate, and temperature in the shear bands becomes much larger than elsewhere. To predict the beginning stage of *significant* flow localization with any reasonable accuracy, except perhaps for materials with a very low strain-rate sensitivity, it seems necessary to devise a new criterion. To this end, in what follows we attempt to formulate a simple new criterion for significant adiabatic flow localization in viscoplastic solids.

3.2 Localization Criterion

Here we do not neglect elasticity and thermal expansion effects, and we take the rate constitutive equation for the stress to be given by

$$\mathbf{T}^{\nabla} = \mathcal{L}[\mathbf{D} - \mathbf{D}^{p}] - \mathbf{\Pi}\dot{\theta}$$

where with $\mathbf{W}$ denoting the spin tensor,

$$\mathbf{T}^{\nabla} \equiv \dot{\mathbf{T}} - \mathbf{W}\mathbf{T} + \mathbf{T}\mathbf{W},$$

is the Jaumann derivative of the Cauchy stress; with μ and κ the elastic shear and bulk moduli and $\mathcal{I}$ and $\mathbf{I}$ the fourth and second order identity tensors,

$$\mathcal{L} \equiv 2\,\mu\mathcal{I} + (\kappa - (2/3)\,\mu)\mathbf{1} \otimes \mathbf{1}$$

is the fourth order isotropic elasticity tensor; with α the coefficient of thermal expansion,

$$\mathbf{\Pi} \equiv 3\kappa\alpha\mathbf{1}$$

is the second order isotropic stress-temperature tensor; $\mathbf{D}$ is the streching tensor, and the flow rule is taken as

$$\mathbf{D}^{p} = \dot{\bar{\gamma}}^{p}(\mathbf{T}'/2\bar{\tau}),$$

where $\mathbf{T}'$ is the deviatoric part of Cauchy stress tensor $\mathbf{T}$, $\bar{\tau}$ is the equivalent shear stress, and

$$\dot{\bar{\gamma}}^{p} = f(\bar{\tau}, \bar{\gamma}^{p}, \theta)$$

is the equivalent plastic shear strain-rate. As before, it is assumed that the strain-rate function f can be inverted to give $\bar{\tau}$ in terms of $\bar{\gamma}^{p}$, $\dot{\bar{\gamma}}^{p}$ and θ; see equation (72).

Differentiation of (72) with respect to time gives

$$\dot{\bar{\tau}} = S\,\dot{\bar{\gamma}}^p + R\,\frac{d}{dt}(\dot{\bar{\gamma}}^p) - T\,\dot{\theta}, \tag{80}$$

where S, R and T are the rates of strain hardening, strain-rate hardening and thermal softening defined in equations (73)–(75). For adiabatic deformations the energy balance equation is given by (76). Substituting for $\dot{\theta}$ from (76) into (80) and rearranging, one obtains

$$\frac{d}{dt}(\dot{\bar{\gamma}}^p) + P\dot{\bar{\gamma}}^p = Q, \tag{81}$$

where P is defined in (79) and $Q \equiv (\dot{\bar{\tau}}/R)$. This equation was first derived by Shawki [1986] who points out that it may be viewed "locally" as a nonlinear ordinary differential equation for $\dot{\bar{\gamma}}^p$. This equation has the (implicit) "solution":

$$\dot{\bar{\gamma}}^p = \dot{\bar{\gamma}}_i^p \exp(\lambda)\left[1 + \left(\dot{\bar{\gamma}}_i^p\right)^{-1} \int_{t_i}^{t} Q \exp(-\lambda) dt\right], \tag{82}$$

where $\dot{\bar{\gamma}}_i^p$ is the value of $\dot{\bar{\gamma}}^p$ at some initial time t_i, and

$$\lambda \equiv \int_{t_i}^{t} (-P)\, dt = \int_{t_i}^{t} \left[-\left\{\frac{S - (\omega\,\bar{\tau}/\rho\,c)\,T}{R}\right\}\right] dt. \tag{83}$$

Note that equations (82) and (83) hold for *arbitrary* three-dimensional adiabatic deformations of bodies obeying the generic form of the constitutive equations assumed here.

For $S > 0$, $R > 0$, $T > 0$, the linear perturbation stability analysis gave the result that in homogeneous plane adiabatic motions shear band instability becomes *possible* when the parameter P becomes negative. Semiatin et al. [1984] have previously deduced a "flow localization parameter" α (see their equation (15) in ref. 16) which is proportional to the flow softening rate and inversely proportional to the strain rate sensitivity. From their numerous studies they have concluded that *noticeable localization*

usually does not occur until $\alpha \approx 5$. If we interpret[4] their α as $(-P/\dot{\bar{\gamma}}^p)$, then a possible criterion for noticeable flow localization is that P should be "sufficiently negative". Such a criterion has also been suggested by Shawki [1986] who uses G (see his equation (2.172)) to denote the parameter that we have here called P.

Semiatin and Jonas [1984, p. 75] remark, "the α parameter provides an insight into the tendency to form shear bands as well as the likely degree of localization or severity of shear banding. Although the $\alpha = 5$ criterion is principally a rule of thumb, process modeling using finite element methods has confirmed the usefulness of this parameter." A few pages later (p. 84) they remark, "Another feature illustrated by the process simulation results is the fact that flow localization is a process not an event. Strain and strain-rate concentrations do not occur instantaneously. For this reason, flow localization cannot be expected to appear fully developed when α reaches some critical value (such as 5) at some point in the flow field."

Based on these remarks, and as is clearly suggested by equations (82) and (83), we note that the occurrence of a large value of the equivalent plastic shear strain-rate *at a material point* depends not only on the instantaneous sign of P or an instantaneous negative value of P, but on the sign and value of the integrated history λ of $-P$. Inspection of equation (82) reveals that in general there is a complicated interaction between the term $\exp(\lambda)$ and the term in the square brackets. However, it can be argued that the term in the square bracket of the equation (82) is bounded between the numbers one and zero such that the dominant term which contributes to the high value of the equivalent plastic shear strain-rate is $\exp(\lambda)$ (See Appendix C). Thus a simple criterion ("rule of thumb") for the localization of plastic deformation is

[4]The considerations of Semiatin, Jonas and co-workers are tied very closely to a particular power-law type constitutive equation for the shear stress.

$$\lambda > \lambda_c. \tag{84}$$

The satisfaction of this criterion at a material point should indicate that the equivalent plastic shear strain-rate at that point is very high.

To make this criterion specific we need to specify the lower limit of integration t_i in equations (82) and (83), and specify the value of λ_c in (84). Two possible choices for t_i are:

1. $t_i = 0$.

2. t_i = the time when P first changes sign from positive to negative.

Recall that as long as P is positive the linear perturbation analysis predicts that the material is stable and the necessary condition for the formation of shear bands is not satisfied. Thus for materials which exhibit some strain hardening, if choice 1 is made then λ is accumulating a negative contribution[5] until such time as P turns negative. Since, as graphically commented by R. J. Clifton[6], "You can't put stability in the bank!", this choice for the lower limit of integration is not attractive, and the choice for t_i to be preferred is the time when P first changes sign from positive to negative. In this case λ is always positive, and λ_c has to be "sufficiently positive". As with the α-criterion of Semiatin, Jonas and co-workers, there does not appear to be a rigorous way to precisely specify the value of λ_c. However, it should be possible to "calibrate" the value of λ_c by performing full non-linear finite-element analyses of representative numerical experiments such as plane-strain tension and compression, and axi-symmetric tension and compression for different constitutive functions.

[5]For materials which show no strain hardening λ is always positive.

[6]Private communication with Anand.

Localization of deformation into a region (band-like or otherwise) is an initiation and growth phenomenon in which the strain, strain-rate and temperature in the region becomes much larger than elsewhere. In what follows we report on a numerical experiment which demonstrates a procedure for obtaining a calibration of the critically positive value of λ by performing simulations of the plane strain tension and compression tests. We show that by monitoring the nucleation and growth of regions of λ, we can follow the initiation and development of regions of intense plastic deformation in the body. The appearance of a significant sized region of "significantly positive" λ in the body *correlates* very well with the beginning of significant flow localization as judged from the distortion of the finite-element mesh, the contours of the equivalent plastic shear strain, shear strain-rate and temperature, and also with the rapid drop in the load carrying capacity of the specimen. In the plane strain tension and compression test simulations the shape of the region of localized plastic flow which evolves naturally is a band-like region.

Chapter 4
Numerical Examples

For the class of large deformation rate constitutive equations for isotropic thermo-elasto-viscoplasticity described in the previous section, Anand et al. [1985] have developed special semi-implicit time-integration procedure, and they have incorporated this time-integration procedure into the general-purpose, non-linear finite element computer program ABAQUS [1984]. The numerical simulation reported here was performed by using this computer code.

The particular constitutive function for the equivalent tensile stress $\bar{\tau}$ used in the numerical analysis is an equation proposed by Lindholm and Johnson [1983]. These authors have reported dynamic torsion test data obtained from short gage-length, thin-walled tubular specimens made from several metals, and they have proposed a constitutive equation for the shear stress which accounts for strain hardening, strain-rate hardening and thermal softening. For small elastic strains and under the assumption of isotropy the constitutive equation proposed by these authors may be interpreted to have the following form:

$$\bar{\tau} = (A + B\,(\bar{\gamma}^p)^n)\,[1 + C\ln(\dot{\bar{\gamma}}^p/\dot{\gamma}_0)]\bar{f}(\theta), \tag{85}$$

where

$$\bar{f}(\theta) = [(\theta_m - \theta)/(\theta_m - \theta_0)]^a, \tag{86}$$

and A, B, C, n, $\dot{\gamma}_0$ and a are material constants, θ_0 is a reference temperature and θ_m is the melting temperature. In their experiments Lindholm and Johnson found the steel AMS 6418 to be very vulnerable to shear localization. Another material

alumimum 2024-T351 has also been selected for the numerical analysis. This material has rate sensitivity and strain hardening capability much higher than those of AMS 6418 steel and is expected to have much higher resistance to shear localization. Thus it is interesting to investigate whether λ_c in our integral criterion can be calibrated to the same value for these significantly different materials. For these two materials Lindholm and Johnson report the values of the material constants in equation (85) and (86) as shown in Table 1. Further, the selected values for the fraction of plastic work converted to heat, mass density, specific heat and elastic bulk and shear moduli for these two materials are also listed in Table 1.

Table 1. Material constants for AMS 6418 steel and aluminum 2024-T351.

material constants	AMS 6418 steel	Aluminum 2024-T351
A (MPa)	896	152
B (MPa)	200	202
n	0.18	0.34
C	0.01	0.015
$\dot{\gamma}_0$ (sec^{-1})	1.0	1.0
θ_m $(^\circ K)$	1763	775
ω	0.90	0.90
ρ (kg/m^3)	7,750	2,770
c $(J/kg^\circ K)$	477	875
κ (MPa)	160,000	68,000
μ (MPa)	82,000	26,000

Lindholm and Johnson have proposed the value $a = 1$ in equation (86), however to accelerate the localization process in our numerical simulation, we have used the value $a = 2$.

The numerical examples considered here are the simulations of (1) plane strain compression, (2) plane strain tension and (3) bending of a u-notched specimen under plane

strain conditions. Plane strain compression and tension problems have been chosen to investigate whether the value of λ_c in our integral criterion can be calibrated to the same value for those two different deformation processes both known to be vulnerable to shear localization. It has been found that $\lambda_c \approx 10$ serves well to predict the beginning of significant shear localization in all the different combinations of deformation processes and material properties described above. The problem of plane strain bending of a U-notched specimen has been chosen to investigate the applicability of the $\lambda > \lambda_c$ criterion for shear localization in an extremely inhomogenous deformation processes.

Each mesh consists of ABAQUS continuum plane strain 4-node isoparametric quadrilateral (CPE4) elements. The mesh for numerical simulation has been refined in the region where deformation localization is expected. Finite element analyses of shear bands based on fine meshes of quadrilateral elements built up from four crossed triangles have been previously used (e.g., LeMonds and Needleman [1986] and Becker and Needleman [1986]) to numerically capture sharply localized shear bands. In the problems of adiabatic plane strain compression and tension, shear bands form across the specimen and thus it is possible to refine the mesh with a proper pre-orientation to capture the sharpest shear bands for given element size. Proper pre-orientation of the mesh with crossed-triangular elements has been obtained by a trial and error effort. In these regions two of the nodes of a typical quadrilateral element have been collapsed to produce a triangular element, and such triangular elements are arranged to build quadrilaterals made from four crossed triangles. In the problem of the bending of a U-notched specimen, there nucleates a deformation localization zone on the free surface of the notch after a certain amount of deformation and then it subsequently propagates

into the deforming zone under the notch. There is no shear band which encompasses the entire deformation field within the specimen. In this sense, flow localization in this problem is highly local when compared against the cases of plane strain compression and tension. Moreover, as the deformation field is extremely inhomogeneous, it is difficult to monitor the nucleation and development of shear localization until there is a global mesh distortion. Thus even though the mesh has been refined in the deformation zone under the notch using the four node quadrilateral elements, further trial and error effort to refine the mesh with the optimum pre-orientation of the triangular elements has not been made for this problem.

The boundary conditions on plane strain compression and tension specimen have been chosen such that nominal plastic shear strain rate of $\sim 1000\,\mathrm{sec}^{-1}$ is obtained in the prospective localization zone of each specimen. In the numerical analysis *the effects of inertia are neglected* and using the static procedures of the finite element code ABAQUS the full non-linear solution to the problem has been obtained. Values of the equivalent plastic shear strain $\bar{\gamma}^p$, equivalent plastic shear strain rate $\dot{\bar{\gamma}}^p$, absolute temperature θ, the parameter P and the parameter λ were calculated at every integration point at the end of every displacement increment, and level contours of these variables were obtained at numerous representative increments. A plot of the overall load versus displacement curve was also obtained.

4.1 Plane Strain Compression

A 320 element mesh shown in Fig. 5 has been used to approximate the plane strain compression of AMS 6418 steel and aluminum 2024-T351 between two *frictionless* platens. Triangular elements obtained by collapsing an edge of 4 node continuum elements have been used to capture the sharp shear band at later stages of compression. The top boundary of the mesh respresenting one quadrant of the specimen with initial temperature of $300°K$ has been compressed down at a constant speed without any constraint on the horizontal degrees of freedom. Specimen geometry allows homogeneous deformation under frictionless compression. Hence it is necessary to introduce a small perturbation which can trigger flow localization. An initial temperature perturbation of $1°C$ has been introduced into an element at the lower left corner of the mesh (element A in Fig. 5). Shapes of the deformed mesh and the values of equivalent plastic shear strain $\bar{\gamma}^p$, temperature θ, equivalent plastic shear strain rate $\dot{\bar{\gamma}}^p$, parameters $P \equiv (S - (\omega\bar{\tau}/\rho c)T)/R$ and $\lambda \equiv \int_{t_i}^{t} -P dt$ together with the value of the total load have been monitored throughout the deformation process.

Special attention has been given to three specific moments:

1. Time t_1 at which the value of the parameter P changes its sign throughout the specimen from positive to negative.

2. Time t_2 at which the load carrying capacity of the specimen reaches its maximum value and when there develops a mild flow localization of shear band mode.

3. Time t_3 at which the load carrying capacity of the specimen is decreasing rapidly and most of the deformation is concentrated onto a narrow shear band.

The deformed mesh and the field variable contours together with the total load - time curve are shown for these three time moments in Fig. 6 - Fig. 8 for AMS 6418 steel and in Fig. 9 - Fig. 11 for aluminum 2024-T351.

Before time t_1 the strain hardening has been overcoming the thermal softening even though there is an adiabatic temperature rise. Thus even with the introduction of a finite temperature perturbation at the lower left corner of the mesh, deformation localization has been supressed up to time t_1. At time t_1 as shown in Fig. 6 and Fig. 9, deformation field is essentially homogeneous throughout the specimen. Due to geometric hardening, load is on the increasing slope of its time curve. According to the linear perturbation stability analysis, a necessary condition for the onset of shear localization in plane strain deformation is $P \equiv (S - (\omega\bar{\tau}/\rho c)T)/R < 0$ (cf. chapter 2.3.2). Thus time t_1 is the moment when the growth of field inhomogeneities into a shear band becomes possible. However, no significant localization process has been observed just after time t_1.

At time t_2, as shown in Fig. 7 and Fig. 10, the total load is at its peak value and there has formed a mildly developed shear band. At this time there appears a zone of noticeable region within each specimen where $\lambda > 5$. Subsequent deformation continues to concentrate within this zone which develops into a band-like region shortly. Thus time t_2 can be considered to be a *beginning* of catastrophic shear localization. All five contour plots agree on the location and shape of the localization zone in the form of a band.

After time t_2, the deformation localization develops significantly. A severely deformed mesh now clearly shows the shear band. The load carrying capacity is decreasing rapidly and the shear localization at this stage is essentially catastrophic. Time t_3

has been chosen to show a fully developed stage of the shear localization with moderate distortion of the elements inside the band (Figs. 8 and 11). At this time the value of λ in the band is $\lambda \approx 30$. After this stage mesh rezoning is necessary to continue the analysis with any accuracy. Due to the finite size of the elements used for the analysis, there exists a finite lower bound to the numerically obtained band thickness.

4.2 Plane Strain Tension

As AMS 6418 steel and aluminum 2024-T351 can sustain different amounts of strains before the development of adiabatic shear bands, slightly different meshes have been used for the numerical simulations. For AMS 6418 steel a 456 element mesh shown in Fig. 12 and for aluminum 2024-T351 a 520 element mesh shown in Fig. 16 have been chosen to approximate the specimen geometry used by Clausing [1970] To capture the sharp shear bands in the catastrophic stages of the shear localization in each material mesh had to be refined with proper pre-orientation of the quadrilaterals with cross triangles in the central regions of the specimen. By a trial and error approach, the mesh has been refined in the central region of the specimen where most of deformation localization is expected. The top boundary of the one quarter of the specimen shown in Fig. 12 and Fig.16 has been pulled upward at a constant speed which gives a nominal plastic shear strain rate of $\sim 10^3 \text{sec}^{-1}$ in the central gage section with the initial temperature of $300°K$, Due to the geometry of the specimen, deformation is not homogeneous right from the beginning and thus there is no need to introduce a perturbation into the model to trigger the shear localization expected at later stages of deformation. As will be shown later, there is a gradual diffuse necking process observed in the central region of the specimen. As the necking progresses, eventually there appear shear localization zones in the form of bands inside the neck. Subsequently, most of deformation is severely localized onto those bands and the total load decreases rapidly.

As in the previous example, the field variables used to monitor the deformation process are equivalent plastic shear strain $\bar{\gamma}^p$, temperature θ, equivalent plastic shear strain rate $\dot{\bar{\gamma}}^p$ and the parameters P and λ together with the deformed mesh and the

total load.

Special attention has been given to three specific moments:

1. Time t_1 at which the value of the parameter P changes its sign at the center of the specimen from positive to negative.

2. Time t_2 at which the total load begins to drop more rapidly, and there develops a significant amount of flow localization.

3. Time t_3 at which shear localization is in its fully developed catastrophic stage.

At time t_1, as shown in Fig. 13 and Fig. 17, the total load is past its maximum and there is a region of negative P developed at the center of the specimen. Inhomogeneity of the deformation field is very mild throughout the central region of the specimen. According to the linear perturbation stability analysis, with a negative value of P such that $S < (\omega\bar{\tau}/\rho c)T$, it is now the time for the growth of field inhomogeneities to form shear bands. However, due to the stabilizing effect of positive strain rate hardening, the speeds of the growth of field inhomogeneities are not high enough to develop any significant flow localization immediately after time t_1. Up to time t_2 the localization process is very gradual.

At time t_2, a zone of noticeable size where $\lambda > 5 \sim 10$ nucleates at the center of the neck and shortly, it propagates from the center of the neck to the free surface of the specimen to form a band-like region. Localization as evidenced by the five field variable contours has intensified, the load is beginning to drop more rapidly, and the mesh begins to deform heavily; see Fig. 14 and Fig. 18.

At time t_3, the deformation localization is so severe that even without the aid of contour plots, shear bands are readily visible as shown in Fig. 15 and Fig. 19. The

load carrying capacity is dropping rapidly. At this time the value of λ in the band is $\lambda \approx 30$ for AMS 6418 steel and ≈ 18 for aluminum 2024-T351. After time t_3 some elements begin to deform severely, and the subsequent finite element analysis requires mesh rezoning for its accuracy.

4.3 Plane Strain Bending of a U-notched Specimen

A 542 element mesh and accompanying boundary conditions shown in Fig. 20 has been chosen to approximate the specimen geometry and experimental scheme used by Zuber (1985) for this problem. A number of *quasi-static, isothermal* four point bending experiments have been performed by Zuber on polycarbonate, aluminum and a maraging steel specimens. In each material, intense shear localization followed by ductile fracture has been observed. Even though the mechanism of shear localization in adiabatic deformation processes is different from that of quasi-static isothermal processes, the problem of adiabatic plane strain bending of a u-notched specimen has been chosen for the numerical simulation. The deformation field is extremely inhomogenous and unlike the previous cases of plane strain compression and tension where localization began inside the deforming body, shear localization in this case is expected to initiate at the free surface of the notch and then propagate into the material. Due to the inhomogenous nature of the deformation field, the beginning of significant shear localization is less clear when compared with the previous examples. However, it will be demonstrated that the linear perturbation stability analysis still underestimates the time to significant shear localization and this can be greatly improved by the new integral criterion. Again, the field variables $\bar{\gamma}^p$, θ, $\dot{\bar{\gamma}}^p$, P and λ together with the deformed mesh and the total load have been monitored throughout the deformation process. Special attention has been given to three specific moments:

1. Time t_1 at which the parameter P has negative values in the deforming regions under the notch and under the back surface of the notch.

2. Time t_2 at which the parameter λ has values greater than 10 in both of the

deforming regions.

3. Time t_3 at which there are fully developed shear localization zones in both of the deforming regions.

In the beginning of the deformation, strain hardening overcomes the thermal softening such that $P > 0$ throughout the deformation field. After an elapse of a certain amount of time, a small negative P zone nucleates under the root of the notch and this negative P zone propagates into the material quickly. This propagation of negative P zone is stopped by the relatively non-deforming region in the neutral plane of the specimen. After P changes its sign from positive to negative in the deforming region under the notch, there appears another negative P zone in the deforming region under the back surface of the notch. By the time t_1, there are two well developed negative P zones in the two deforming regions separated by a neutral plane as shown in Fig. 21. At this time the total load is past its maximum value on its time trajectory. Even though the deformation field is inhomogenous, there is no significant shear mode localization observed at this stage of deformation. The value of λ is less than its critical value of 10 over the deforming regions except in the vicinity of a small zone on the free surface away from the center of the notch as seen in Fig. 21.

After time t_1, the $\lambda > 10$ zone propagates from its nucleation site into the deforming region under the notch. This propagation of $\lambda > 10$ zone is again stopped by the neutral plane. Highest strain rate is observed at this nucleation site on the free surface off the center of the notch. Then there nucleates another $\lambda > 10$ zone on the back surface of the notch. This $\lambda > 10$ zone also propagates into the deforming region under the back surface of the notch and get stopped by the neutral plane. Thus by the time t_2, there are two $\lambda > 10$ zones developed in the deforming regions under the notch and under

the back surface of the notch as shown in Fig. 22. Deformed mesh and contour plots indicate that there is a localization process centered around the point where $\lambda > 10$ region has first nucleated at time t_1. At this stage, mesh distortion reveals moderate shear localization in the deforming region under the notch.

After time t_2 the shear localization in the deforming region under the notch becomes more developed and mesh distortion becomes more prominent. Along with the shear localization in this region, there develops another shear mode flow localization in the deforming region under the back surface of the notch. Fig. 23 shows a fully developed stage of shear localization at time t_3. At this stage, shear bands are readily observable even without the aid of contour plots due to the heavy distortion of the finite element mesh. The numerical results at this stage is probably inaccurate and mesh rezoning will be necessary to continue the analysis.

Chapter 5
Discussion and Conclusions

In chapter 2, a linear perturbation stability analysis for shear localization in 3 dimensional flow of viscoplastic solids has been performed. Shear localization is regarded as a material instability and a general framework for obtaining a characteristic equation for the shear localization in 3 dimensional flow has been presented from which conditions for the onset of shear localization can be deduced. For the special cases of 2 dimensional plane deformation, conditions for the onset of shear localization have been obtained in terms of the material parameters such as strain hardening, effective thermal softening, strain-rate hardening and pressure sensitivity. It has been demonstrated that linear perturbation stability analysis predicts:

- The necessary conditions for the initiation of shear bands.
- The incipient orientations of the shear bands.
- The incipient rate of growth of the emergent shear bands.

However, it has been widely known from the study of the shear localization in one dimensional simple shear deformation that linear perturbation stability analysis significantly underpredicts the amount of attainable strain prior to the significant development of shear localization. Fully nonlinear numerical simulations of simple shear deformation of viscoplastic solids reveal that there is no noticeable development of shear bands at the moment of shear band initiation predicted from the linear perturbation stability analysis. Significant development of shear localization is usually postponed until much later stages of deformation.

Motivated by these observations, another approach to the problem of shear localization in rate sensitive materials has been considered in chapter 3. For the purpose of the argument, attention has been focused upon the adiabatic shear localization. Again, the phenomenon of shear localization is regarded as a material instability and an attempt is made to devise a criterion for significant shear localization in terms of the material parameters for a class of viscoplastic materials. The development of the new criterion is based upon the fact that due to the autocatalytic nature of adiabatic shear localization, strain rates can be very large within the localization zone once the shear band formation is taking place. A nonlinear first order differential equation for the equivalent plastic shear strain rate $\dot{\bar{\gamma}}^p$ has been obtained for a class of viscoplastic materials undergoing adiabatic deformation. An implicit solution to this equation has been obtained. The form of this solution suggests that unbounded growth of the equivalent plastic shear strain rate $\dot{\bar{\gamma}}^p$ at a material point is possible when a dimensionless, history dependent parameter

$$\lambda \equiv \int_{t_i}^{t} (-P) dt \equiv \int_{t_i}^{t} \left[-\frac{S - (\omega\bar{\tau}/\rho c)T}{R} \right] dt$$

reaches a certain value. Here, the lower limit of the integration t_i has been chosen as the time when P defined in equation (79) changes its sign from positive to negative. This is the time of the initiation of shear localization predicted by linear perturbation stability analysis for plane deformation. Thus a simple criterion for the localization of plastic deformation has been suggested as

$$\lambda > \lambda_c$$

where λ_c is a positive number which can be calibrated for a class of constitutive equations and deformation processes. Attainment of the condition above in the deformation

localization zones will take a finite amount of time from the time t_i and thus the new criterion is supposed to improve the underprediction of the critical strain to significant shear localization from linear perturbation stability analysis. Another feature of the new criterion is that in contrast to the linear perturbation stability analysis which characterizes the initiation of shear localization in terms of the instantaneous values of the material parameters such as P, the new criterion suggests that the catastrophic stage of shear localization is characterized by the time history of P.

Finite element simulations of adiabatic plane strain compression, tension and bending of materials described by a set of viscoplastic constitutive equations have been successfully performed. Elasticity, thermal expansion and large geometry changes are accounted for, but inertial effects have been neglected. The numerical simulations of plane strain compression and tension tests have been used to follow the initiation and growth of a band-like region of localization through slow early growth to severe localization. It is shown, as expected, that the significant stage of severe localization, i.e. when the load starts to drop rapidly, is poorly correlated with the instant when $\{P \equiv (S - (\omega \bar{\tau}/\rho c) T)/R\}$ turns negative. However, the beginning of severe localization correlates fairly well with the time when there first develops a band-like region of $\lambda \equiv \int_{t_i}^{t} P\, dt > \lambda_c \approx 10$ across the specimen.

In order to follow the localization process in an arbitrary deformation history it appears attractive to monitor the parameter λ and its contours in addition to the parameters $(\bar{\gamma}^p, \dot{\bar{\gamma}}^p, \theta)$ and their contours. It is important to note that like $\bar{\gamma}^p$ and θ, the parameter λ depends upon the entire deformation history experienced by each material point. Because of the point-wise nature of the parameter λ, the attainment of a sufficiently positive value of λ does not by itself predict localization which is usually

understood to occur when the strain, strain-rate and temperature in a region (band-like or otherwise) becomes much larger than the regions which surround it. However, by monitoring the nucleation and growth of of a region where λ is positive we would have automatically monitored the region where the strain, strain-rate and temperature are greater than in the regions which surround it. To determine the shape of the region of localized deformation in a given boundary value problem, the full non-linear solution to the problem has to be carried out. In the plane strain compression and tension test simulations the shape of the region of localized flow which evolves naturally is a band-like region. For plane strain bending of a u-notched specimen, due to the severe inhomogeneity of the deformation field the shape of the $\lambda > \lambda_c$ zone was not so simple as in the cases of plane strain compression and tension. However, the formation of significant sized $\lambda > \lambda_c$ zone within the deforming regions of the specimen correlated fairly well with the beginning of the siginficant shear localization in these regions.

For the derivation of the parameter λ, no specific assumption as to the mode of deformation has been made even though the main purpose of the derivation was for the shear mode of localization. Thus it is interesting to see if the same parameter λ can be applied to a different mode of flow localization such as necking in axisymmetric tension.

Apart from the interest in monitoring regions of λ during numerical studies conducted to understand the physical phenomenon of flow localization, the monitoring of this parameter may be useful for determining the stage in a finite element analysis when it may become necessary to start worrying about significant mesh distortion and the need for a re-zoning operation.

There is an another issue in relation to the applicability of the localization criterion

$\lambda > \lambda_c$ to interrupted deformation histories. In situations such as forging, the flow field can be extremely inhomogenous and the boundary conditions can be continuously changing with time due to the change of the workpiece geometry. Thus it is possible that for certain stages of the deformation process shear localization is promoted within the deforming body but later on further development of the shear localization is suppressed by the new loading conditions. In these cases, it is possible that the strain rates in the interrupted shear localization zone are no longer allowed to grow with time but eventually will be forced to return to zero values. On the other hand, there is no upper limit provided for the time integration for the parameter λ defined in equation (83). For the parameter λ to be applicable for such cases of interrupted deformation histories, it should be shown that λ will decrease or at least stop increasing when the values of the strain rates return to zero. For a class of viscoplasic materials for which the flow stress $\bar{\tau}$ is a function of the equivalent plastic shear strain rate $\dot{\bar{\gamma}}^p$ such that

$$\bar{\tau} = g(\bar{\gamma}^p, \dot{\bar{\gamma}}^p, \theta) = u(\bar{\gamma}^p, \varsigma, \theta)$$

with $\varsigma \equiv \ln \dot{\bar{\gamma}}^p$, the strain rate hardening R defined in equation (74) will be inversely proportional to the equivalent plastic shear strain rate $\dot{\bar{\gamma}}^p$ such as

$$R \equiv \partial g / \partial \dot{\bar{\gamma}}^p = \frac{1}{\dot{\bar{\gamma}}^p} \partial u / \partial \varsigma$$

As the parameter P defined in equation (79) is inversely proportional to the strain-rate hardening R, it can be said that for a class of viscoplastic materials (except the linear viscous limit) that

$$P \propto \dot{\bar{\gamma}}^p$$

Thus for viscoplastic materials the value of the parameter P will return to zero and the value of the localization parameter λ will be frozen to its previous value whenever

the strain rates are forced to zero values.

In spite of the efforts made in this thesis, the understanding of the shear localization phenomenon is far from being complete. There are a number of issues upon which our future effort should be concentrated. First of all, the complete feature of the three dimensional generalization of Clifton and Bai's linear perturbation stability analysis has not been fully examined primarily because of the complexity of the coefficient matrix A shown in Appendix A. Even though linear perturbation stability analysis cannot give the critical strains to shear localization in rate-dependent materials, the result is supposed to provide the further understanding of the roles of various features of the three dimensional deformation field. For the simplicity of the mathematical operations, relatively simple constitutive assumptions has been used for the analysis. Obviously, the analysis can be improved by incorporating the effects of elasticity, dilatancy together with pressure sensitivity and more complex features constitutive behavior of anisotropic materials.

The new criterion which employs a dimensionless parameter λ has been developed to overcome the underprediction of the critical strains to shear localizaiton by linear perturbation stability analysis. It has been asserted that due to the autocatalytic nature of the adiabatic shear localization, the critical stage can be determined as when the values of strain, strain rate and temperature in the localization zone become very large compared to their values elsewhere. This approach cannot be applied to quasi-static deformation processes and the study of failure criterion becomes necessary. The study of shear localization cannot be complete without the understanding of failure mechanism by which the shear localization process is terminated in many cases. It might be possible to modify the new criterion such as $\lambda > \lambda_{failure}$ for the catastrophic

stage of shear localization. Of course it is now an open question how $\lambda_{failure}$ should be determined.

Another aspect of the new criterion which should be studied further is that the derivation of λ has not been based upon the spatial gradients of the plastic strain rate. The phenomenon of shear localization is best evidenced by the intense spatial gradients of the field variables such as strains, strain rates and temperature in case of adiabatic deformation rather than their absolute values at each material point. Characterization of the phenomenon in terms of the spatial gradients of the field variables might lead to an improved criterion for shear localization.

To determine the range of the values for λ_c, numerical solution procedures had to be used together with a set of specific constitutive equations. This procedure will be better substantiated with an analysis of the sensitivity of the value of λ_c to the constitutive model.

In all of the numerical examples presented in this thesis, it has been observed that the finite element analysis results become inaccurate when there appears a significant distortion of the mesh due to the shear localization. For the continuation of the analysis without losing its accuracy, it is obvious that mesh rezoning is essential. This capability which is not available at present should be developed into the finite element program in future.

Only numerical simulations have been performed and presented in this thesis. Accurate modeling methodology for the constitutive behavior of viscoplastic materials which incorporates all the important features relevant to the shear localization, criteria for shear mode localization and subsequent failure in their maximum generality, and automatic mesh rezoning capability for finite element analyses should provide the tools

for the quantitative comparison between experiments and model prediction when they are fully developed and integrated.

References

1. Zener, C. and Hollomon, J. H., "Effect of Strain Rate Upon Plastic Flow of Steel", Journal of Applied Physics, **15**(1944), pp. 22-32.

2. Recht, R. F., "Catastrophic Thermoplastic Shear", Journal of Applied Mechanics, Transactions of the ASME, **86**(June 1964), pp. 189-193.

3. Semiatin, S. L. ,Lahoti, G. D. and Oh, S. I., "The Occurance of Shear Bands in Metalworking", in: J. Mescall and V. Weiss (Ed.), Materials Behavior Under High Stress and Ultrahigh Loading Rates, Sagamore Army Materials Research Conference Proceedings, **29**(1983), Plenum Press, pp. 119-160

4. Culver, R. S., "Thermal Instability Strain in Dynamic Plastic Deformation", in: Rhode, R. W., Butcher, B. M., Holland, J. R. and Karnes, C. H. (eds.), Metallurgical Effects at High Strain Rates, The Metallurgical Society of AIME Proceedings, Plenum Press, 1973, pp. 519-530.

5. Costin, L. S, Crisman, E. E., Hawley, R. H. and Duffy, J., "On the Localization of Plastic Flow in Mild Steel Tubes Under Dynamic Torsional Loading", in: J. Harding (Ed.), Mechanical Properties at High Rates of Strain, Proc. 2nd Oxford Conf. 1979, Inst. Phys., London (1980), pp. 90-100

6. Backman, M. E. and Finnegan, S. A., "The Propagation of Adiabatic Shear", in: Rhode, R. W., Butcher, B. M., Holland, J. R. and Karnes, C. H. (eds.), Metallurgical Effects at High Strain Rates, The Metallurgical Society of AIME Proceedings, Plenum Press, 1973, pp. 531-543.

7. Rogers, H. C. and Shastry, C. V., "Material Factors in Adiabatic Shearing in Steels", in: Meyers, Mark A. and Lawrence, E. Murr (eds.), Shock Waves and High-Strain-Rate Phenomena in Metals, Proceedings of the International Conference on Metallurgical Effects on High-Strain-Rate Deformation and Fabrication, June 22-26, 1980, Albuquerque, New Mexico, Plenum Press, New York, 1981, pp. 285-298.

8. Leech, Patrick W., "Observations of Adiabatic Shear Band Formation in 7039 Aluminum Alloy", Metallurgical Transactions A, **16A**(October 1985), pp. 1900-1903.

9. Thornton, Peter A. and Heiser, Francis A., "Observations on Adiabatic Shear Zones in Explosively Loaded Thick-Wall Cylinders", Metallurgical Transactions, **2**(1971), pp. 1496-1499.

10. Staker, M. R., "The Relation Between Adiabatic Shear Instabilty Strain and Material Properties", Acta Metallurgica, **29**(1981), pp. 683-689.

11. Bird, J. E. and Carlson, J. M., "Shear Band Formation During Sheet Forming", Journal of Metals, November, 1986, pp. 47-54.

12. Charalambakis, Nicolas, "Behavior and Asymptotic Stability of Thermomechanical Processes", Int J. Engng. Sci., **24**(1986), pp. 755-764.

13. Anand, L. and Spitzig, W. A., "Initiation of Localized Shear Bands in Plane Strain", J. Mech. Phys. Solids, **28**(1980), pp. 113-128.

14. Rudnicki J. W. and Rice, J. R., "Conditions for the Localization of Deformation in Pressure-sensitive Dilatant Materials", J. Mech. Phys. Solids, **23**(1975) pp.

371-394.

15. Rice, J. R., "The Localization of Plastic Deformation", in: Koiter, W. T. (ed.), Theoretical and Applied Mechanics, Proceedings of the 14th International Congress of Theoretical and Applied Mechanics, Delft, the Netherlands, 30 August - 4 Septmeber, 1976, Volume I, North-Holland, Amsterdam, 1977, p. 207.

16. Semiatin, S. L., Staker, M. R. and Jonas, J. J., "Plastic Instability and Flow Localization in Shear at High Rates of Deformation", Acta Metall. **32**(1984), pp. 1349-1354.

17. Clifton, R. J., Chap. 8 in Materials Response to Ultra-High Loading Rates, NRC Report. NMAB-356, 1980, pp. 129-142.

18. Bai, Y. L., "Thermo-plastic Instability in Simple Shear", J. Mech. Phys. Solids, **30** (1982), pp. 195-207

19. Burns, T. J., "Approximate Linear Stability Analysis of a Model of Adiabatic Shear Band Formation", Quart. Appl. Math. **43**(1985), pp. 65-84

20. Rabotnov, G. N. and Shesterikov, S. A., "Creep Stability of Columns and Plates", J. Mech. Phys. Solids, **6**(1957), pp. 27-34.

21. Hoff, N. J., "A Survey of the Theories of Creep Buckling", Proceedings of the 3rd U.S. National Congress of Applied Mechanics, Brown University, Providence, R.I., 1958, pp. 29-49.

22. Fressengeas, C. and Molinari, A., "Inertia and Thermal Effects on the Localization of Plastic Flow", Acta Metallurgica, **33**(1985), pp. 387-396.

23. Hutchinson, J. W. and Obrecht, H., "Tensile Instabilities in Strain-Rate Dependent Materials", in: Taplin, D. M. R. (ed.), Fracture 1977, Proceedings of the 4th International Congress on Fracture, Waterloo, Canada, June 19-24, 1977, University of Waterloo Press, pp. 101-113.

24. Merzer, A. M., "Modelling of Adiabatic Shear Band Development from Small Imperfections", J. Mech. Phys. Solids, **30**(1982), pp. 323

25. Wright, T. W and Batra, R. C., " The Initiation and Growth of Adiabatic Shear Bands", International Journal of Plasticity, **1**(1985), pp. 205

26. Shawki, T. G., "Analysis of Shear Band Formation at High Strain Rates and the Visco-plastic Response of Polycrystals", Ph. D. Thesis, Division of Engineering, Brown University, Providence, R.I., June 1985

27. Clifton, R. J., Duffy, J., Hartley, K. A. and Shawki, T. G., "On Critical Conditions for Shear Band Formation at High Strain Rates", Scripta Metall., **18**(1984), pp. 443-448

28. Molinari, A. and Clifton, R. J., "Analytical Characterization of Shear Localization in Thermoviscoplastic Materials", Brown University Technical Report, ARO Grant DAAG29-85-K-0003, Report No. 4, December, 1986.

29. Semiatin, S. L. and Jonas, J. J., Formability & Workability of Metals: Plastic Instability & Flow Localization, ASM series in metal processing;2(1984), American Society for Metals.

30. Anand, L., Lush, A., Briceno, M. and Parks, D., "A Time-Integration Procedure for a Set of Internal Variable Type Elasto-Viscoplastic Constitutive Equations",

M. I. T. Report of Research In Mechanics of Materials, 1985

31. Hibbit, H. D., "ABAQUS/EPGEN, A General Purpose Finite Element Code With Emphasis on Nonlinear Applications", Nuclear Engineering Design, **77**(1984), pp. 271-297; Reference Manuals (Sept. 1984), Hibbit, Karlsson and Sorensen Inc., Providence, R.I..

32. Lindholm, U. S. and Johnson, G. R., "Strain-Rate Effects in Metals at Large Shear Strains", in: J. Mescall and V. Weiss (Ed.), Material Behavior Under High Stress and Ultrahigh Loading Rates, Sagamore Army Materials Research Conference Proceedings, **29**(1983), Plenum Press, pp.61

33. LeMonds, J. and Needleman, A., "Finite Element Analyses of Shear Localization in Rate and Temperature Dependent Solids", Army Research Office Report No. DAAG 29-85-K-0003/4, May 1986.

34. Becker, R. and Needleman, A., "Effect of Yield Surface Curvature on Necking and Failure in Porous Solids", Journal of Applied Mechanics, Transactions of the ASME, **53**(1986), pp.491-499.

35. Clausing, D. P., "Effect of Plastic Strain Rate on Ductility and Toughness", International Journal of Fracture Mechanics, **6**(1970), pp. 71

36. Zuber, P. J., "Initiation of Ductile Fracture from Shear Bands in U-Notched Four Point Bend Tests", Master Thesis, 1985, Massachusetts Institute of Technology.

Appendix A. The entries of the matrix A

The entries of the coefficient matrix **A** in (35) are:

$$A_{11} = \xi^2 \left[\left\{ R^\circ + \frac{S^\circ}{\eta} - \left(\frac{\bar{\tau}^\circ}{\dot{\bar{\gamma}}^\circ} \right) \right\} \left(\frac{2}{\dot{\bar{\gamma}}^\circ} \right)^2 \alpha_1^2 n_1^2 + \frac{\bar{\tau}^\circ}{\dot{\bar{\gamma}}^\circ} \right] + \rho\eta$$

$$A_{12} = \xi^2 \left[\left\{ R^\circ + \frac{S^\circ}{\eta} - \left(\frac{\bar{\tau}^\circ}{\dot{\bar{\gamma}}^\circ} \right) \right\} \left(\frac{2}{\dot{\bar{\gamma}}^\circ} \right)^2 \alpha_1 \alpha_2 n_1 n_2 \right]$$

$$A_{13} = \xi^2 \left[\left\{ R^\circ + \frac{S^\circ}{\eta} - \left(\frac{\bar{\tau}^\circ}{\dot{\bar{\gamma}}^\circ} \right) \right\} \left(\frac{2}{\dot{\bar{\gamma}}^\circ} \right)^2 \alpha_1 \alpha_3 n_1 n_3 \right]$$

$$A_{14} = (i\xi) T^\circ \left(\frac{2}{\dot{\bar{\gamma}}^\circ} \right) \alpha_1 n_1$$

$$A_{15} = (i\xi) \left\{ 1 - \mathcal{P}^\circ \left(\frac{2}{\dot{\bar{\gamma}}^\circ} \right) \alpha_1 \right\} n_1$$

$$A_{21} = \xi^2 \left[\left\{ R^\circ + \frac{S^\circ}{\eta} - \left(\frac{\bar{\tau}^\circ}{\dot{\bar{\gamma}}^\circ} \right) \right\} \left(\frac{2}{\dot{\bar{\gamma}}^\circ} \right)^2 \alpha_1 \alpha_2 n_1 n_2 \right]$$

$$A_{22} = \xi^2 \left[\left\{ R^\circ + \frac{S^\circ}{\eta} - \left(\frac{\bar{\tau}^\circ}{\dot{\bar{\gamma}}^\circ} \right) \right\} \left(\frac{2}{\dot{\bar{\gamma}}^\circ} \right)^2 \alpha_2^2 n_2^2 + \left(\frac{\bar{\tau}^\circ}{\dot{\bar{\gamma}}^\circ} \right) \right] + \rho\eta$$

$$A_{23} = \xi^2 \left[\left\{ R^\circ + \frac{S^\circ}{\eta} - \left(\frac{\bar{\tau}^\circ}{\dot{\bar{\gamma}}^\circ} \right) \right\} \left(\frac{2}{\dot{\bar{\gamma}}^\circ} \right)^2 \alpha_2 \alpha_3 n_2 n_3 \right]$$

$$A_{24} = (i\xi) T^\circ \left(\frac{2}{\dot{\bar{\gamma}}^\circ} \right) \alpha_2 n_2$$

$$A_{25} = (i\xi) \left\{ 1 - \mathcal{P}^\circ \left(\frac{2}{\dot{\bar{\gamma}}^\circ} \right) \alpha_2 \right\} n_2$$

$$A_{31} = \xi^2 \left[\left\{ R^\circ + \frac{S^\circ}{\eta} - \left(\frac{\bar{\tau}^\circ}{\dot{\bar{\gamma}}^\circ} \right) \right\} \left(\frac{2}{\dot{\bar{\gamma}}^\circ} \right)^2 \alpha_1 \alpha_3 n_1 n_3 \right]$$

$$A_{32} = \xi^2 \left[\left\{ R^\circ + \frac{S^\circ}{\eta} - \left(\frac{\bar{\tau}^\circ}{\dot{\bar{\gamma}}^\circ} \right) \right\} \left(\frac{2}{\dot{\bar{\gamma}}^\circ} \right)^2 \alpha_2 \alpha_3 n_2 n_3 \right]$$

$$A_{33} = \xi^2 \left[\left\{ R^\circ + \frac{S^\circ}{\eta} - \left(\frac{\bar{\tau}^\circ}{\dot{\bar{\gamma}}^\circ} \right) \right\} \left(\frac{2}{\dot{\bar{\gamma}}^\circ} \right)^2 \alpha_3^2 n_3^2 + \left(\frac{\bar{\tau}^\circ}{\dot{\bar{\gamma}}^\circ} \right) \right] + \rho\eta$$

$$A_{34} = (i\xi) T^\circ \left(\frac{2}{\dot{\bar{\gamma}}^\circ} \right) \alpha_3 n_3$$

$$A_{35} = (i\xi) \left\{ 1 - P^\circ \left(\frac{2}{\dot{\bar{\gamma}}^\circ} \right) \alpha_3 \right\} n_3$$

$$A_{41} = (i\xi) \left\{ \left(R^\circ + \frac{S^\circ}{\eta} \right) \dot{\bar{\gamma}}^\circ + \bar{\tau}^\circ \right\} \left(\frac{2}{\dot{\bar{\gamma}}^\circ} \right) \alpha_1 n_1$$

$$A_{42} = (i\xi) \left\{ \left(R^\circ + \frac{S^\circ}{\eta} \right) \dot{\bar{\gamma}}^\circ + \bar{\tau}^\circ \right\} \left(\frac{2}{\dot{\bar{\gamma}}^\circ} \right) \alpha_2 n_2$$

$$A_{43} = (i\xi) \left\{ \left(R^\circ + \frac{S^\circ}{\eta} \right) \dot{\bar{\gamma}}^\circ + \bar{\tau}^\circ \right\} \left(\frac{2}{\dot{\bar{\gamma}}^\circ} \right) \alpha_3 n_3$$

$$A_{44} = \left\{ - \left(\frac{\rho c}{\omega} \eta + \frac{\kappa}{\omega} \xi^2 + T^\circ \dot{\bar{\gamma}}^\circ \right) \right\}$$

$$A_{45} = P^\circ \dot{\bar{\gamma}}^\circ$$

$$A_{51} = n_1$$

$$A_{52} = n_2$$

$$A_{53} = n_3$$

$$A_{54} = 0$$

$$A_{55} = 0$$

Appendix B. The entries of the matrix B

The entries of the coefficient matrix **B** in (41) are

$$B_{11} = \xi^2 \left[\left\{ R^\circ + \frac{S^\circ}{\eta} - \left(\frac{\bar{\tau}^\circ}{\dot{\bar{\gamma}}^\circ} \right) \right\} n_1^2 + \left(\frac{\bar{\tau}^\circ}{\dot{\bar{\gamma}}^\circ} \right) \right] + \rho\eta$$

$$B_{12} = -\xi^2 \left[\left\{ R^\circ + \frac{S^\circ}{\eta} - \left(\frac{\bar{\tau}^\circ}{\dot{\bar{\gamma}}^\circ} \right) \right\} n_1 n_2 \right]$$

$$B_{13} = (i\xi) T^\circ n_1$$

$$B_{14} = (i\xi)(1 - P^\circ) n_1$$

$$B_{21} = B_{12}$$

$$B_{22} = \xi^2 \left[\left\{ R^\circ + \frac{S^\circ}{\eta} - \left(\frac{\bar{\tau}^\circ}{\dot{\bar{\gamma}}^\circ} \right) \right\} n_2^2 + \left(\frac{\bar{\tau}^\circ}{\dot{\bar{\gamma}}^\circ} \right) \right] + \rho\eta$$

$$B_{23} = -(i\xi) T^\circ n_2$$

$$B_{24} = (i\xi)(1 + P^\circ) n_2$$

$$B_{31} = (i\xi) \left\{ \left(R^\circ + \frac{S^\circ}{\eta} \right) \dot{\bar{\gamma}}^\circ + \bar{\tau}^\circ \right\} n_1$$

$$B_{32} = -(i\xi) \left\{ \left(R^\circ + \frac{S^\circ}{\eta} \right) \dot{\bar{\gamma}}^\circ + \bar{\tau}^\circ \right\} n_2$$

$$B_{33} = \left\{ - \left(\frac{\rho c}{\omega} \eta + \frac{\kappa}{\omega} \xi^2 + T^\circ \dot{\bar{\gamma}}^\circ \right) \right\}$$

$$B_{34} = P^\circ \dot{\bar{\gamma}}^\circ$$

$$B_{41} = n_1$$

$$B_{42} = n_2$$

$$B_{43} = B_{44} = 0$$

Appendix C. Time behavior of the term

$$1 + (\dot{\bar{\gamma}}^p)^{-1} \int_{t_i}^{t} Q \exp(-\lambda) dt$$

We assume that material has strain hardening, thermal softening and strain-rate hardening capabilities which are all positive. When such a material is subjected adiabatic deformation, the flow stress $\bar{\tau}$ will increase initially due to strain hardening but the effect of temperature rise will ultimately overcome the effect of strain hardening and thus the flow stress will begin to decrease with time. At material points located in a adiabatic flow localization zone this process will continue due to its autocatalytic nature. Thus at such material points the time histories of flow stress $\bar{\tau}$ and the term Q defined in relation to equation (81) can be represented by the time trajectories such as shown in Fig. 24(a) and Fig. 24(b). We also note that from equations (76) and (80) we have

$$\dot{\bar{\tau}} = R \left\{ \frac{d}{dt}(\dot{\bar{\gamma}}^p) + P\dot{\bar{\gamma}}^p \right\}$$

where P has been defined in equation (79). For most engineering materials the contribution from the strain rate hardening to the total value of the flow stress $\bar{\tau}$ is small when compared to the contributions from the strain hardening or thermal softening (eg., ref. Table 1). For such materials the following approximation can be made:

$$\dot{\bar{\tau}} \approx RP\dot{\bar{\gamma}}^p$$

Hence for a given deformation history at a materal point within a flow localization zone, the time when the flow stress $\bar{\tau}$ reaches its maximum value will be approximately equal to the time t_i when P changes its sign from positive to negative such as sketched in Fig. 24(c). From the given time history of P sketched in Fig. 24(c), the time

trajectory of the parameter λ defined in equation (83) and hence the time trajectory of the term $Q\exp(-\lambda)$ has been sketched in Fig. 24(d) and Fig. 24(e). From Fig. 24(e) it is obvious that the term $1 + (\dot{\bar{\gamma}}^p)^{-1}\int_{t_i}^{t} Q\exp(-\lambda)dt$ will have a value of 1 at time t_i and will subsequently continue to decrease monotonically. In view of the fact that the equivalent plastic shear strain rate $\dot{\bar{\gamma}}^p$ cannot have negative values and from the equation (82) it is also clear that the term $1 + (\dot{\bar{\gamma}}^p)^{-1}\int_{t_i}^{t} Q\exp(-\lambda)dt$ also cannot have negative values. Thus as sketched in Fig. 24(f), the term $1 + (\dot{\bar{\gamma}}^p)^{-1}\int_{t_i}^{t} Q\exp(-\lambda)dt$ will continue to decrease from its value of 1 at time t_i to a positive finite value or zero value asymptotically. Thus we can conclude that within a adiabatic flow localization zone

$$0 \leq 1 + (\dot{\bar{\gamma}}^p)^{-1}\int_{t_i}^{t} Q\exp(-\lambda)dt \leq 1 \quad \text{for} \quad t \geq t_i$$

Appendix D. ABAQUS Input Files

For each of the numerical simulations presented in chapter 4, three input files have been provided. Following is the description of these files.

- Input Data File

  This file defines the model in terms of mesh geometry, boundary conditions, material properties, numerical solution procedure, and the format of the solution output to be recorded. For the three types (compression, tension and bending) of the problems the Input Data Files are essentially similar to each other. An input data file for the problem of plane strain tension of 2024-T351 Aluminum is shown here.

- User-Defined Material Subroutine UMAT

  This file contains the information regarding the specific set of constitutive equations and the associated numerical integration procedure. This subroutine is called at each integration point during the ABAQUS solution procedure.

- User-Defined Displacement Boundary Condition Subroutine DISP

  This file is used to prescribe the kinematic boundary conditions for the model defined by the Input Date File. This subroutine is called at each increment of the solution process.

```
*HEADING
520 ELEMENT MODEL FOR 1100 ALUMINUM, PLANE STRAIN TENSION.
*NODE
    1 .0000E+00 .1200E+02 .0000E+00
    2 .4000E+01 .1200E+02 .0000E+00
    3 .8000E+01 .1200E+02 .0000E+00
    4 .1200E+02 .1200E+02 .0000E+00
    5 .1600E+02 .1200E+02 .0000E+00
    6 .0000E+00 .1400E+02 .0000E+00
    7 .4000E+01 .1400E+02 .0000E+00
    8 .8000E+01 .1400E+02 .0000E+00
    9 .1200E+02 .1400E+02 .0000E+00
   10 .1600E+02 .1400E+02 .0000E+00
   11 .0000E+00 .1600E+02 .0000E+00
   12 .4000E+01 .1600E+02 .0000E+00
   13 .8000E+01 .1600E+02 .0000E+00
   14 .1200E+02 .1600E+02 .0000E+00
   15 .1600E+02 .1600E+02 .0000E+00
   16 .0000E+00 .1900E+02 .0000E+00
   17 .4000E+01 .1900E+02 .0000E+00
   18 .8000E+01 .1900E+02 .0000E+00
   19 .1200E+02 .1900E+02 .0000E+00
   20 .1600E+02 .1900E+02 .0000E+00
   21 .0000E+00 .2200E+02 .0000E+00
   22 .4000E+01 .2200E+02 .0000E+00
   23 .8000E+01 .2200E+02 .0000E+00
   24 .1200E+02 .2200E+02 .0000E+00
   25 .1600E+02 .2200E+02 .0000E+00
   26 .0000E+00 .2500E+02 .0000E+00
   27 .4000E+01 .2500E+02 .0000E+00
   28 .8000E+01 .2500E+02 .0000E+00
   29 .1200E+02 .2500E+02 .0000E+00
   30 .1600E+02 .2500E+02 .0000E+00
    .     .          .          .
    .     .          .          .
    .     .          .          .
    .     .          .          .
    .     .          .          .
    .     .          .          .
  308 .1600E+02 .1000E+02 .0000E+00
  309 .1000E+01 .1050E+02 .0000E+00
  310 .0000E+00 .1100E+02 .0000E+00
  311 .2000E+01 .1100E+02 .0000E+00
  312 .3000E+01 .1050E+02 .0000E+00
  313 .5000E+01 .1050E+02 .0000E+00
  314 .4000E+01 .1100E+02 .0000E+00
  315 .7000E+01 .1050E+02 .0000E+00
  316 .6000E+01 .1100E+02 .0000E+00
  317 .9000E+01 .1050E+02 .0000E+00
  318 .8000E+01 .1100E+02 .0000E+00
  319 .1100E+02 .1050E+02 .0000E+00
  320 .1000E+02 .1100E+02 .0000E+00
  321 .1300E+02 .1050E+02 .0000E+00
  322 .1200E+02 .1100E+02 .0000E+00
  323 .1500E+02 .1050E+02 .0000E+00
  324 .1400E+02 .1100E+02 .0000E+00
  325 .1600E+02 .1100E+02 .0000E+00
  326 .1000E+01 .1150E+02 .0000E+00
  327 .2000E+01 .1200E+02 .0000E+00
  328 .3000E+01 .1150E+02 .0000E+00
  329 .5000E+01 .1150E+02 .0000E+00
  330 .7000E+01 .1150E+02 .0000E+00
  331 .6000E+01 .1200E+02 .0000E+00
```

```
  332 .9000E+01 .1150E+02 .0000E+00
  333 .1100E+02 .1150E+02 .0000E+00
  334 .1000E+02 .1200E+02 .0000E+00
  335 .1300E+02 .1150E+02 .0000E+00
  336 .1500E+02 .1150E+02 .0000E+00
  337 .1400E+02 .1200E+02 .0000E+00
*ELEMENT, TYPE=CPE4
    1  119  117  118  118
    2  118  114  119  119
    3  120  117  119  119
    4  119  114  116  116
    5  113  111  112  112
    6  116  111  113  113
    7  113  108  110  110
    8  112  108  113  113
    9  107  105  106  106
   10  106  102  107  107
   11  107  102  104  104
   12  110  105  107  107
   13  104  101   99   99
   14   99  101  100  100
   15  100   96   99   99
   16   99   96   98   98
   17  121  117  120  120
   18  118  117  121  121
   19  116  114  115  115
   20  115  111  116  116
   21  112  111  115  115
   22  115  114  118  118
   23  137  134  118  118
   24  121  136  118  118
   25  118  134  115  115
   26  118  136  137  137
   27  109  105  110  110
   28  110  108  109  109
   29  106  105  109  109
   30  109  108  112  112
    .    .    .    .    .
    .    .    .    .    .
    .    .    .    .    .
    .    .    .    .    .
    .    .    .    .    .
    .    .    .    .    .
    .    .    .    .    .
  490   54   57   72   53
  491   53   72   80   52
  492   52   80   88   51
  493   56   58   59   57
  494   57   59   73   72
  495   72   73   81   80
  496   80   81   89   88
  497   58   60   61   59
  498   59   61   74   73
  499   73   74   82   81
  500   81   82   90   89
  501   60   62   63   61
  502   61   63   75   74
  503   74   75   83   82
  504   82   83   91   90
  505   62   64   65   63
  506   63   65   76   75
  507   75   76   84   83
  508   83   84   92   91
```

```
   509    64    66    67    65
   510    66    68    69    67
   511    68    70    71    69
   512    65    67    77    76
   513    76    77    85    84
   514    84    85    93    92
   515    67    69    78    77
   516    69    71    79    78
   517    77    78    86    85
   518    85    86    94    93
   519    78    79    87    86
   520    86    87    95    94
*NSET,NSET=E1
98,99,104,107,110,113,116,119,120
*NSET,NSET=E2,GENERATE
123,310,17
*NSET,NSET=E2,GENERATE
1,51,5
*NSET,NSET=E2,GENERATE
88,92,1
*NSET,NSET=E2
97,98
*NSET,NSET=E3
92,93,94,95
*ELSET,ELSET=C
44,75,107,139,171,203,235,331
*ELSET,ELSET=C
16,13,11,7
*EQUATION
2
93,2,1.,92,2,-1.
2
94,2,1.,92,2,-1.
2
95,2,1.,92,2,-1.
*MPC
1,327,1,2
1,331,2,3
1,334,3,4
1,337,4,5
*PLOT
520 ELEMENT MESH
10,10,2.5,2.5
*DETAIL
0.0,0.0,0.0,17.0,18.5,0.0
*DRAW
*BOUNDARY,OP=NEW
E1,2,,0.
E2,1,,0.
E3,2,,0.
*MATERIAL
*USER MATERIAL,CONSTANTS=15
0.02,0.75,0.9,152.0,300.0,26000.0,68000.0,6.7D-6,
2.77,0.875,1.0,0.015,202.,0.34,775.0
*DEPVAR
8
*RESTART,WRITE,FREQUENCY=10
*STEP,INC=200,CYCLE=6,NLGEOM,AMP=RAMP
*VISCO,PTOL=10.0,CETOL=2.E-3
4.0E-8,6.0000E-4,1.0E-10
*BOUNDARY,OP=MOD
E3,2,,0.
*EL FILE,ELSET=C,DEPVAR,FREQ=1
```

```
2,2
2,2,2
1,1,1,1
*EL PRINT,DEPVAR,ELSET=C,FREQ=500
2,2
2,2,2
1,1,1,1
*NODE FILE,NSET=E3,FREQ=1
2,1,1,1,1,2
*NODE PRINT,NSET=E3,FREQ=500
2,1,1,1,1,2
*PLOT,FREQ=10
DEFORMED MESH
*DETAIL
0.0,0.0,0.0,17.0,32.0,0.0
*DISPLACED
1,1.,1
*PLOT,FREQ=10
EQUIVALENT PLASTIC STRAIN
*DETAIL
0.0,0.0,0.0,17.0,32.0,0.0
*CONTOUR
84
*PLOT,FREQ=10
EQUIVALENT PLASTIC SHEAR STRAIN RATE
*DETAIL
0.0,0.0,0.0,17.0,32.0,0.0
*CONTOUR
83
*PLOT,FREQ=10
TEMPERATURE
*DETAIL
0.0,0.0,0.0,17.0,32.0,0.0
*CONTOUR
82
*PLOT,FREQ=10
P
*DETAIL
0.0,0.0,0.0,17.0,32.0,0.0
*CONTOUR
85
*PLOT,FREQ=10
LAMBDA_1
*DETAIL
0.0,0.0,0.0,17.0,32.0,0.0
*CONTOUR
86
*PLOT,FREQ=10
LAMBDA_2
*DETAIL
0.0,0.0,0.0,17.0,32.0,0.0
*CONTOUR
87
*END STEP
```

```
      SUBROUTINE UMAT(STRESS,STATEV,DDSDDE,SSE,SPD,SCD,STRAN,DSTRAN,
     1  TIME,DTIME,TEMP,DTEMP,PREDEF,DPRED,MATERL,NDI,NSHR,NTENS,
     2  NSTATV,PROPS,NPROPS,COORDS)
C**********************************************************************
C  Isotropic Thermo-Elasto-Viscoplasticity with pressure sensitive
C  plastic flow and plastic dilatancy.
C**********************************************************************
C  This UMAT version interfaces with the *VISCO procedure in ABAQUS.
C  Automatic timestep control is done using the CEMAX parameter. The
C  timestep is decreased if CEMAX exceeds CETOL.
C**********************************************************************
C  This UMAT version is not for use in plane stress or any other cases
C  where more strain terms than stress terms are used.
C**********************************************************************
C State Variables:
C   STATEV(1) = S        (plastic flow resistance,tensile,suggested
C                         units are N/m2)
C   STATEV(2) = TH       (temperature,suggested units are Deg.K)
C Five more are for debugging and plotting purposes.
C   STATEV(3) = GAMPBDOT(plastic shear strain rate)
C   STATEV(4) = GAMPB                  (plastic shear strain)
C   STATEV(5) = P :(SS-(OMEGA*TAUB/RHO*C)*T)/R
C   STATEV(6) = LAMBDA_1 = INTEGRAL OF P SINCE t_{0}.
C    WHERE
C         SS=dTAUB/dGAMPB     ; STRAIN HARDENING
C          R=dTAUB/dGAMPBDOT  ; STRAIN RATE HARDENING
C          T=-dTAUB/dTH       ; THERMAL SOFTENING
C   STATEV(7) = LAMBDA_2 = INTEGRAL OF (-P) SINCE P CHANGES NEGATIVE.
C   STATEV(8) = THE VALUE OF GAMDOT WHEN P CHANGES NEGATIVE.
C      APRIL 13, 1987  KWON HEE KIM
C**********************************************************************
C Contents of PROPS vector in this version:
C J   PROPS(J)
C---  ----------
C 1   PLSLMT -- limit on equiv. plastic tensile strain increment
C 2   PHI -- degree of implicitness (ranges from 0 to 1)
C 3   OMEGA -- fraction of plastic work going into adiabatic heating
C 4   S0 -- initial value for internal variable S
C 5   T0 -- initial value for temperature
C 6   AMU -- shear modulus
C 7   AKAPPA -- bulk modulus
C 8   ALPHA -- thermal expansion coefficient
C 9   RHO -- density
C 10  C -- specific heat
C 11  GAMDOT0 -- REFERENCE STRAIN RATE
C 12  CM -- RATE CONSTANT
C 13  B -- STRENGTH COEFFICIENT
C 14  N -- STRAIN HARDENINNG EXPONENT
C 15  TM -- MELTING TEMPERATURE
C**********************************************************************
C See subroutines UMPROP, GAMDOT, and SDOT for suggested units for
C the above properties.
C**********************************************************************
C The parameter PHI controls the degree of implicitness of the
C integration procedure.
C    PHI=0.0   ---- explicit
C    PHI=1.0   ---- fully implicit
C Suggested value of PHI: equal to or greater than 0.50
C**********************************************************************
C The parameter OMEGA controls whether the problem is isothermal or
C adiabatic.
C    OMEGA=0.0  ---- isothermal
C    OMEGA=1.0  ---- adiabatic
```

```
C Suggested value for fast deformations is 0.9
C*************************************************************************
      IMPLICIT REAL*8(A-H,O-Z)
C*************************************************************************
C Common blocks CERROR and CONSTS appear here exactly as they exist in
C ABAQUS version 4-5-159. They will generally be different for other
C ABAQUS versions.
C*************************************************************************
      COMMON/CERROR/RESMAX(30),JNREMX(30),ERRMAX(2),CETOL,CSLIM,
     1  CEMAX,PCTOL,TLIMIT,PSUBIN,RESMIN,DUMAX(30),JNDUMX(30),ERRPRE,
     2  UDELSS,PTOL,AMTOL,DMKET,DMRETL,SIGTOL,DSIGMX,UTOL,UMAX,U4MAX,
     3  VMAX,V4MAX,AMAX,A4MAX,TMAX,EPPMAX,RMAX,R4MAX,NGOPEN,NGCLOS,
     4  ROTTOL,ROTFAC,JRIKND,NINCCS,RIKUB,RIKUMX,RIKMU,RIKLAM,RIKDLA,
     5  RIKRO,RIKOLD,RIKLMX,QMAX,DUMAXP,STRRAT,PCUT,RIKDLO
C*************************************************************************
      COMMON/CONSTS/PI,SIN60,COS60,KCROS2(3),KCROS3(3),ZERO,LZERO,LONE,
     1  ONE,TWO,HALF,ABIG,ASMALL,BCBIG,LOCSHR(2,3),THIRD,PRECIS,BLANK
C*************************************************************************
      DIMENSION STRESS(NTENS),STATEV(NSTATV),DDSDDE(NTENS,NTENS),
     1  STRAN(NTENS),DSTRAN(NTENS),PREDEF(1),DPRED(1),PROPS(NPROPS),
     2  COORDS(3)
C*************************************************************************
      SQART3=TWO*SIN60
      NDIP1=NDI+1
      PHIDT=PROPS(2)*DTIME
C*************************************************************************
C Initialize the state variables, if necessary.
C*************************************************************************
      IF (STATEV(1).LE.ZERO) THEN
      STATEV(1)=PROPS(4)
      STATEV(2)=PROPS(5)
      STATEV(4)=ZERO
      STATEV(6)=ZERO
      STATEV(7)=ZERO
      END IF
C*************************************************************************
C Set the state variables.
C*************************************************************************
      S=STATEV(1)
      TH=STATEV(2)
      GAMPB=STATEV(4)
C*************************************************************************
C Subroutine UMPROP determines AMU,AKAPPA,ALPHA,RHO,and C based upon
C the temperature TH, using data supplied in PROPS. For the present
C case, the properties are assumed constant and input directly in PROPS.
C In other cases, additional data constants defining functions of TH for
C each property may be input.
C*************************************************************************
      CALL UMPROP (AMU,AKAPPA,ALPHA,RHO,C,TH,PROPS,NPROPS)
C*************************************************************************
C Pressure PB and equivalent shear stress TAUB
C*************************************************************************
      CALL SINV (STRESS,SINV1,SINV2)
      TAUB=SINV2/SQART3
      TAUBOLD=TAUB
      PB=-SINV1
C*************************************************************************
C Subroutine GAMDOT determines the equivalent plastic shear strain rate
C F and its derivatives PDA,PDB,PDC,PDD with respect to TAUB,PB,TH,and
C S, respectively. To make the subsequent calculations more convenient,
C PDB,PDC, and PDD are returned as:
C         RATIOB =  PDB/PDA
C         RATIOC =  PDC/PDA
```

```
C          RATIOD =  PDD/PDA
C*************************************************************************
      CALL GAMDOT (IERROR,TAUB,PB,TH,S,PROPS,NPROPS,SQART3,
     1             F1,PDA,RATIOB,RATIOC,RATIOD)
      IF(IERROR.EQ.1)THEN
      WRITE(6,5000)
 5000 FORMAT(1H1,10X,43H**ERROR IN UMAT -- INPUT STRESS INCORRECT     )
      WRITE(6,5001)
 5001 FORMAT(11X,32HTAUB TOO LARGE FOR GAMDOT CALC     )
      STOP
      END IF
      AMUB=AMU*TAUB/(TAUB+AMU*PHIDT*F1)
C*************************************************************************
C Subroutine SBETA determines the value of the plastic dilatancy
C factor BETA. Presently set to zero.
C*************************************************************************
      CALL SBETA (TAUB,PB,TH,S,BETA)
C*************************************************************************
      IF (PROPS(3).GT.ZERO) THEN
      CON1=PROPS(3)*(TAUB-BETA*PB)/(RHO*C)
      ELSE
      CON1=ZERO
      END IF
C*************************************************************************
C Subroutine SDOT determines the hardening rate H and the static
C restoration rate RDOT.
C*************************************************************************
      CALL SDOT(TAUB,PB,TH,S,GAMPB,AMU,PROPS,NPROPS,SQART3,F1,H,RDOT)
      DR=RDOT*DTIME
C*************************************************************************
      G=AMU-(RATIOB*AKAPPA*BETA+RATIOC*CON1+RATIOD*H)
      V=PHIDT*PDA*G
      V1=F1*DTIME/(ONE+V)
      V2=PHIDT*PDA/(ONE+V)
C*************************************************************************
C Trace of strain increment -- DVOL
C*************************************************************************
      DVOL=ZERO
      DO 10 K1=1,NDI
   10 DVOL=DVOL+DSTRAN(K1)
C*************************************************************************
C Convert stress to deviatoric stress.
C*************************************************************************
      DO 20 K1=1,NDI
   20 STRESS(K1)=STRESS(K1)+PB
C*************************************************************************
C Deviatoric stress times strain increment -- SDSI
C*************************************************************************
      SDSI=ZERO
      DO 30 K1=1,NTENS
   30 SDSI=SDSI+STRESS(K1)*DSTRAN(K1)
C*************************************************************************
C Effective plastic shear strain increment.
C*************************************************************************
      DGAMPB=V1+V2*(AMU*SDSI/TAUB-AKAPPA*RATIOB*DVOL)
C*************************************************************************
C Increments DS and DTH.
C*************************************************************************
      DS=H*DGAMPB-DR
      DTH=CON1*DGAMPB
C*************************************************************************
C Constants for Jacobian and stress increment.
C*************************************************************************
```

```
      V3=TWO*AMUB
      V11=AKAPPA-TWO*THIRD*AMUB
      V4=V11*DVOL
      V5=AKAPPA*ALPHA*DTH/THIRD
      V6=AKAPPA*BETA*DGAMPB
      V7=V4-V5-V6
      V8=AMU*DGAMPB/TAUB-(AMU-AMUB)*SDSI/TAUB**2
      V9=AMUB
      V12=(V2*AMU**2+AMUB-AMU)/TAUB**2
      V13=-V2*AKAPPA*RATIOB*AMU/TAUB
      V14=V2*AKAPPA*(AMU/TAUB)*(BETA+CON1*ALPHA/THIRD)
      V15=-V2*AKAPPA**2*RATIOB*(BETA+CON1*ALPHA/THIRD)
      V16=V11-V15
C*************************************************************************
C Calculate the Jacobian, which is nonsymmetric unless V13=V14. This
C is generally true only if OMEGA=0, BETA=0, and PDB=0. Otherwise,
C ABAQUS will use only the symmetric part of the Jacobian unless an
C unsymmetric Jacobian has been called for on the title card.
C Note that STRESS used here is the deviatoric stress.
C*************************************************************************
C The Jacobian has been made symmetric in this version.
C*************************************************************************
      V13=HALF*(V13+V14)
      V14=V13
C*************************************************************************
      DO 40 K1=1,NTENS
      DO 40 K2=1,NTENS
   40 DDSDDE(K1,K2)=-V12*STRESS(K1)*STRESS(K2)
      DO 50 K1=1,NDI
      DO 50 K2=1,NTENS
      DDSDDE(K1,K2)=DDSDDE(K1,K2)-V14*STRESS(K2)
   50 DDSDDE(K2,K1)=DDSDDE(K2,K1)-V13*STRESS(K2)
      DO 60 K1=1,NDI
      DDSDDE(K1,K1)=DDSDDE(K1,K1)+V3
      DO 60 K2=1,NDI
   60 DDSDDE(K1,K2)=DDSDDE(K1,K2)+V16
      IF (NSHR.GT.0) THEN
      DO 70 K1=NDIP1,NTENS
   70 DDSDDE(K1,K1)=DDSDDE(K1,K1)+V9
      END IF
C*************************************************************************
C Calculate complete STRESS at the end of the increment using the
C deviatoric stress at the beginning of the increment.
C*************************************************************************
      DO 80 K1=1,NDI
   80 STRESS(K1)=(ONE-V8)*STRESS(K1)+V3*DSTRAN(K1)+V7-PB
      IF (NSHR.GT.0) THEN
      DO 90 K1=NDIP1,NTENS
   90 STRESS(K1)=(ONE-V8)*STRESS(K1)+V9*DSTRAN(K1)
      END IF
C*************************************************************************
C Update the state variables.
C*************************************************************************
      CALL SINV (STRESS,SINV1,SINV2)
      TAUB=SINV2/SQART3
      TAUBNEW=TAUB
      PB=-SINV1
      TH=TH+DTH
      S=S+DS
      CALL GAMDOT (IERROR,TAUB,PB,TH,S,PROPS,NPROPS,SQART3,
     1             F2,PDA,RATIOB,RATIOC,RATIOD)
      IF(IERROR.EQ.1)THEN
      CEMAX=TWO*CETOL
```

```
      F2=F1
      END IF
      STATEV(1)=S
      STATEV(2)=TH
      STATEV(3)=F2
      STATEV(4)=STATEV(4)+DGAMPB
      CON3=PROPS(3)*TAUB/(RHO*C)
      CON4=STATEV(5)
      STATEV(5)=PDA*(-1.*H*RATIOD-CON3*RATIOC)
      STATEV(6)=STATEV(6)+(CON4+STATEV(5))*DTIME/2
      IF(STATEV(5).GE.0.0) THEN
      STATEV(8) = STATEV(3)
      GO TO 100
      END IF
      STATEV(7)=STATEV(7)-(CON4+STATEV(5))*DTIME/2
C*************************************************************************
C Comparison of the plastic strain rates before and after the time
C increment. To be used by the automatic integration scheme of ABAQUS.
C Note that the factor SQART3 is used to convert shear strain to
C tensile strain.
C*************************************************************************
100   DIFF=DTIME*DABS(F1-F2)/SQART3
      CEMAX=DMAX1(CEMAX,DIFF)
C*************************************************************************
C Check magnitude of plastic strain increment against a reference level.
C This allows the automatic timestep control in ABAQUS to limit the size
C of the plastic strain increment using the variable CEMAX.
C*************************************************************************
      PLSLMT=PROPS(1)*SQART3
      IF (PLSLMT.GT.ZERO) THEN
      PLSCHK=(DGAMPB/PLSLMT)*CETOL
      CEMAX=DMAX1(CEMAX,PLSCHK)
      END IF
      RETURN
      END
C*************************************************************************

C*************************************************************************
      SUBROUTINE UMPROP (AMU,AKAPPA,ALPHA,RHO,C,TH,PROPS,NPROPS)
C*************************************************************************
C Determine the following constants for the material:
C AMU ---- shear modulus (suggested units: N/m2)
C AKAPPA - bulk modulus (suggested units: N/m2)
C ALPHA -- thermal expansion coefficient (suggested units: 1/Deg.K)
C RHO ---- mass density (suggested units: kg/m3)
C C ------ specific heat (suggested units: Joules/kg/Deg.K)
C In general, these properties are functions of temperature, but in
C the present case they are input directly, assuming no temperature
C dependence. Additional entries in PROPS could be used to define them
C as functions of temperature.
C*************************************************************************
      IMPLICIT REAL*8(A-H,O-Z)
C*************************************************************************
      DIMENSION PROPS(NPROPS)
C*************************************************************************
      AMU=PROPS(6)
      AKAPPA=PROPS(7)
      ALPHA=PROPS(8)
      RHO=PROPS(9)
      C=PROPS(10)
C*************************************************************************
      RETURN
      END
```

```
C*********************************************************************

C*********************************************************************
      SUBROUTINE SBETA (TAUB,PB,TH,S,BETA)
C*********************************************************************
C Subroutine SBETA determines the plastic dilatancy factor.
C*********************************************************************
      IMPLICIT REAL*8(A-H,O-Z)
C*********************************************************************
      BETA=0.0D+0
C*********************************************************************
      RETURN
      END
C*********************************************************************

C*********************************************************************
      SUBROUTINE GAMDOT (IERROR,TAUB,PB,TH,S,PROPS,NPROPS,SQART3,
     1                   F,PDA,RATIOB,RATIOC,RATIOD)
C*********************************************************************
C Subroutine GAMDOT determines the equivalent plastic shear strain rate
C and its derivatives PDA,PDB,PDC,PDD with respect to TAUB,PB,TH,and S,
C respectively. Note that the following derivative terms are returned:
C             RATIOB = PDB/PDA
C             RATIOC = PDC/PDA
C             RATIOD = PDD/PDA
C*********************************************************************
      IMPLICIT REAL*8(A-H,O-Z)
C*********************************************************************
      COMMON/CONSTS/PI,SIN60,COS60,KCROS2(3),KCROS3(3),ZERO,LZERO,LONE,
     1  ONE,TWO,HALF,ABIG,ASMALL,BCBIG,LOCSHR(2,3),THIRD,PRECIS,BLANK
C*********************************************************************
      DIMENSION PROPS(NPROPS)
C*********************************************************************
C Material parameters defining the equivalent plastic shear strain rate
C PROPS(11)=GAMDOT0 REFERENCE STRAIN RATE
C PROPS(12)=CM RATE CONSTANT
C PROPS(13)=B -- STRENGTH COEFFICIENT
C PROPS(14)=N -- STRAIN HARDENING EXPONENT
C PROPS(15)=TM -- MELTING TEMPERATURE
C*********************************************************************
      IF(TAUB.LT.1.E-20) TAUB=1.E-20
      THFAC=((PROPS(15)-TH)/(PROPS(15)-PROPS(5)))**2
      SEFF=S*THFAC
      IF(SEFF.LE.0.0D0)THEN
      PRINT*,' SEFF.LE.0'
      CALL XIT
      END IF
      CHECK1=DLOG10(DABS(TAUB-SEFF))
      CHECK2=DLOG10(SEFF*PROPS(12))+40.D0
      IF(CHECK1.GT.CHECK2)THEN
      IERROR=1
      RETURN
      END IF
      XP=ONE/PROPS(12)
      FAC=((TAUB/SEFF)-ONE)*XP
      CHECK=DLOG10(PROPS(11))+(FAC/2.3026D0)
C*********************************************************************
      IF (CHECK.GT.40.D0) THEN
      IERROR=1
      ELSE IF (CHECK.GT.-40.D0)THEN
      F=PROPS(11)*DEXP(FAC)
      PDA=F*XP/SEFF
      RATIOB=ZERO
```

```
      RATIOC=2.D0*TAUB/(PROPS(15)-TH)
      RATIOD=-TAUB/S
      ELSE
      F=ZERO
      PDA=ZERO
      RATIOB=ZERO
      RATIOC=ZERO
      RATIOD=ZERO
      END IF
C*************************************************************************
C*************************************************************************
      RETURN
      END
C*************************************************************************
C*************************************************************************
      SUBROUTINE SDOT (TAUB,PB,TH,S,GAMPB,AMU,PROPS,NPROPS,SQART3,
     +                 F,H,RDOT)
C*************************************************************************
C This subroutine determines the hardening rate H.
C*************************************************************************
      IMPLICIT REAL*8(A-H,O-Z)
C*************************************************************************
      COMMON/CONSTS/PI,SIN60,COS60,KCROS2(3),KCROS3(3),ZERO,LZERO,LONE,
     1  ONE,TWO,HALF,ABIG,ASMALL,BCBIG,LOCSHR(2,3),THIRD,PRECIS,BLANK
C*************************************************************************
      DIMENSION PROPS(NPROPS)
C*************************************************************************
C Material parameters determining the rate of hardening:
C PROPS(13)=B -- STRENGTH COEFFICIENT IN STRAIN HARDENING EXPRESSION
C PROPS(14)=N -- STRAIN HARDENING EXPRESSION
C*************************************************************************
C Calculate H.
C CALCULATE RDOT
C*************************************************************************
      B= PROPS(13)
      AN = PROPS(14)
      IF (GAMPB.LE.0.001) THEN
      GAMPB=0.001
      END IF
      H= AN*B*GAMPB**(AN-ONE)
      RDOT=ZERO
      RETURN
      END
```

```
SUBROUTINE DISP (U,KSTEP,KINC,TIME,NODE,JDOF)
IMPLICIT REAL*8(A-H,O-Z)
D =21478.52286*TIME
U = 0.0
IF (JDOF.EQ.2 .AND. NODE.EQ.92)U = D
RETURN
END
```

List of Figures

Fig. 1 Schematic behavior of the function $f_2 = \cos(2\chi)[\cos(2\chi) + P^\circ]$ with respect to χ at a fixed P°. The maximum negative value of f_2 is $f_2^* = -(P^\circ/2)^2$, and it occurs at orientations $\chi^* = \pm[(\pi/4) + (P^\circ/4)]$.

Fig. 2a Schematic behavior of the function $H(\chi) = [\rho c S^\circ \chi_1 - \omega \bar{\tau}^\circ T^\circ(2\chi_1 - 1)]$, where $\chi_1 = \sin^2 2\chi$ with respect to orientation χ.

Fig. 2b Schematic behavior of the function $R^\circ\chi_1 + \mu^\circ(1 - \chi_1)$ as a function of orientation χ.

Fig. 3 Schematic of shear band orientations with respect to the maximum stretching direction $\hat{\mathbf{e}}_1$ in a simple shearing motion for which the velocity is given by $\mathbf{v} = 2\alpha(\mathbf{e}_1 \otimes \mathbf{e}_2)(\mathbf{x} - \mathbf{0})$.

Fig. 4 Shear bands in polycarbonate. Thin polished sections from a region near point A in the skectch above were viewed in transmission (dark-field) through a polarizing microscope. Note that two sets of shear bands are formed.

Fig. 5 Finite element mesh for the simulation of plane strain tests on AMS 6418 steel and aluminum 2024-T351. The 320 element mesh represents one quarter of the specimen.

Fig. 6 Deformed mesh and the contour plots of the parameters $\bar{\gamma}^p$, θ, $\dot{\bar{\gamma}}^p$, P and λ at time t_1 when P changes its sign from positive to negative throughout the specimen. Adiabatic plane strain compression of AMS 6418 steel.

Fig. 7 Deformed mesh and the contour plots of the parameters $\bar{\gamma}^p$, θ, $\dot{\bar{\gamma}}^p$, P and λ at time t_2 when there necleates a zone of noticeable size where $\lambda > 10$ in the specimen. Note that the total load is at its maximum and contours show definite signs of localization. Adiabatic plane strain compression of AMS 6418 steel.

Fig. 8 Deformed mesh and the contour plots of the parameters $\bar{\gamma}^p$, θ, $\dot{\bar{\gamma}}^p$, P and λ at time t_3 when shear localization is fully developed. Note that the total load is rapidly decreasing and mesh is heavily distorted along the shear band. Adiabatic plane strain compression of AMS 6418 steel.

Fig. 9 Deformed mesh and the contour plots of the parameters $\bar{\gamma}^p$, θ, $\dot{\bar{\gamma}}^p$, P and λ at time t_1 when P changes its sign from positive to negative throughout the specimen. Adiabatic plane strain compression of aluminum 2024-T351.

Fig. 10 Deformed mesh and the contour plots of the parameters $\bar{\gamma}^p$, θ, $\dot{\bar{\gamma}}^p$, P and λ at time t_2 when there necleates a zone of noticeable size where $\lambda > 10$ in the specimen. Note that the total load is at its maximum and contours show definite signs of localization. Adiabatic plane strain compression of aluminum 2024-T351.

Fig. 11 Deformed mesh and the contour plots of the parameters $\bar{\gamma}^p$, θ, $\dot{\bar{\gamma}}^p$, P and λ at time t_3 when shear localization is fully developed. Note that the total load is rapidly decreasing and mesh is heavily distorted along the shear band. Adiabatic plane strain compression of aluminum 2024-T351.

Fig. 12 Finite element mesh for the simulation of a plane strain tension test on AMS 6418 steel. The 456 element mesh represents one quarter of the specimen. All subsequent figures show only the region A and the associated level contours of various quantities.

Fig. 13 Deformed mesh and the contour plots of the parameters $\bar{\gamma}^p$, θ, $\dot{\bar{\gamma}}^p$, P and λ at time t_1 when there first forms a region of negative P across the neck of the specimen. Adiabatic plane strain tension of AMS 6418 steel.

Fig. 14 Deformed mesh and the contour plots of the parameters $\bar{\gamma}^p$, θ, $\dot{\bar{\gamma}}^p$, P and λ at time t_2 when there necleates a zone of noticeable size where $\lambda > 10$ in the at the central region of the neck. Note that the total load at the beginning of the secondary slope and the level contours show definite signs of shear localization. Adiabatic plane strain tension of AMS 6418 steel.

Fig. 15 Deformed mesh and the contour plots of the parameters $\bar{\gamma}^p$, θ, $\dot{\bar{\gamma}}^p$, P and λ at time t_3 when shear localization is fully developed. Note that the total load is rapidly decreasing and mesh is heavily distorted along the shear band. Adiabatic plane strain tension of AMS 6418 steel.

Fig. 16 Finite element mesh for the simulation of a plane strain tension test on aluminum 2024-T351. The 520 element mesh represents one quarter of the specimen. All subsequent figures show only the region A and the associated level contours of various quantities.

Fig. 17 Deformed mesh and the contour plots of the parameters $\bar{\gamma}^p$, θ, $\dot{\bar{\gamma}}^p$, P and λ at time t_1 when there first forms a region of negative P across the neck of the specimen. Adiabatic plane strain tension of aluminum 2024-T351.

Fig. 18 Deformed mesh and the contour plots of the parameters $\bar{\gamma}^p$, θ, $\dot{\bar{\gamma}}^p$, P and λ at time t_2 when there necleates a zone of noticeable size where $\lambda > 10$ in the at the central region of the neck. Note that the total load at the beginning of the secondary slope and the level contours show definite signs of shear localization. Adiabatic plane strain tension of aluminum 2024-T351.

Fig. 19 Deformed mesh and the contour plots of the parameters $\bar{\gamma}^p$, θ, $\dot{\bar{\gamma}}^p$, P and λ at time t_3 when shear localization is fully developed. Note that the total load is rapidly decreasing and mesh is heavily distorted along the shear band. Adiabatic plane strain tension of aluminum 2024-T351.

Fig. 20 Finite element mesh for the simulation of adiabatic plane strain bending of a U-notched AMS 6418 steel specimen. The 542 element mesh represents one half of the specimen.

All subsequent figures show only the region A and the associated level contours of various quantities.

Fig. 21 Deformed mesh and the contour plots of the parameters $\bar{\gamma}^p$, θ, $\dot{\bar{\gamma}}^p$, P and λ at time t_1 when there first forms two regions of negative P in the deforming regions under the notch and under the back surface of the notch. The deformation field is extremely inhomogenous but there are no signs of shear localization. Adiabatic plane strain bending of a U-notched AMS 6418 steel specimen.

Fig. 22 Deformed mesh and the contour plots of the parameters $\bar{\gamma}^p$, θ, $\dot{\bar{\gamma}}^p$, P and λ at time t_2 when there forms two zones of noticeable size where $\lambda > 10$ in both of the deforming regions under the notch and under the back surface of the notch. Deformed mesh begins to show signs of shear localization at this stage. Adiabatic plane strain bending of a U-notched AMS 6418 steel specimen.

Fig. 23 Deformed mesh and the contour plots of the parameters $\bar{\gamma}^p$, θ, $\dot{\bar{\gamma}}^p$, P and λ at time t_3 when shear localization is fully developed. Mesh is heavily distorted along the shear bands in two regions above and below the neutral plane. Adiabatic plane strain bending of a U-notched AMS 6418 steel specimen.

Fig. 24 Qualitative time trajectories of the field variables related to the term $[1+(\dot{\bar{\gamma}}^p)^{-1}\int_{t_i}^{t} Q\exp(-\lambda)dt]$ in equation (82).

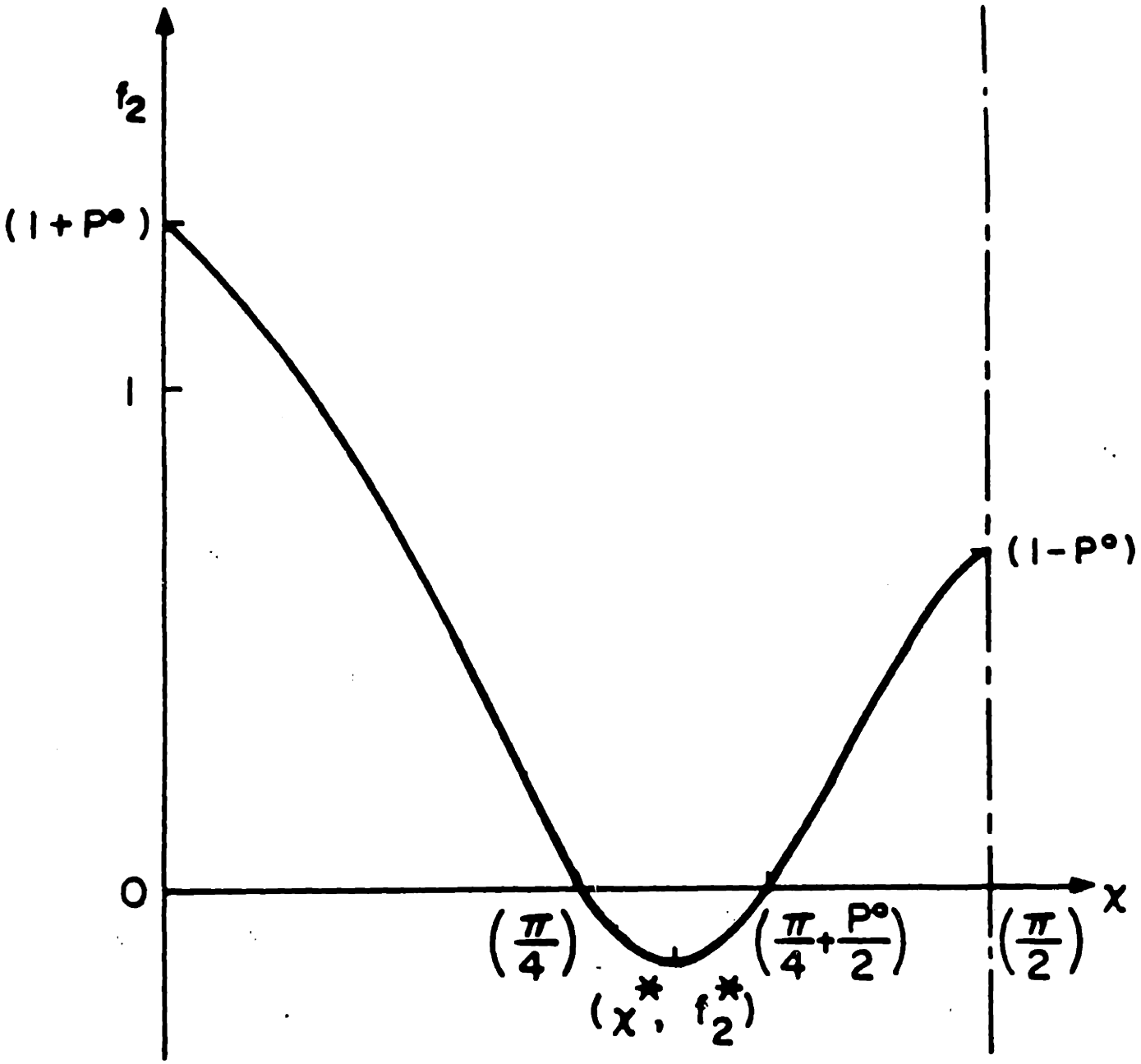

Fig. 1 Schematic behavior of the function $f_2 = \cos(2\chi)[\cos(2\chi) + P^\circ]$ with respect to χ at a fixed P°. The maximum negative value of f_2 is $f_2^* = -(P^\circ/2)^2$, and it occurs at orientations $\chi^* = \pm[(\pi/4) + (P^\circ/4)]$.

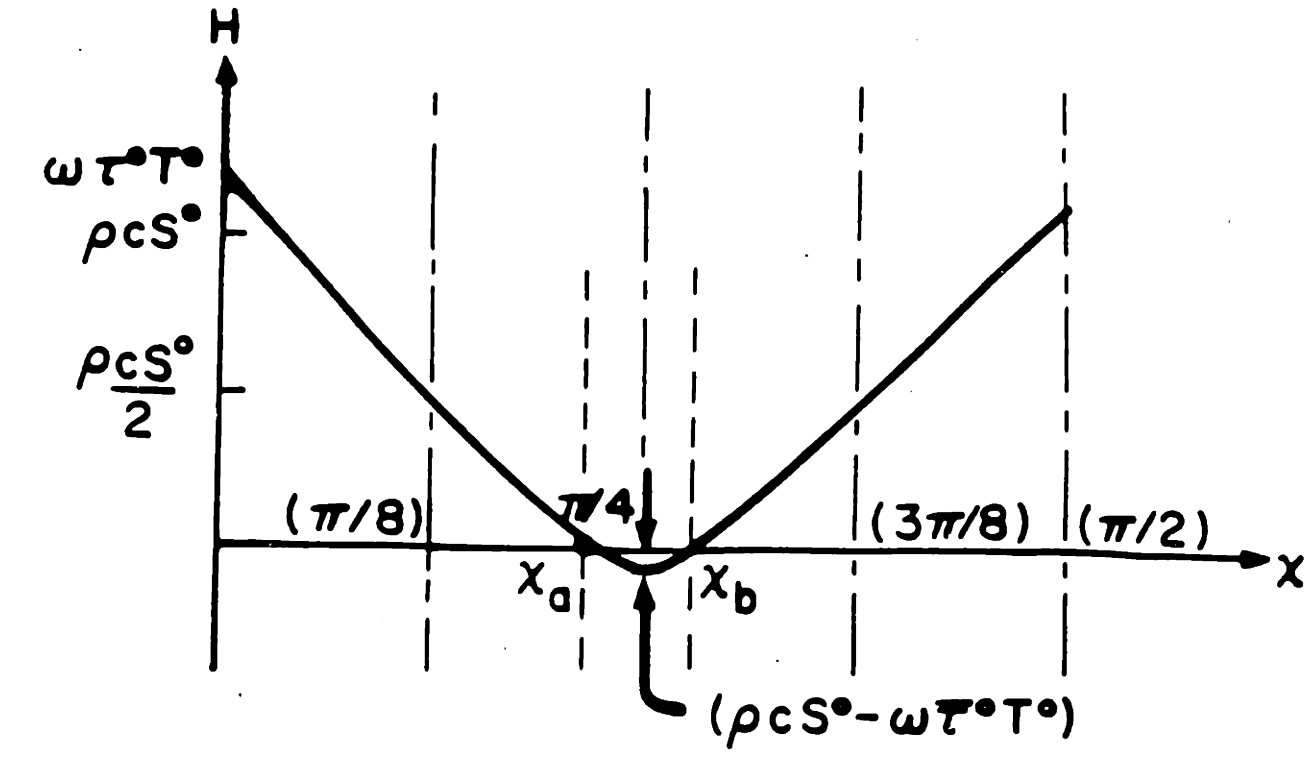

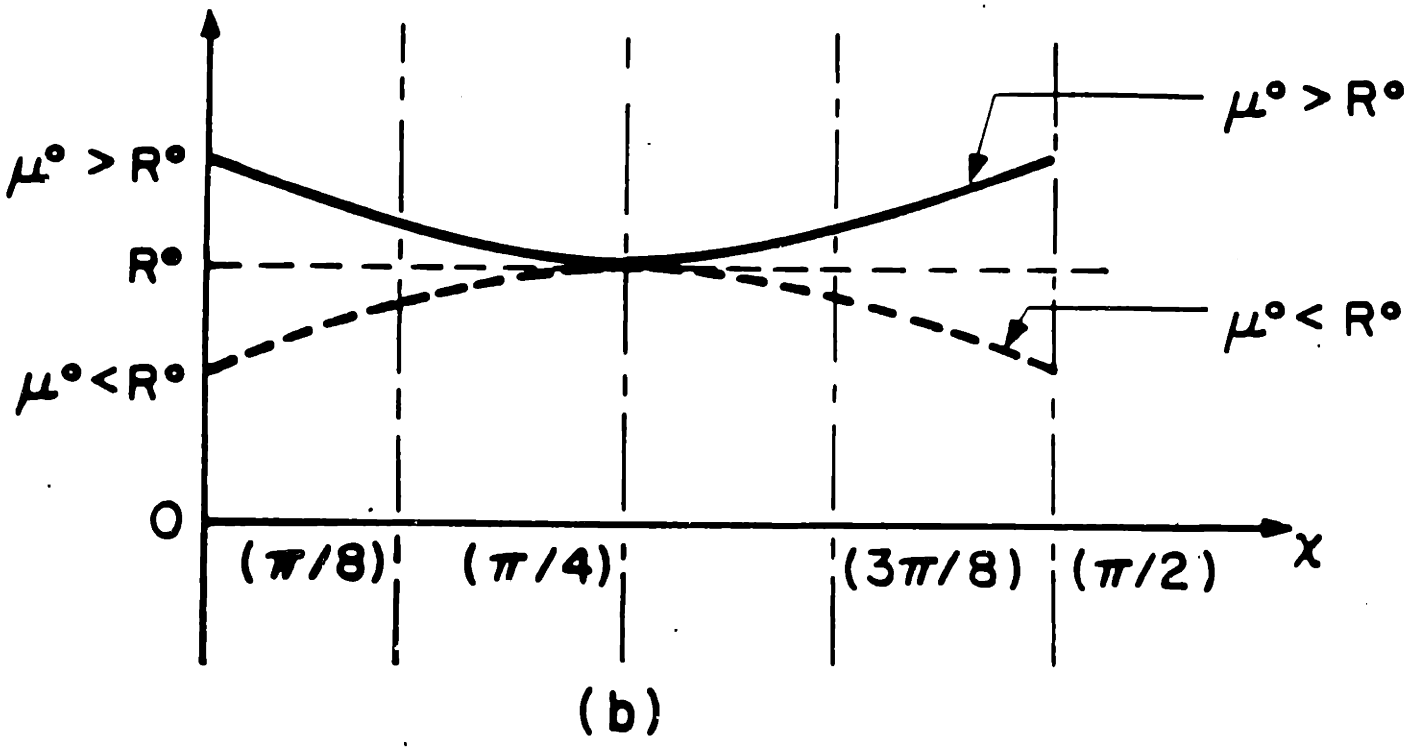

Fig. 2a Schematic behavior of the function $H(\chi) = [\rho cS^\circ \chi_1 - \omega\bar{\tau}^\circ T^\circ(2\chi_1 - 1)]$, where $\chi_1 = \sin^2 2\chi$ with respect to orientation χ.

2b Schematic behavior of the function $R^\circ\chi_1 + \mu^\circ(1 - \chi_1)$ as a function of orientation χ.

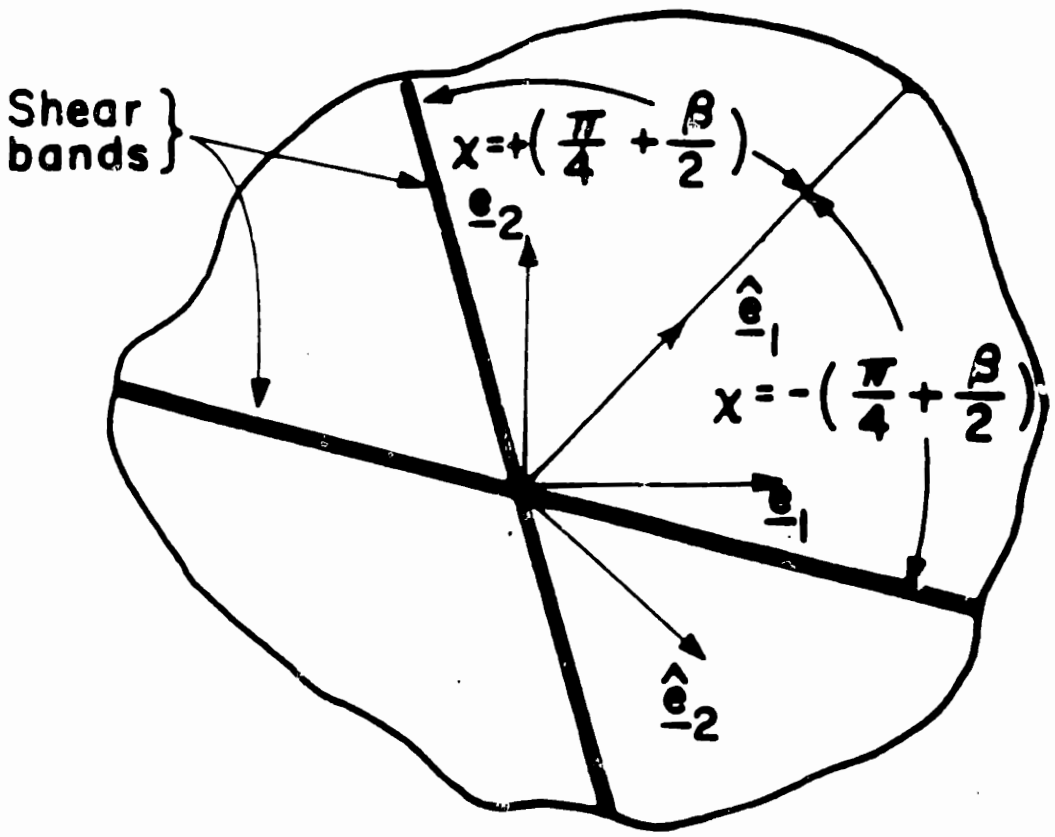

Fig. 3 Schematic of shear band orientations with respect to the maximum stretching direction $\hat{\mathbf{e}}_1$ in a simple shearing motion for which the velocity is given by $\mathbf{v} = 2\alpha(\mathbf{e}_1 \otimes \mathbf{e}_2)(\mathbf{x} - 0)$.

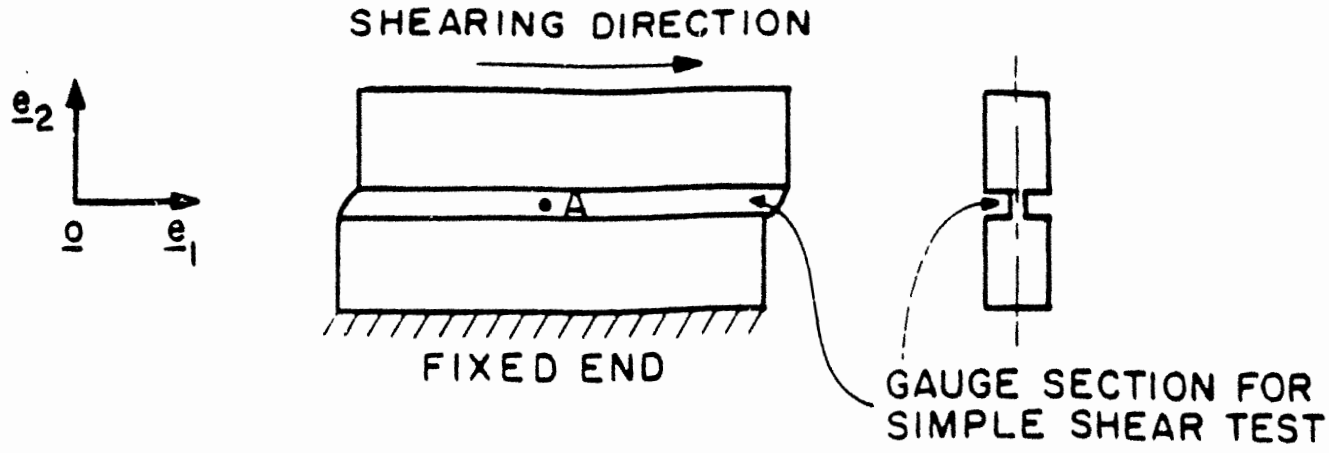

The micrograph below was taken from a region near point A which is sufficiently removed from end effects.

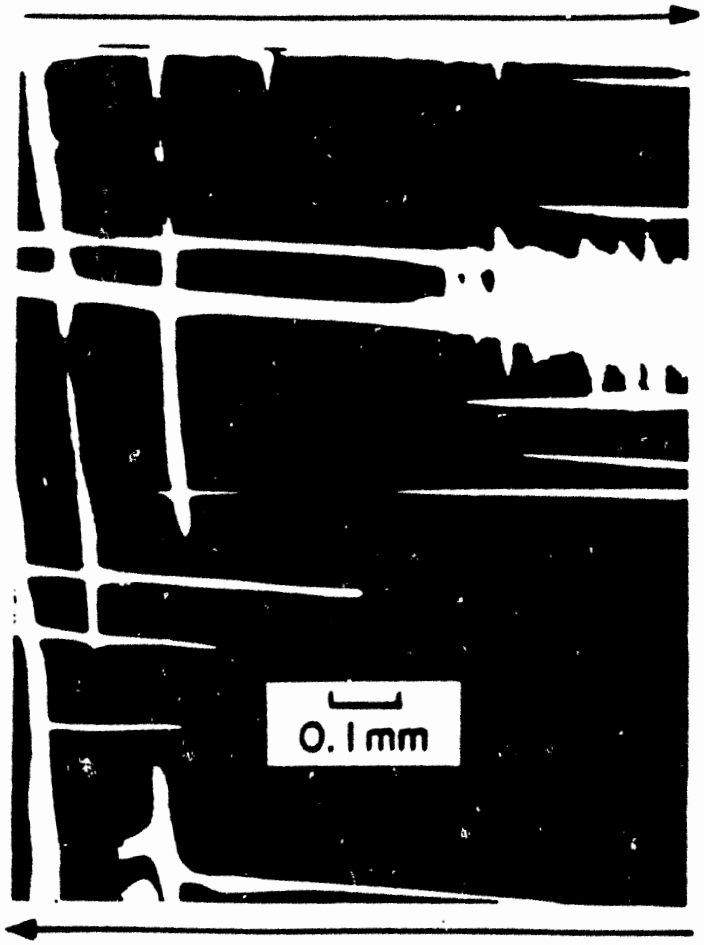

Fig. 4 Shear bands in polycarbonate. Thin polished sections from a region near point A in the skectch above were viewed in transmission (dark-field) through a polarizing microscope. Note that two sets of shear bands are formed.

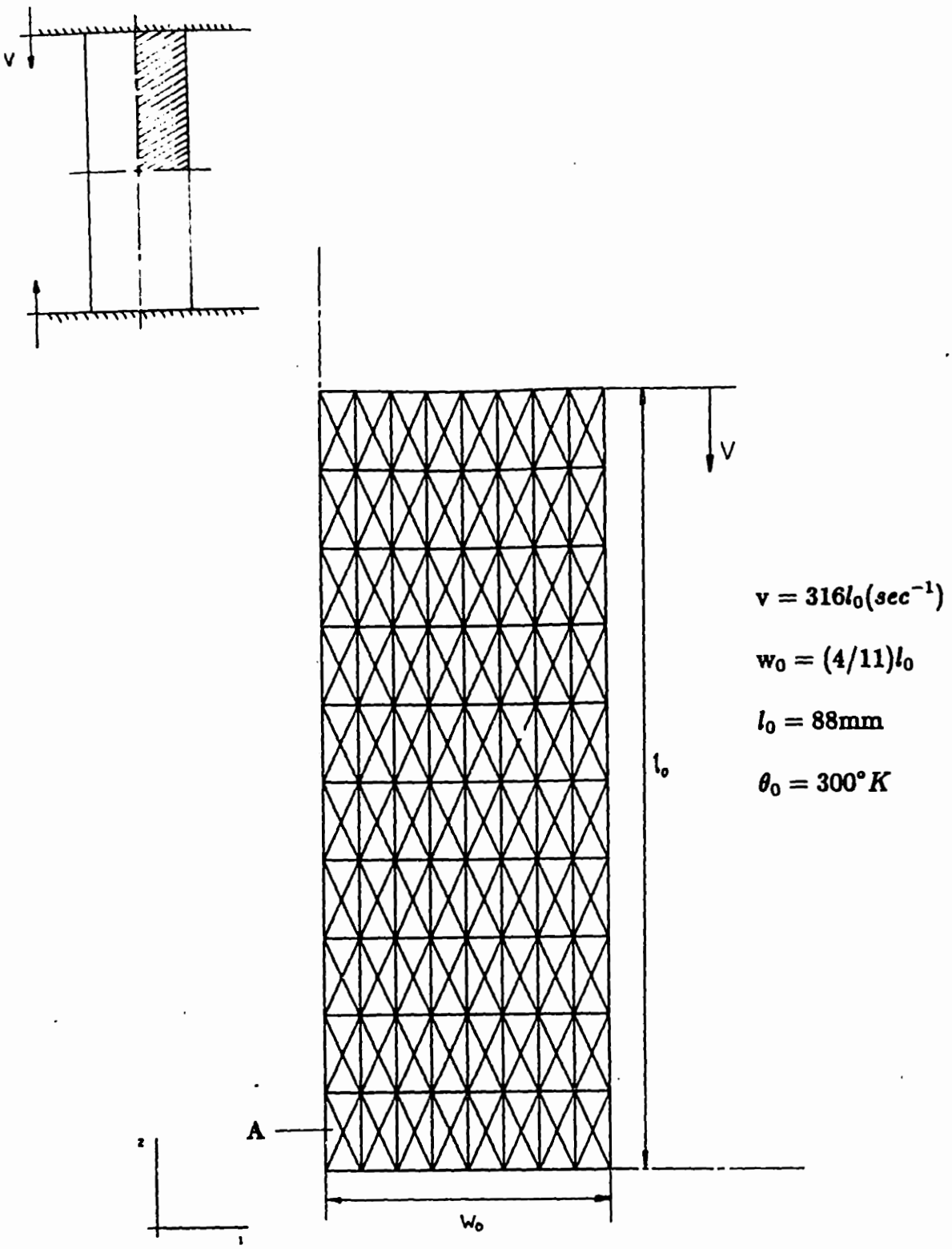

Fig. 5 Finite element mesh for the simulation of plane strain tests on AMS 6418 steel and aluminum 2024-T351. The 320 element mesh represents one quarter of the specimen.

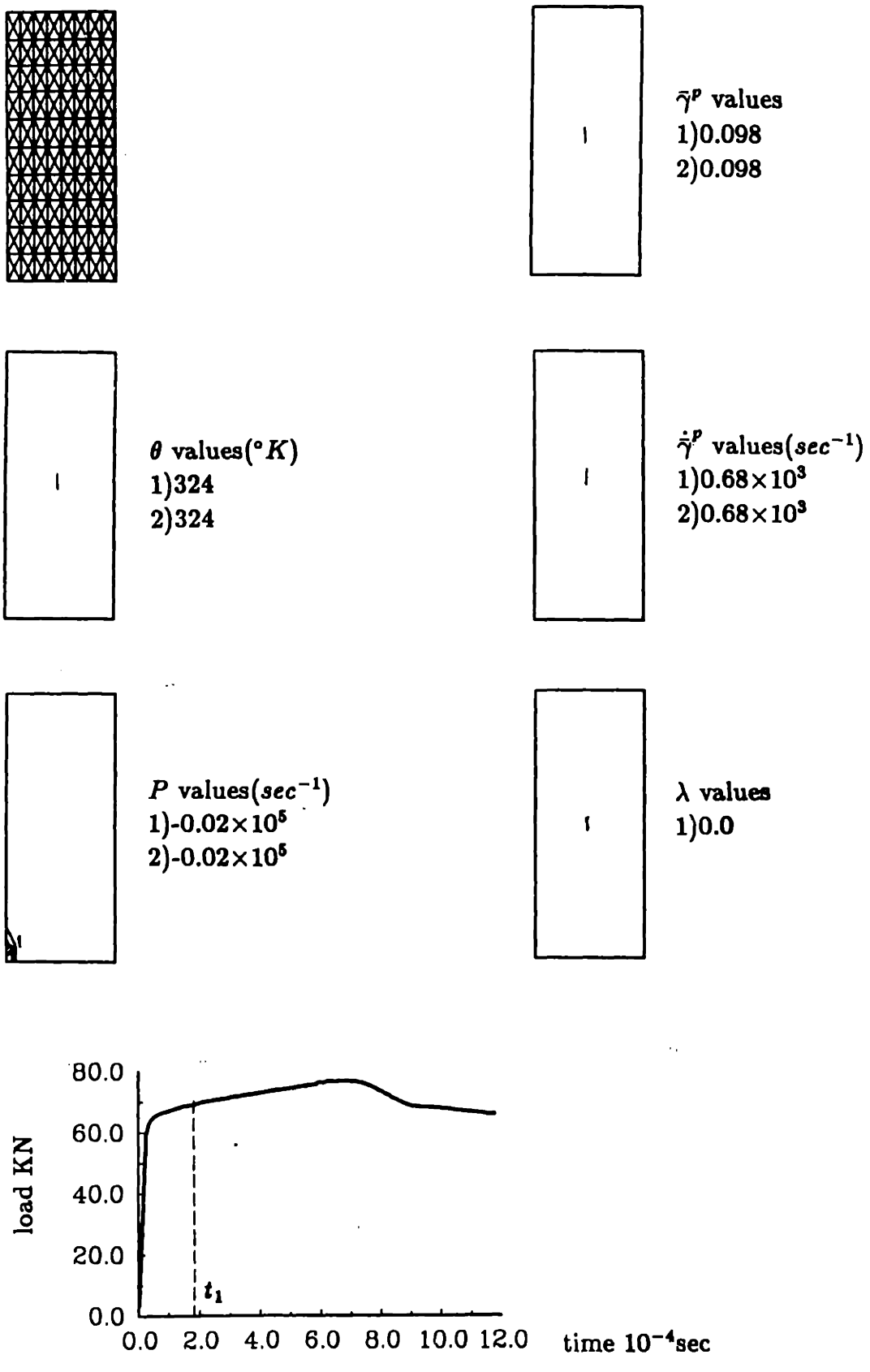

Fig. 6 Deformed mesh and the contour plots of the parameters $\bar{\gamma}^p$, θ, $\dot{\bar{\gamma}}^p$, P and λ at time t_1 when P changes its sign from positive to negative throughout the specimen. Adiabatic plane strain compression of AMS 6418 steel.

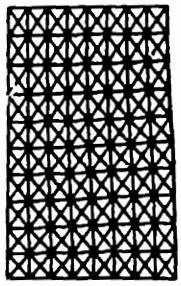

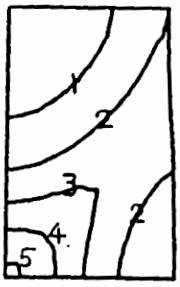

$\bar{\gamma}^p$ values
1)0.45
2)0.50
3)0.55
4)0.60
5)0.65

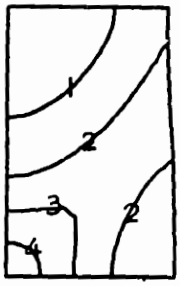

θ values($^\circ K$)
1)410
2)423
3)436
4)450

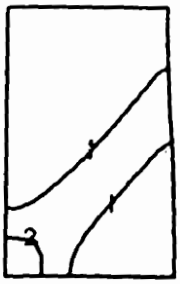

$\dot{\bar{\gamma}}^p$ values(sec^{-1})
1)1.33×10^3
2)2.66×10^3

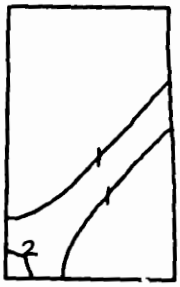

P values(sec^{-1})
1)-0.5×10^5
2)-1.0×10^5

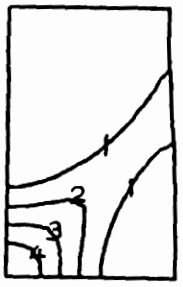

λ values
1)10.0
2)11.0
3)12.0
4)13.0

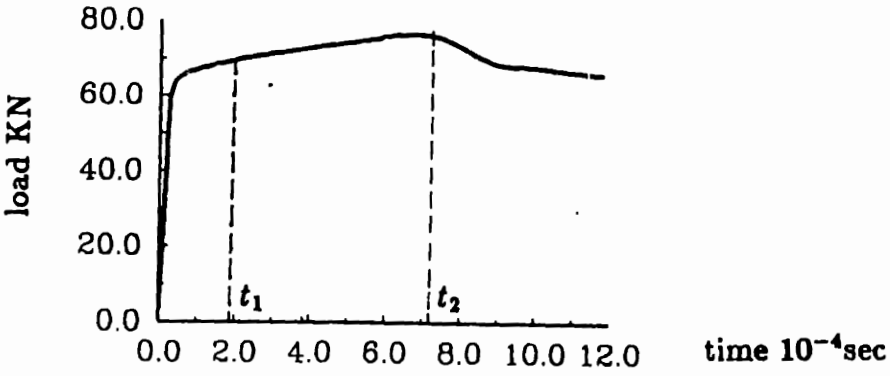

Fig. 7 Deformed mesh and the contour plots of the parameters $\bar{\gamma}^p$, θ, $\dot{\bar{\gamma}}^p$, P and λ at time t_2 when there necleates a zone of noticeable size where $\lambda > 10$ in the specimen. Note that the total load is at its maximum and contours show definite signs of localization. Adiabatic plane strain compression of AMS 6418 steel.

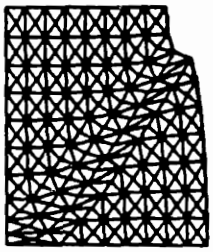

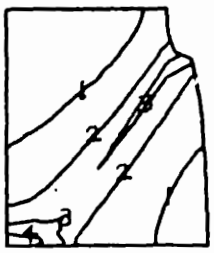

$\bar{\gamma}^p$ values
1)0.5
2)1.0
3)1.5
4)2.0

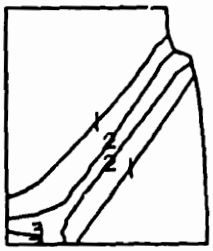

θ values($^\circ K$)
1)500
2)600
3)700

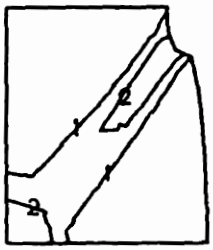

$\dot{\bar{\gamma}}^p$ values(sec^{-1})
1)1.33×10^3
2)2.66×10^3

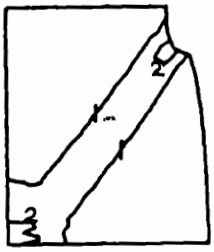

P values(sec^{-1})
1)-0.5×10^5
2)-1.0×10^5

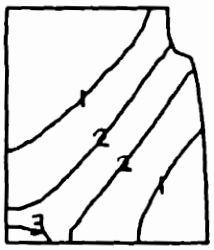

λ values
1)10.0
2)30.0
3)50.0

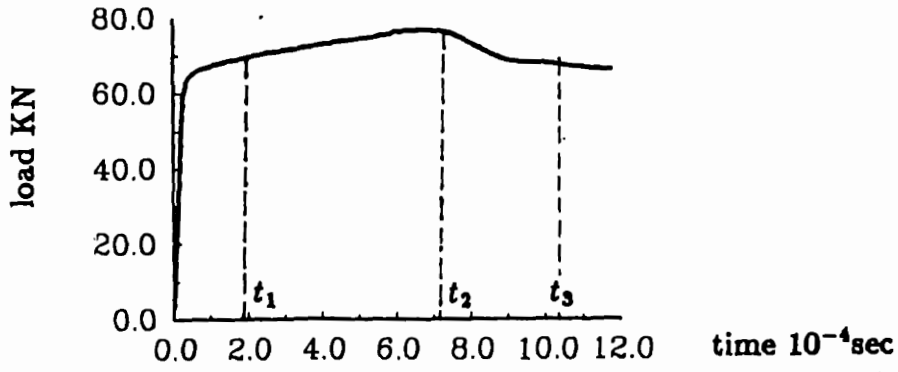

Fig. 8 Deformed mesh and the contour plots of the parameters $\bar{\gamma}^p$, θ, $\dot{\bar{\gamma}}^p$, P and λ at time t_3 when shear localization is fully developed. Note that the total load is rapidly decreasing and mesh is heavily distorted along the shear band. Adiabatic plane strain compression of AMS 6418 steel.

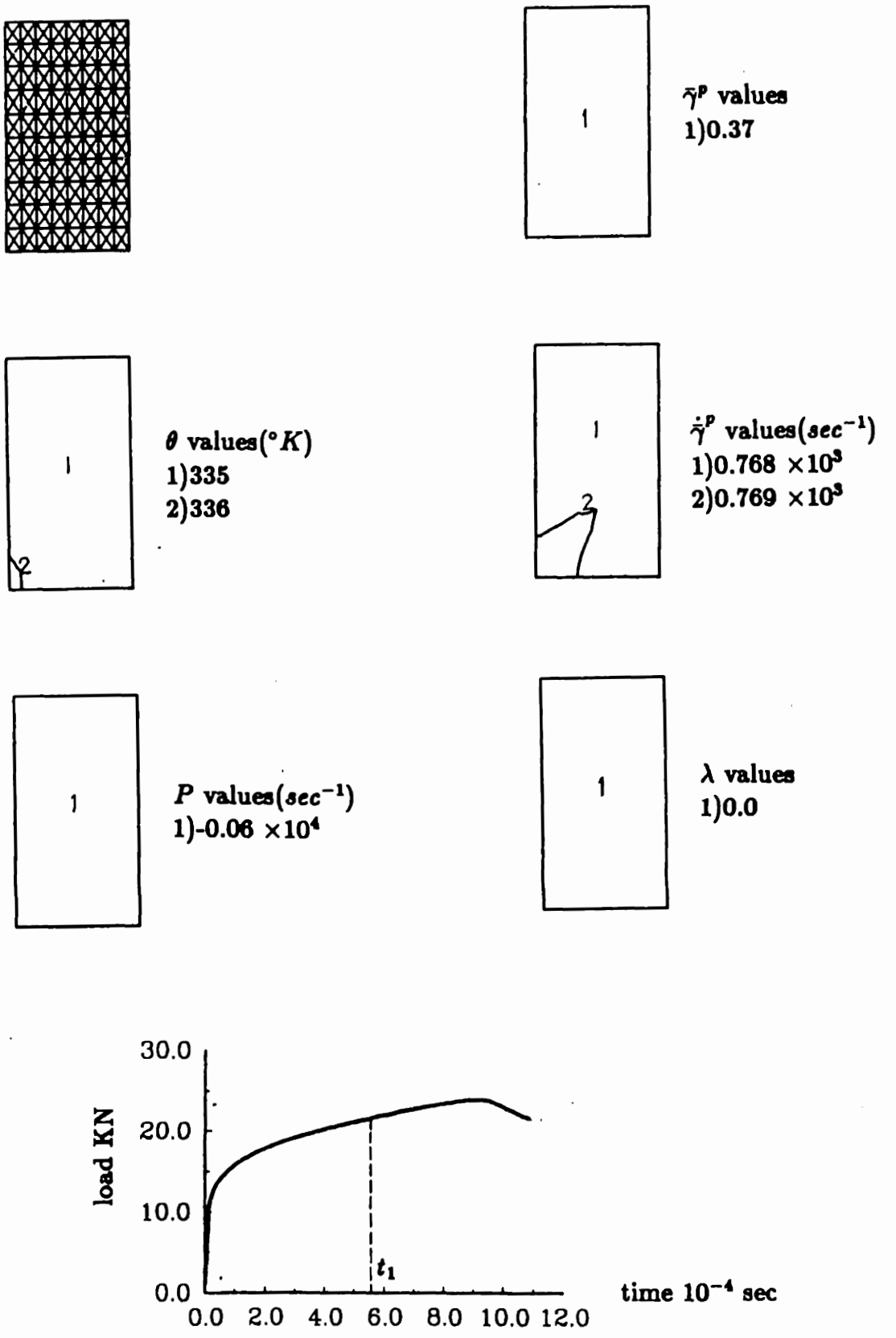

Fig. 9 Deformed mesh and the contour plots of the parameters $\bar{\gamma}^p$, θ, $\dot{\bar{\gamma}}^p$, P and λ at time t_1 when P changes its sign from positive to negative throughout the specimen. Adiabatic plane strain compression of aluminum 2024-T351.

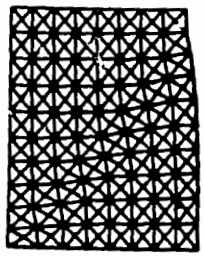

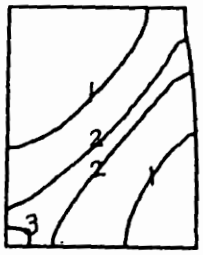

$\bar{\gamma}^p$ values
1)0.68
2)0.92
3)1.16

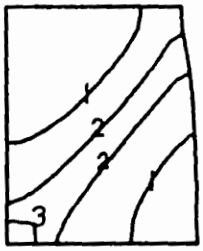

θ values($^\circ K$)
1)367
2)388
3)409

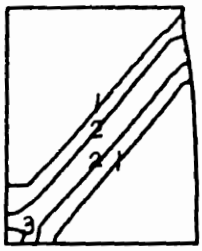

$\dot{\bar{\gamma}}^p$ values(sec^{-1})
1)0.8 $\times 10^3$
2)3.2 $\times 10^3$
3)5.6 $\times 10^3$

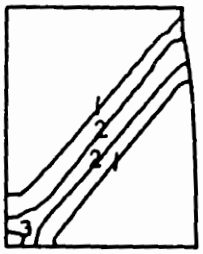

P values(sec^{-1})
1)-0.2$\times 10^5$
2)-0.8$\times 10^5$
3)-1.4$\times 10^5$

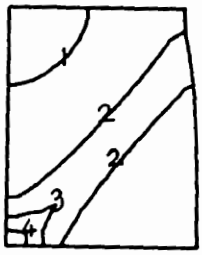

λ values
1)2.0
2)6.0
3)10.0
4)14.0

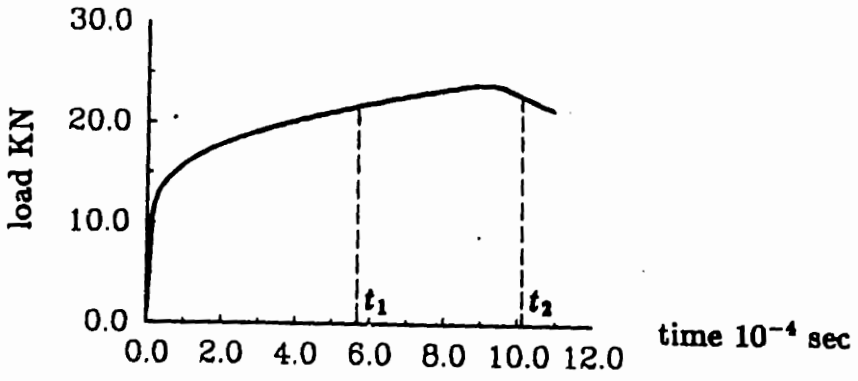

Fig. 10 Deformed mesh and the contour plots of the parameters $\bar{\gamma}^p$, θ, $\dot{\bar{\gamma}}^p$, P and λ at time t_2 when there necleates a zone of noticeable size where $\lambda > 10$ in the specimen. Note that the total load is at its maximum and contours show definite signs of localization. Adiabatic plane strain compression of aluminum 2024-T351.

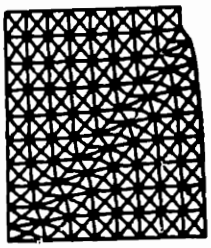

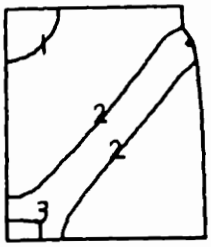

$\bar{\gamma}^p$ values
1)0.6
2)1.0
3)1.4

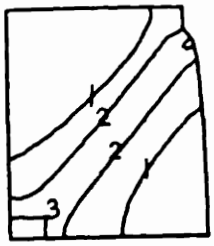

θ values($^\circ K$)
1)370
2)400
3)430

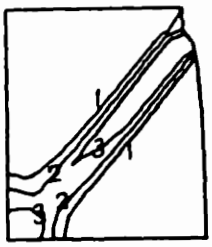

$\dot{\bar{\gamma}}^p$ values(sec^{-1})
1)1.2 $\times 10^3$
2)2.4 $\times 10^3$
3)3.6 $\times 10^3$

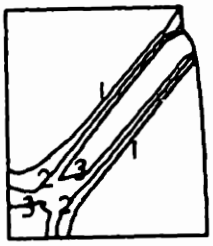

P values(sec^{-1})
1)-0.2$\times 10^5$
2)-0.5$\times 10^5$
3)-0.8$\times 10^5$

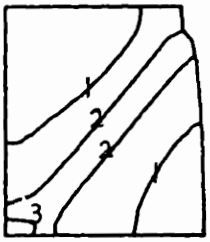

λ values
1) 3.0
2)12.0
3)21.0

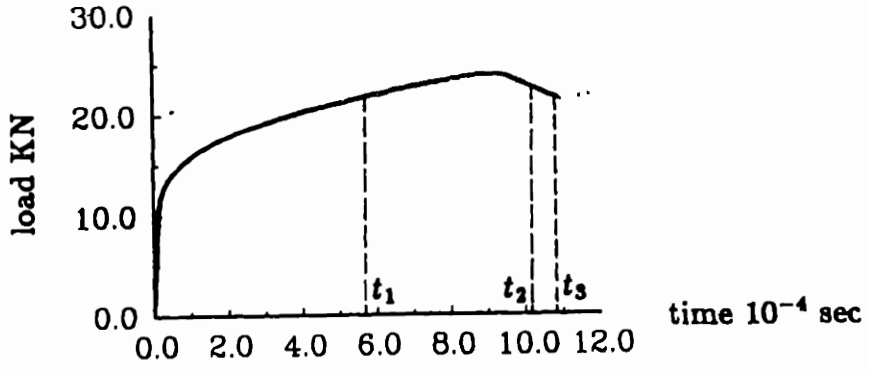

Fig. 11 Deformed mesh and the contour plots of the parameters $\bar{\gamma}^p$, θ, $\dot{\bar{\gamma}}^p$, P and λ at time t_3 when shear localization is fully developed. Note that the total load is rapidly decreasing and mesh is heavily distorted along the shear band. Adiabatic plane strain compression of aluminum 2024-T351.

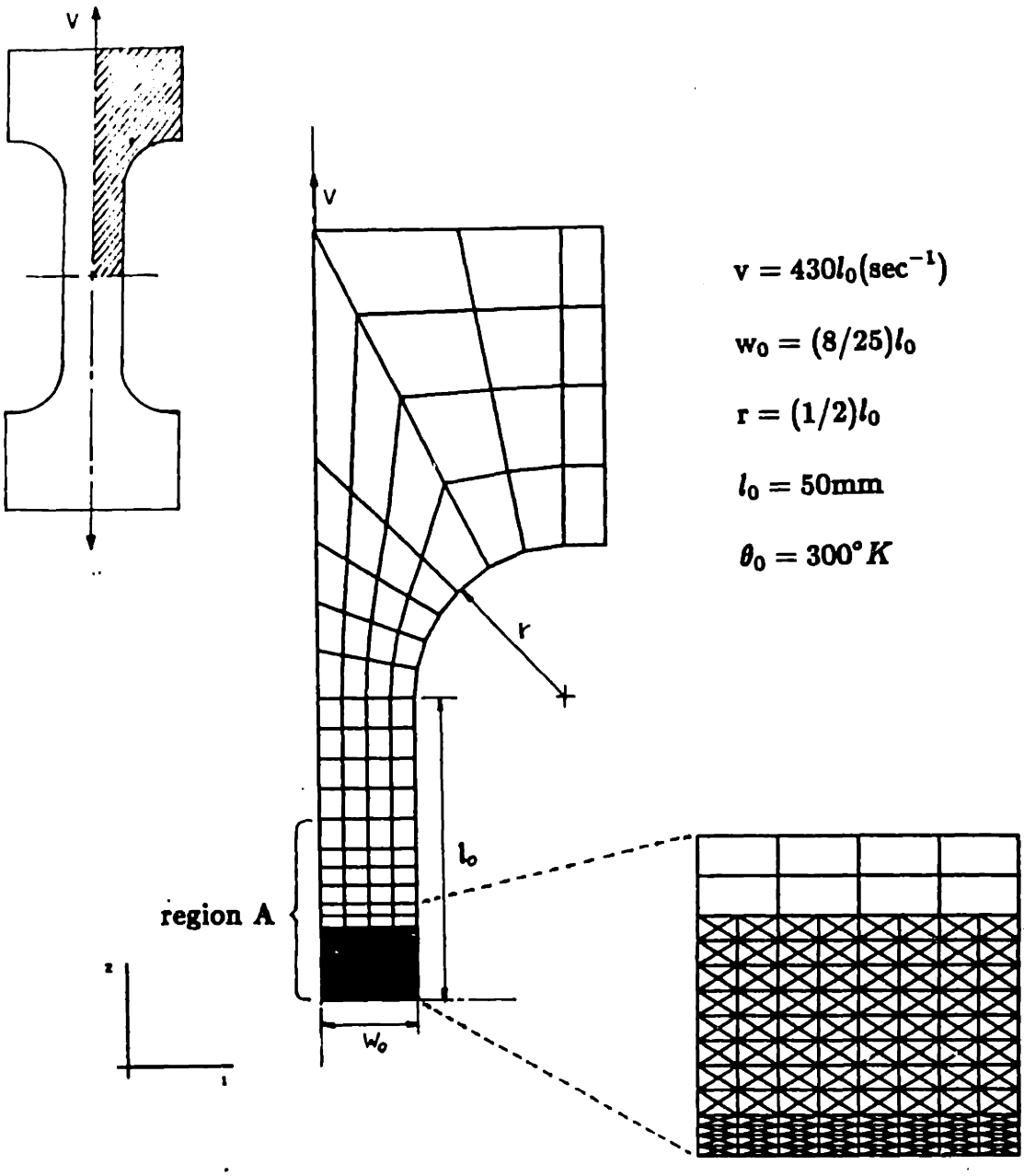

Fig. 12 Finite element mesh for the simulation of a plane strain tension test on AMS 6418 steel. The 456 element mesh represents one quarter of the specimen. All subsequent figures show only the region A and the associated level contours of various quantities.

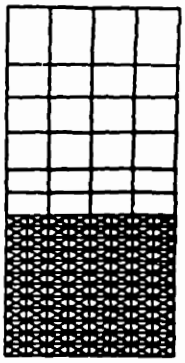

region A
(see Fig. 12)

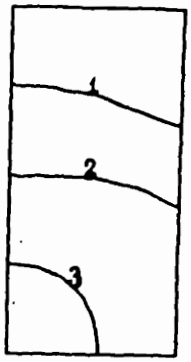

$\bar{\gamma}^p$ values
1)0.07
2)0.08
3)0.09

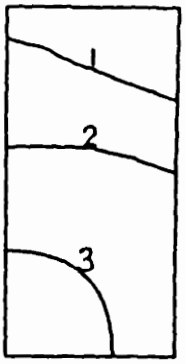

θ values($^\circ K$)
1)316
2)319
3)322

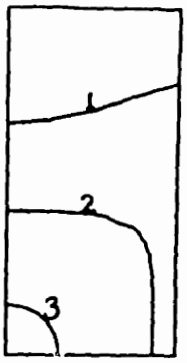

$\dot{\bar{\gamma}}^p$ values(sec^{-1})
1)0.9×10^3
2)1.5×10^3
3)2.1×10^3

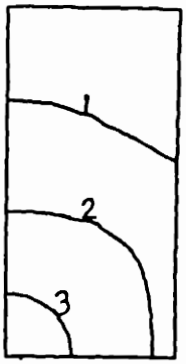

P values(sec^{-1})
1) 0.0
2)-0.5×10^4
3)-1.0×10^4

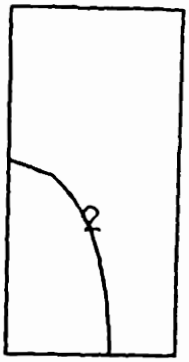

λ values
1)0.0
2)0.0

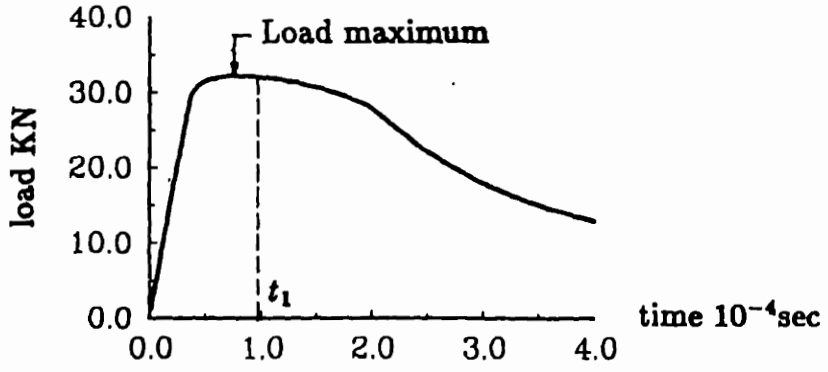

Fig. 13 Deformed mesh and the contour plots of the parameters $\bar{\gamma}^p$, θ, $\dot{\bar{\gamma}}^p$, P and λ at time t_1 when there first forms a region of negative P across the neck of the specimen. Adiabatic plane strain tension of AMS 6418 steel.

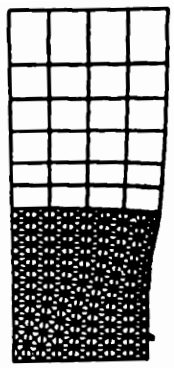

region A
(see Fig. 12)

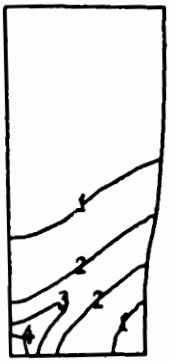

$\bar{\gamma}^p$ values
1)0.2
2)0.4
3)0.6
4)0.8

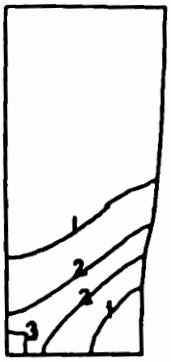

θ values($^\circ K$)
1)360
2)420
3)480

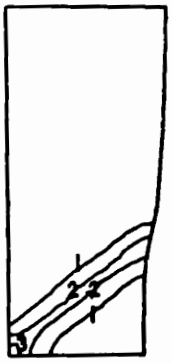

$\dot{\bar{\gamma}}^p$ values(sec^{-1})
1)0.3×10^4
2)1.2×10^4
3)2.1×10^4

P values(sec^{-1})
1) 0.0
2)-2.0×10^5
3)-4.0×10^5
4)-6.0×10^5

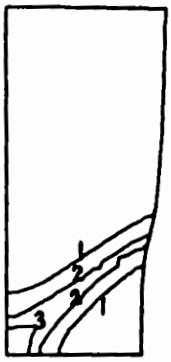

λ values
1) 5.0
2)10.0
3)15.0

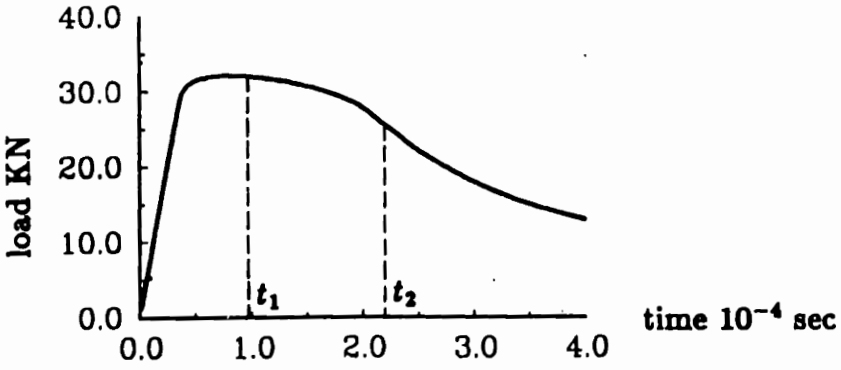

Fig. 14 Deformed mesh and the contour plots of the parameters $\bar{\gamma}^p$, θ, $\dot{\bar{\gamma}}^p$, P and λ at time t_2 when there necleates a zone of noticeable size where $\lambda > 10$ in the at the central region of the neck. Note that the total load at the beginning of the secondary slope and the level contours show definite signs of shear localization. Adiabatic plane strain tension of AMS 6418 steel.

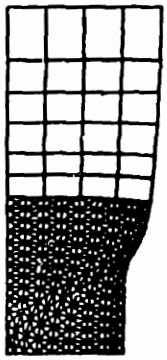

region A
(see Fig. 12)

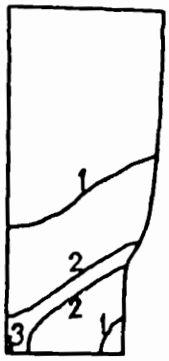

$\bar{\gamma}^p$ values
1)0.2
2)1.0
3)1.8

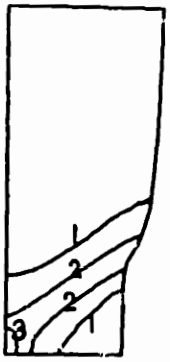

θ values($^\circ K$)
1)380
2)500
3)620

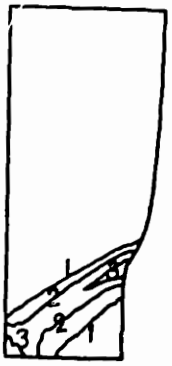

$\dot{\bar{\gamma}}^p$ values(sec^{-1})
1)0.2×10^4
2)0.8×10^4
3)1.4×10^4

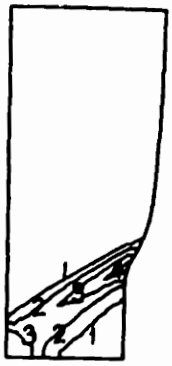

P values(sec^{-1})
1)-0.5×10^5
2)-2.0×10^5
3)-3.5×10^5
4)-5.0×10^5

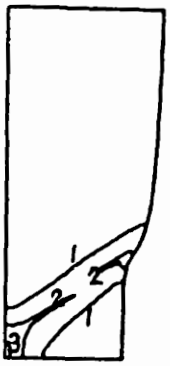

λ values
1)10.0
2)30.0
3)50.0

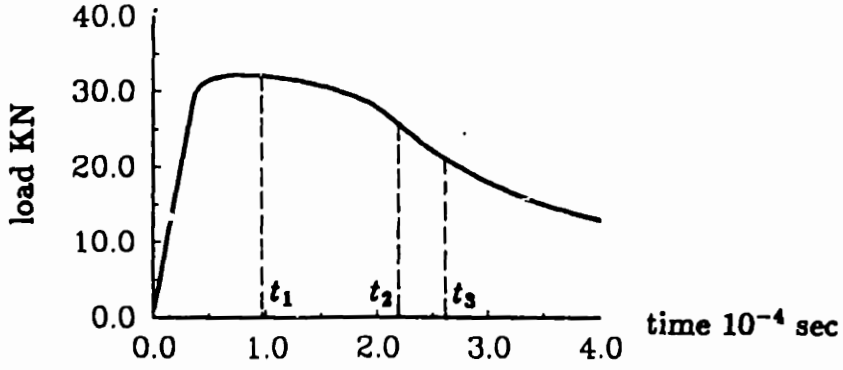

Fig. 15 Deformed mesh and the contour plots of the parameters $\bar{\gamma}^p$, θ, $\dot{\bar{\gamma}}^p$, P and λ at time t_3 when shear localization is fully developed. Note that the total load is rapidly decreasing and mesh is heavily distorted along the shear band. Adiabatic plane strain tension of AMS 6418 steel.

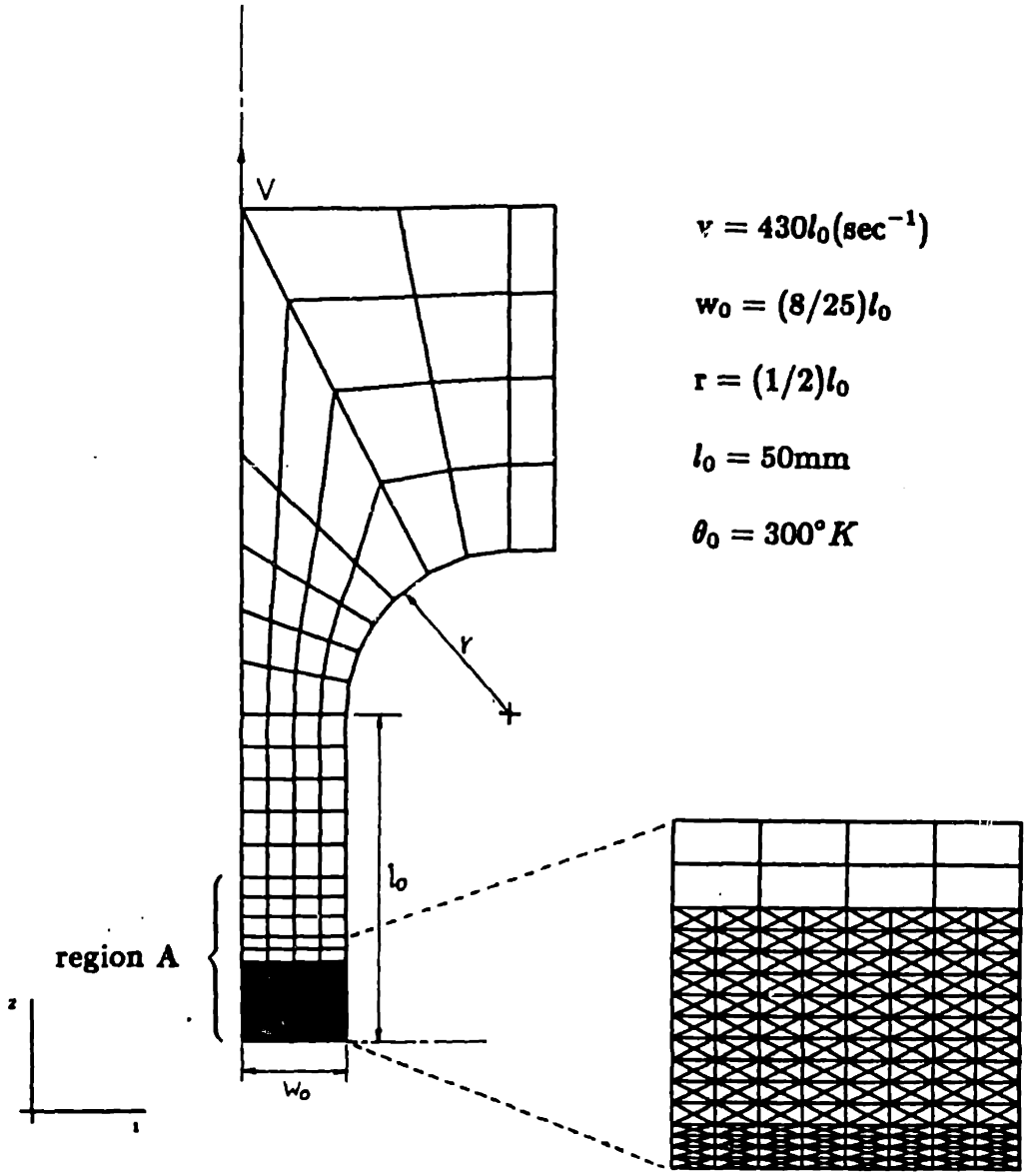

Fig. 16 Finite element mesh for the simulation of a plane strain tension test on aluminum 2024-T351. The 520 element mesh represents one quarter of the specimen. All subsequent figures show only the region A and the associated level contours of various quantities.

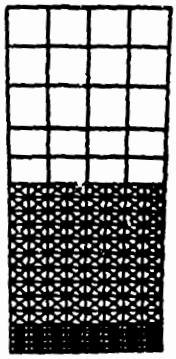

region A
(see Fig. 16)

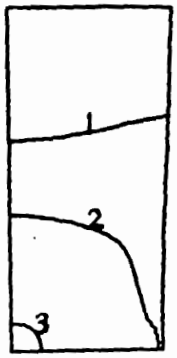

$\bar{\gamma}^p$ values
1)0.32
2)0.38
3)0.44

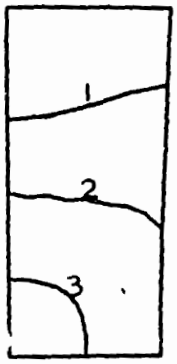

θ values($^\circ K$)
1)329
2)335
3)341

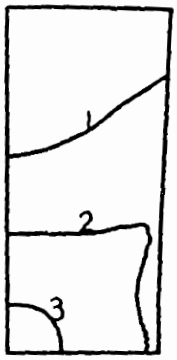

$\dot{\bar{\gamma}}^p$ values(sec^{-1})
1)0.8 $\times 10^3$
2)2.0 $\times 10^3$
3)3.2 $\times 10^3$

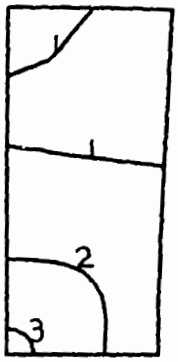

P values(sec^{-1})
1)+0.2$\times 10^4$
2)-1.0$\times 10^4$
3)-2.2$\times 10^4$

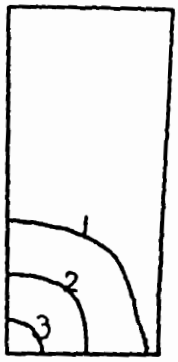

λ values
1)0.03
2)0.15
3)0.27

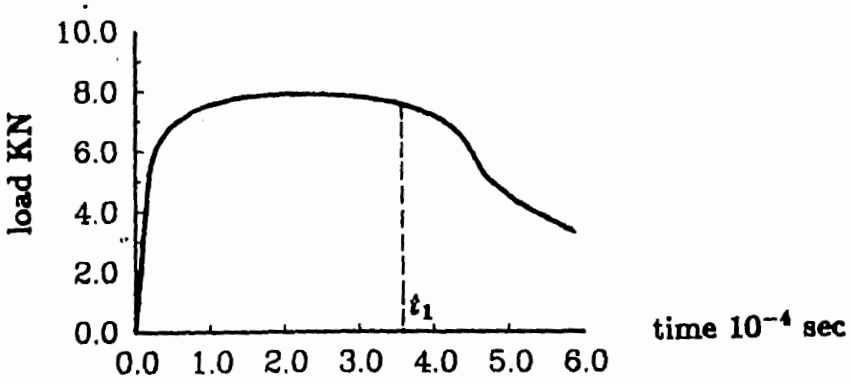

Fig. 17 Deformed mesh and the contour plots of the parameters $\bar{\gamma}^p$, θ, $\dot{\bar{\gamma}}^p$, P and λ at time t_1 when there first forms a region of negative P across the neck of the specimen. Adiabatic plane strain tension of aluminum 2024-T351.

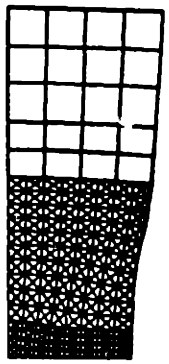

region A
(see Fig. 16)

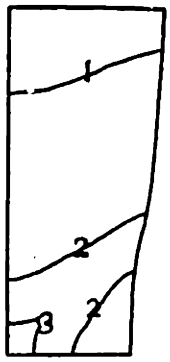

$\bar{\gamma}^p$ values
1)0.30
2)0.60
3)0.90

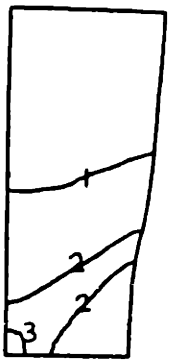

θ values($^\circ K$)
1)340
2)370
3)400

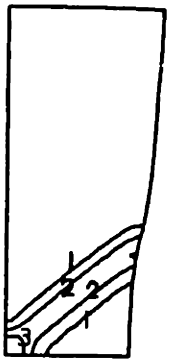

$\dot{\bar{\gamma}}^p$ values(sec^{-1})
1) 3.0×10^3
2) 9.0×10^3
3)15.0×10^3

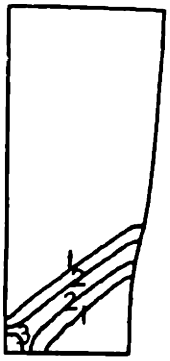

P values(sec^{-1})
1)-0.6×10^5
2)-2.2×10^5
3)-3.8×10^5

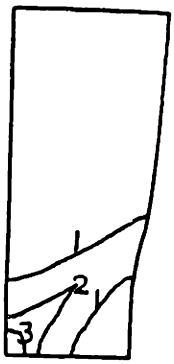

λ values
1)2.0
2)6.0
3)10.0

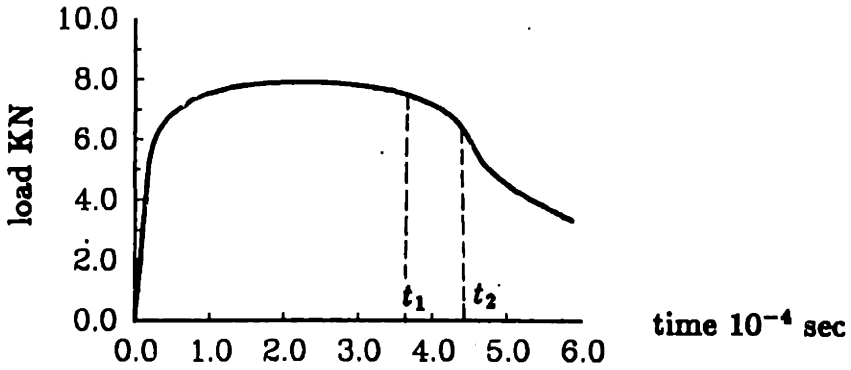

Fig. 18 Deformed mesh and the contour plots of the parameters $\bar{\gamma}^p$, θ, $\dot{\bar{\gamma}}^p$, P and λ at time t_2 when there necleates a zone of noticeable size where $\lambda > 10$ in the at the central region of the neck. Note that the total load at the beginning of the secondary slope and the level contours show definite signs of shear localization. Adiabatic plane strain tension of aluminum 2024-T351.

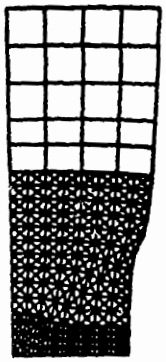

region A
(see Fig. 16)

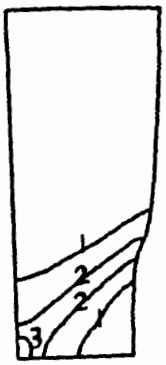

$\bar{\gamma}^p$ values
1)0.6
2)1.0
3)1.4

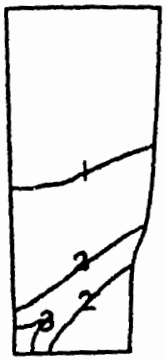

θ values($^\circ K$)
1)340
2)380
3)420

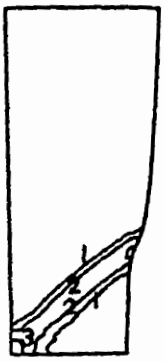

$\dot{\bar{\gamma}}^p$ values(sec^{-1})
1) 4.0×10^3
2)12.0×10^3
3)20.0×10^3

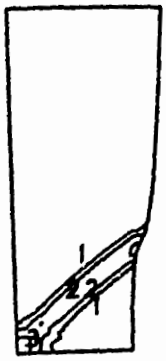

P values(sec^{-1})
1)-1.0×10^5
2)-3.0×10^5
3)-5.0×10^5

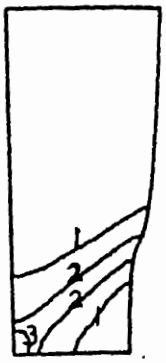

λ values
1) 2.0
2)10.0
3)18.0

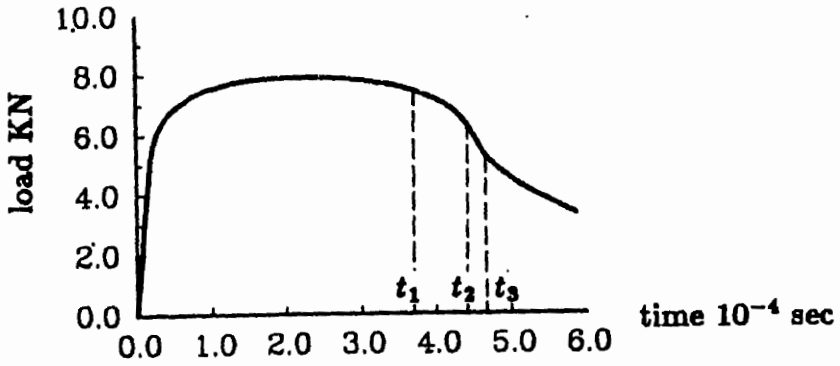

Fig. 19 Deformed mesh and the contour plots of the parameters $\bar{\gamma}^p$, θ, $\dot{\bar{\gamma}}^p$, P and λ at time t_3 when shear localization is fully developed. Note that the total load is rapidly decreasing and mesh is heavily distorted along the shear band. Adiabatic plane strain tension of aluminum 2024-T351.

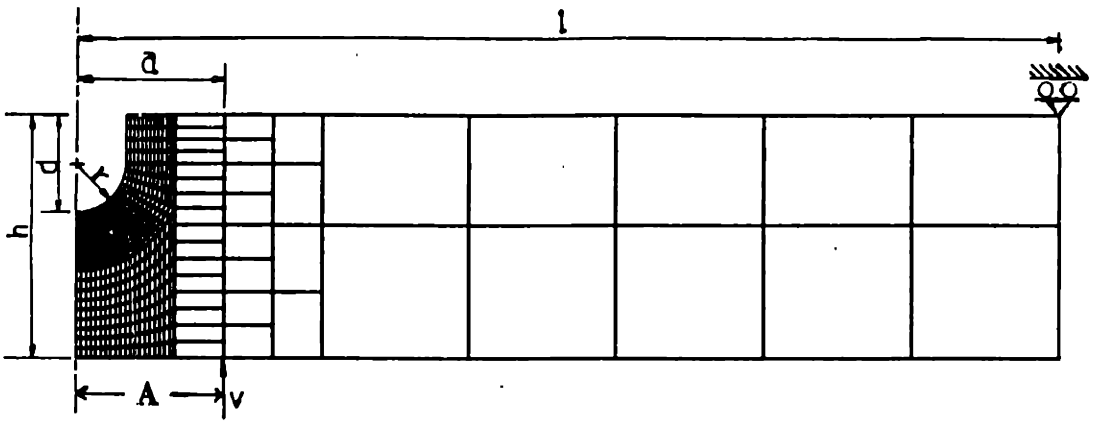

$h = (1/4)\, l$
$a = (3/20)\, l$
$r = (1/20)\, l$
$d = (1/10)\, l$
$v = 850\, l\, (sec^{-1})$
$l = 100\,\text{mm}$
$\theta_0 = 300°K$

Fig. 20 Finite element mesh for the simulation of adiabatic plane strain bending of a U-notched AMS 6418 steel specimen. The 542 element mesh represents one half of the specimen. All subsequent figures show only the region A and the associated level contours of various quantities.

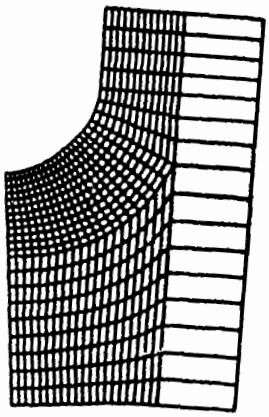

region A
(see Fig. 20)

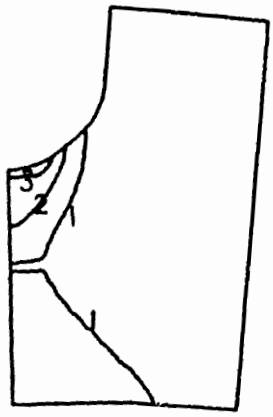

$\bar{\gamma}^p$ values
1)0.02
2)0.22
3)0.42

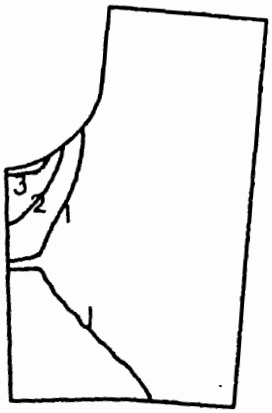

θ values($^\circ K$)
1)305
2)355
3)405

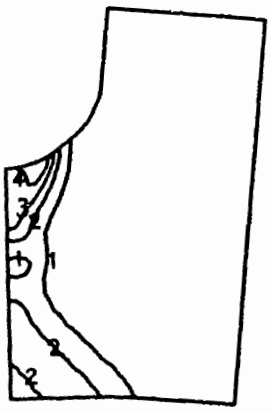

$\dot{\bar{\gamma}}^p$ values(sec^{-1})
1)0.05×10^4
2)0.20×10^4
3)0.35×10^4
4)0.50×10^4

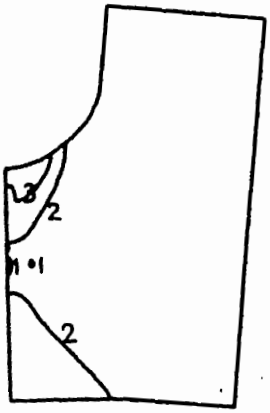

P values(sec^{-1})
1) 0.8×10^5
2)-0.2×10^5
3)-1.2×10^5

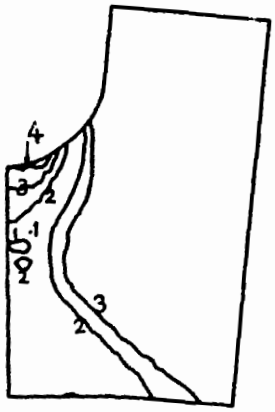

λ values
1) 2.0
2) 5.0
3) 8.0
4) 10.0

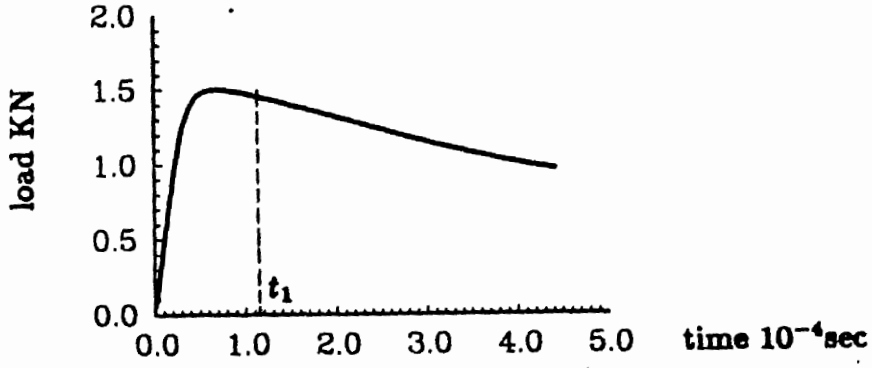

Fig. 21 Deformed mesh and the contour plots of the parameters $\bar{\gamma}^p$, θ, $\dot{\bar{\gamma}}^p$, P and λ at time t_1 when there first forms two regions of negative P in the deforming regions under the notch and under the back surface of the notch. The deformation field is extremely inhomogenous but there are no signs of shear localization. Adiabatic plane strain bending of a U-notched AMS 6418 steel specimen.

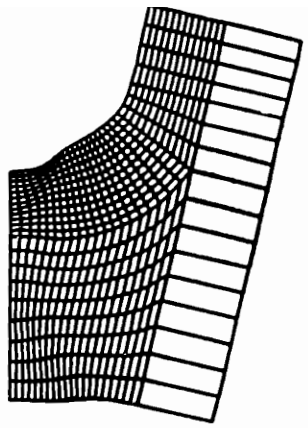

region A
(see Fig. 20)

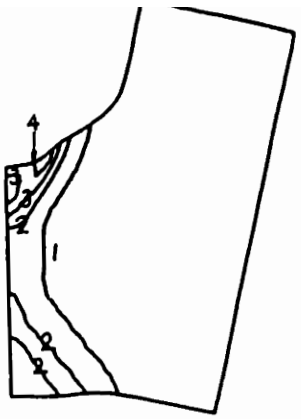

$\bar{\gamma}^p$ values
1)0.1
2)0.5
3)0.9
4)1.3

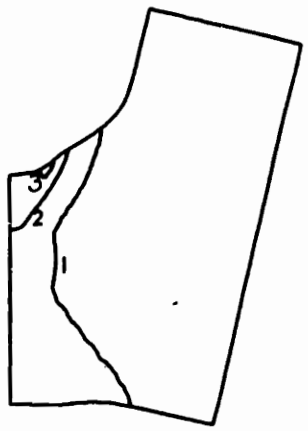

θ values($^\circ K$)
1)310
2)460
3)610

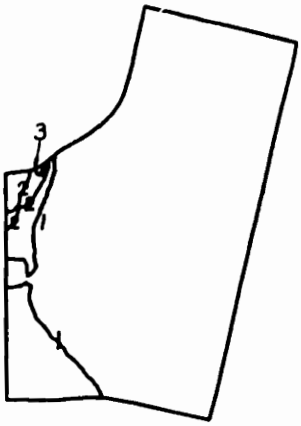

$\dot{\bar{\gamma}}^p$ values(sec^{-1})
1)0.1×10^4
2)0.6×10^4
3)1.1×10^4

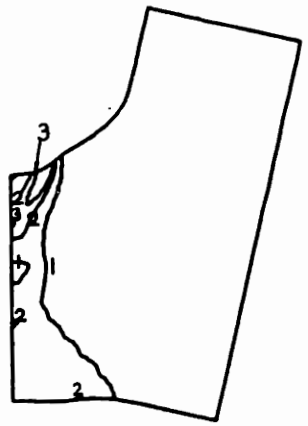

P values(sec^{-1})
1)-0.1×10^5
2)-1.1×10^5
3)-2.1×10^5

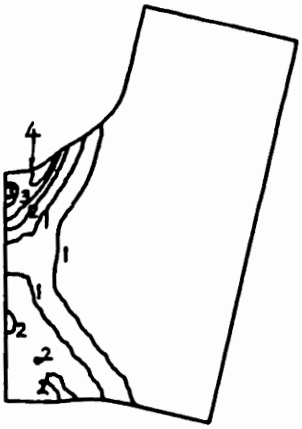

λ values
1) 0.0
2)15.0
3)25.0
4)35.0

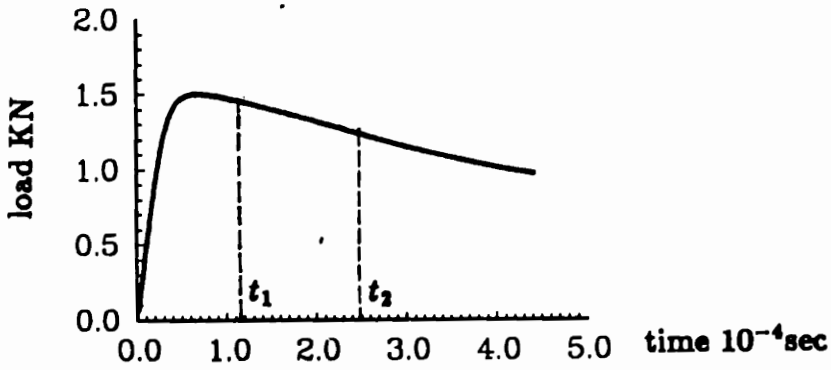

Fig. 22 Deformed mesh and the contour plots of the parameters $\bar{\gamma}^p$, θ, $\dot{\bar{\gamma}}^p$, P and λ at time t_2 when there forms two zones of noticeable size where $\lambda > 10$ in both of the deforming regions under the notch and under the back surface of the notch. Deformed mesh begins to show signs of shear localization at this stage. Adiabatic plane strain bending of a U-notched AMS 6418 steel specimen.

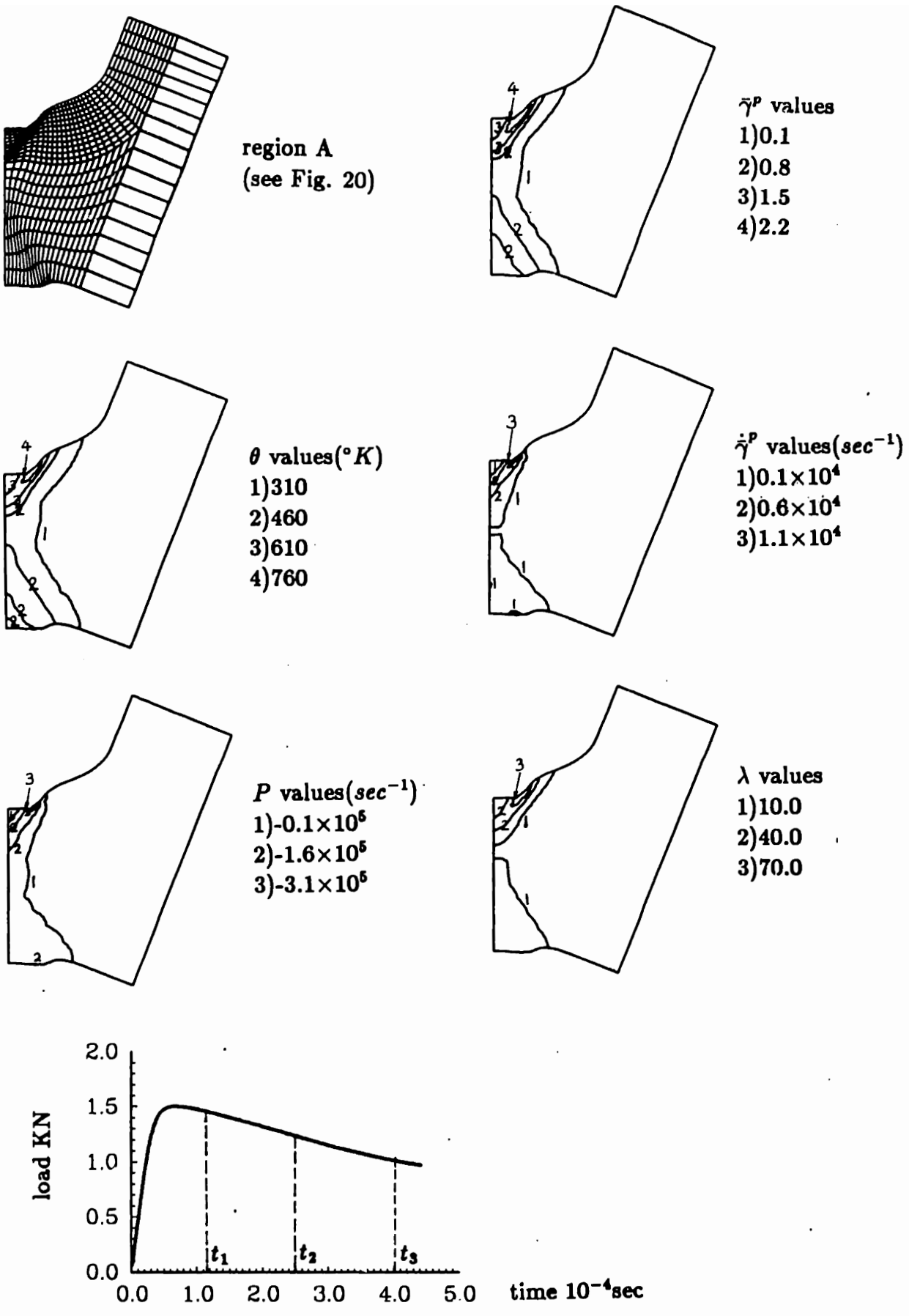

Fig. 23 Deformed mesh and the contour plots of the parameters $\bar{\gamma}^p$, θ, $\dot{\bar{\gamma}}^p$, P and λ at time t_3 when shear localization is fully developed. Mesh is heavily distorted along the shear bands in two regions above and below the neutral plane. Adiabatic plane strain bending of a U-notched AMS 6418 steel specimen.

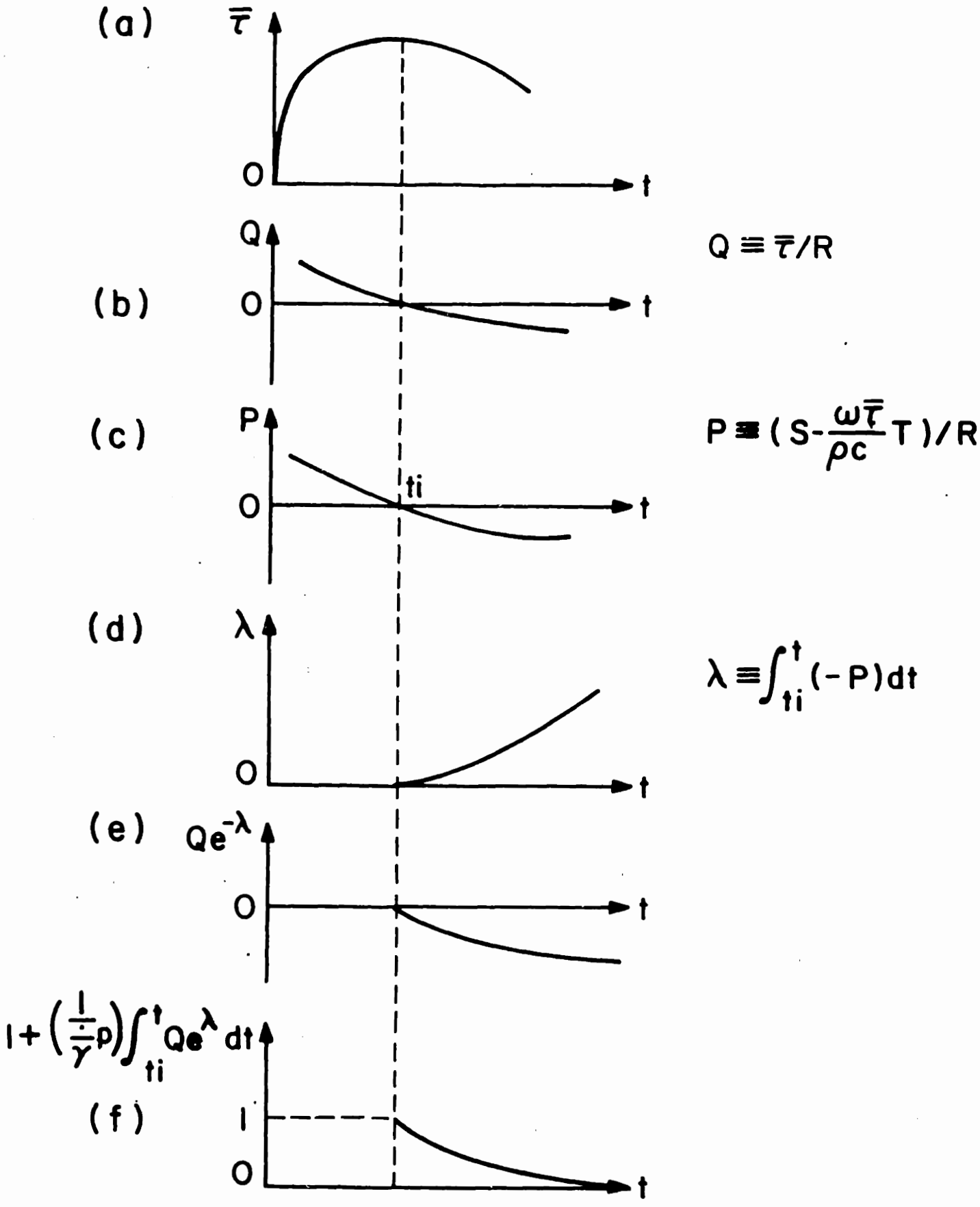

Fig. 24 Qualitative time trajectories of the field variables related to the term $[1 + (\dot{\gamma}^p)^{-1} \int_{t_i}^{t} Q \exp(-\lambda) dt]$ in equation (82).